Dissertation
submitted to the
Combined Faculties for the Natural Sciences and for Mathematics
of the Ruperto-Carola University of Heidelberg, Germany
for the degree of
Doctor of Natural Sciences

presented by

Master of Science Andrea Scarpa
born in Venice, Italy
Oral-examination: 20.04.2018

The Arabidopsis tasiARFs pathway: unraveling its role in root and embryo development

Referees: Prof. Dr. Alexis Maizel
Prof. Dr. Karin Schumacher

Table of contents

List of abbreviations

A	adenine
A. tumefaciens	*Agrobacterium tumefaciens*
AA	amino acid
AGO	ARGONAUTE
amiRNA	artificial micro RNA
Arabidopsis	*Arabidopsis thaliana*
ARE	auxin responsive element
ARF	AUXIN RESPONSE FACTOR
AUX/IAA	AUXIN/INDOLE-3-ACETIC ACID
b	base
BC	back-cross
BDL	BODENLOS
BOG	*BROTHER OF GEORGE*
bp	base pair
C	cytosine
cDNA	complementary DNA
CDS	coding sequence
Col-0	Columbia
CTRL	control
DMSO	Dimethyl sulfoxide
dsRNA	double-strand RNA
E. coli	*Escherichia coli*
easiRNAs	epigenetically activated small interfering RNA
EDTA	Ethylenediaminetetraacetic acid
EMS	ethyl methanesulfonate
F	filial generation
G	guanine
gDNA	genomic DNA
GFP	GREEN FLUORESCENT PROTEIN
GK	GABI-Kat
Glu	glutamate
Gly	glycine
GRG	*GEORGE*
GUS	*β-glucuronidase*
H2B	histone H2B
HA	human influenza hemagglutinin
IAA	indole-3-acetic acid
ISH	*in situ* hybridization
LR	lateral root
LRD	lateral root density
LRIS	lateral root induction system
MES	2-(N-morpholino)ethanesulfonic acid
miRNA	micro RNA
MMC	megaspore mother cell

MP	MONOPTEROS
mPS-PI	modified pseudo-Schiff propidium iodide
mRNA	messenger RNA
MS	Murashige and Skoog
NB	northern blot
NGS	next-generation sequencing
NLS	nuclear localization signal
NPA	N-1-naphthylphthalamic acid
nt	nucleotide
OD	optical density
phasiRNA	phased small interfering RNA
PI	propidium iodide
PR	primary root
PTGS	post-transcriptional gene silencing
QC	quiescent center
qPCR	quantitative PCR
RFP	RED FLUORESCENT PROTEIN
RISC	RNA-induced silencing complex
SAM	shoot apical meristem
siRNA	small interfering RNA
SNP	single-nucleotide polymorphism
SPL	SQUAMOSA PROMOTER BINDING PROTEIN-LIKE
T	thymine
T-DNA	transfer DNA
TAE	Tris-acetate-EDTA
TAS3	*TRANS-ACTING SIRNA3*
tasiARFs	*TRANS-ACTING SIRNA3*-derived trans-acting small-interfering RNAs
tasiRNAs	trans-acting small-interfering RNAs
Tris	tris(hydroxymethyl)aminomethane
U	uracil
UBQ	UBIQUITIN
WT	wild type

Summary

The phytohormone auxin controls a wide spectrum of biological processes by regulating the activity of AUXIN RESPONSE FACTORS (ARFs) transcription factors. ARFs are also post-transcriptionally regulated by *TRANS-ACTING SIRNA3* (*TAS3*)-derived trans-acting small-interfering RNAs (tasiARFs). The tasiARFs pathway is highly conserved in land plants, regulating functions ranging from developmental timing to lateral roots formation. This pathway is also present in primary root tip and in embryo, where its function(s) remains elusive. A modifier genetic screen using a transcriptional reporter for *MIR390A*, a tasiARFs pathway element, identified a mutant with no expression in the primary root tip. The mutation was mapped to AT1G75860, a gene of unknown function. Here, we tried to assign a function for this pathway in embryo and primary root, we further characterized the AT1G75860 mutant, and we also tested a possible interaction with the miR156/SQUAMOSA PROMOTER BINDING PROTEIN-LIKE (SPL) pathway in the control of lateral root development.

AT1G75860-mutant and -T-DNA lines were characterized regarding *MIR390A* presence in the primary root tip. We performed an allelism test between the mutant and the T-DNA lines; we tried to complement the mutant and, after more rounds of backcross, we tested if there was still linkage between mutation and phenotype. The results could not link the mutation with the phenotype, and indicated that the *MIR390A* transcriptional reporter might not faithfully reflect *MIR390A* expression pattern.

We tested for functions of the tasiARFs pathway in the primary root. We used mutants, gain-of-functions, or overexpressors of this pathway and looked for a primary root growth or meristem size phenotype in normal and abiotic-stress conditions. However, no primary root phenotype could be identified.

To check if there is an interaction between the tasiARFs and miR156/SPLs pathways in lateral root development, we tested, by qPCR and using the *MIR390A* transcriptional reporter, the response of one pathway to perturbations in the other. Due to inconsistences between experiments and methods for miR156 detection, only miR390 response could be examined, but no conclusive proof of interactions could be obtained.

Finally, regarding the role of the tasiARFs pathway in embryo, we could show that elements of the tasiARFs pathway are expressed and actively repress the expression of *ARF3.* Furthermore, using mutants of this pathway, we confirmed its role in control of seed number, and we propose a possible novel role in endosperm development.

Zusammenfassung

Das Phytohormon Auxin reguliert die Aktivität der Transkriptionsfaktoren *Auxin Response Factors* (ARFs) und kontrolliert dadurch eine breite Palette an biologischen Prozessen. Die ARFs werden außerdem posttranskriptionell von den trans-agierenden kleinen interferierenden RNAs (tasiARFs) reguliert, die von *TRANS-ACTING SIRNA3* (*TAS3*) abstammen. Der tasiARF-Weg ist in Landpflanzen hochkonserviert und reguliert Prozesse von Entwicklungstiming bis Seitenwurzelbildung. Der tasiARF-Weg ist ebenso im Embryo und in der Wurzelspitze aktiv, wo die Funktionen jedoch nur schwer definierbar sind. Durch einen genetischen Screen für Modifikatoren mit einem transkriptionellen Reporter für *MIR390A*, einem Bestandteil des tasiARF-Wegs, wurde eine Mutante identifiziert, der die Expression in der Wurzelspitze fehlte. Die Mutation wurde in AT1G75860, einem Gen mit unbekannter Funktion, ermittelt. Die AT1G75860-Mutante wurde weiter charakterisiert um eine Funktion im tasiARF-Weg in Embryo oder Wurzelspitze zuzuordnen. Im Rahmen dessen wurde auch eine potentielle Interaktion mit dem miR156/*Squamosa Promoter Binding Protein-Like* (SPL)-Weg in der Kontrolle der Seitenwurzelbildung untersucht.

Die Existenz von *MIR390A* in der Wurzelspitze wurde sowohl in der AT1G75860-Mutante als auch in T-DNA-Insertionslinien untersucht. Ebenso wurde ein Allelismus Test zwischen der Mutante und den Insertionslinien durchgeführt und eine Komplementation der Mutante versucht. Nach mehreren Rückkreuzungen wurde außerdem getestet ob noch ein Zusammenhang von Mutation und Phänotyp nachweisbar ist. Die Ergebnisse dieser Experimente konnten keinen Zusammenhang von Mutation und Phänotyp mehr nachweisen, sondern weisen darauf hin, dass der transkriptionelle Reporter für *MIR390A* das *MIR390A*-Expressionsmuster nicht unverfälscht widergibt.

In der Wurzelspitze wurde mit „loss-of-function“-, „gain-of-function“- und Überexpressionsmutanten nach Effekten des tasiARF-Wegs gesucht. Weder unter Standard- noch unter Stressbedingungen konnten Veränderungen im Hauptwurzelwachstum oder in der Meristemgröße gefunden werden.

Um eine mögliche Interaktion von tasiARF- und miR156/SPL-Weg zu untersuchen wurden die Reaktionen des einen Wegs auf Störungen des anderen Wegs getestet. Durch Unstimmigkeiten zwischen Experimenten und Methoden zur miR156-Detektion konnten nur die miR390-Antworten analysiert werden. Es konnten jedoch keine schlüssigen Beweise für Interaktionen der beiden Wege gefunden werden.

Schließlich konnten wir zeigen, dass Komponenten des tasiARF-Wegs im Embryo exprimiert sind und aktiv die Expression von *ARF3* unterdrücken. Durch Mutanten konnte die Rolle des tasiARF-Wegs in der Kontrolle der Samenanzahl bestätigt werden, außerdem schlagen wir eine mögliche neue Rolle in der Endosperm-Entwicklung vor.

General introduction

The general aim of this thesis is to elucidate the role in root and embryo development of the *TAS3*-derived trans-acting small-interfering RNAs (tasiRNAs) pathway, a type of post-transcriptional gene silencing (PTGS). This pathway controls several auxin responsive factors (ARFs) by the production of small interfering RNAs that are called tasiARFs.

In this introduction, embryo and root development will be shortly described; then the different mechanisms of PTGS in plants, with a special emphasis on the tasiARFs pathway and its role during embryo and root development regulation will be reviewed. Given the central role played by auxin during plant development and as the tasiARFs pathway modulate some of its essential components, I will first provide key elements about auxin signaling.

1 Auxin signaling

Auxin is one of the mayor phytohormones. Although many auxinic compounds have been identified, indole-3-acetic acid (IAA) is the major naturally occurring auxin in plants. Auxin has been shown to be involved in several developmental and adaptative processes, like embryogenesis, tropism, organogenesis, root and shot development and homeostasis, and plant-pathogen interactions (Salehin *et al.*, 2015).

Auxin effect is mediated through the nuclear receptor transport inhibitor response 1/auxin-related F-box proteins (TIR1/AFB) family (Li, Xie*, et al.*, 2016). F-box proteins act as substrate recognition elements for the Skp1-Cullin1-F-box protein (SCF), a multimeric complex of ubiquitin ligases. By binding to auxin, TIR1/AFP targets AUXIN/INDOLE-3-ACETIC ACID (AUX/IAA) repressors for ubiquitination and thus degradation, releasing their repression of auxin response factors (ARFs). AUX/IAAs repression is mediated by the co-repressor protein TOPLESS (TPL) (Salehin *et al.*, 2015). ARFs are transcription factors that bind to auxin responsive elements (AREs) controlling gene expression. AREs have a TGTCNN consensus core sequence, which often is TGTCTC (ARF1 and ARF5 have been shown to bind preferentially to the sequence TGTCGG) (Boer *et al.*, 2014). However, it must be noticed that, because *circa* half of *Arabidopsis thaliana* (in short, Arabidopsis) genes have at least one ARE in the first kilobase of their promoter, palindromic or direct repetitions of the consensus, or a consensus overlapping or adjoining coupling elements is necessary for auxin response (Mironova *et al.*, 2014). Most ARFs have an N-terminal DNA binding domain, a middle region containing an activation or a repression domain, and a C-terminal dimerization domain, which mediates dimerization with ARFs or AUX/IAAs (Li, Xie*, et al.*, 2016). It has been proposed that ARFs dimerization may act as molecular caliper to

discriminate uniquely spaced palindromic AREs (Dinesh *et al.*, 2015). So far, 22 ARF genes and one pseudogene have been identified in Arabidopsis (Li, Xie, *et al.*, 2016).

Auxin levels are controlled by local biosynthesis and degradation and by polar auxin transport. In the root, auxin polar transport follows a reverse fountain pattern, moving rootward in the stele till the root tip, where first moves toward the outer layers and then shootward. Auxin PIN-FORMED (PIN) efflux carriers with polarized tissue-specific subcellular localization, and AUXIN1 (AUX1) and LIKE AUX1 (LAX) influx carriers control the reverse fountain flow (Band *et al.*, 2014).

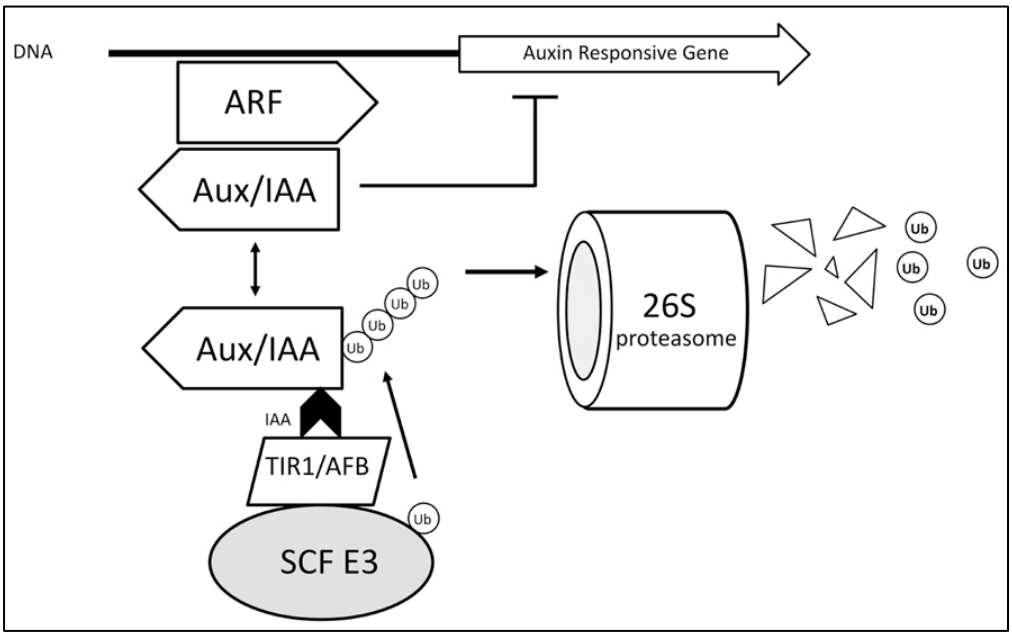

Figure 1. Model for auxin-mediated IAA-ARFs transcription activation. Adapted from (da Costa *et al.*, 2013). Under © https://creativecommons.org/licenses/by/3.0/.

The other auxin receptor, AUXIN BINDING PROTEIN 1 (ABP1), was thought to control auxin response in a non-transcriptional way by forming a complex with plasma membrane-localized receptor-like transmembrane kinases (TMKs) (T. D. Xu *et al.*, 2014). However, recent findings seemed to rule out a role of APB1 in auxin signaling (Gao *et al.*, 2015).

2 Embryonic and post embryonic development of Arabidopsis

2.1 Embryonic development: from ovule formation to germination

2.1.1 Arabidopsis flower

Ovule and pollen formation, fertilization, embryo development, and seed maturation, all occur in the flower. Arabidopsis flower has a concentric organ arrangement of 4 whorls: sepals, petals, stamens, and carpels. Externally, 4 sepals protect the bud and alternate with a

more internal ring of 4 petals providing further protection and controlling interactions with biotic factors. The next whorl is formed by 6 stamens, 4 long and 2 short, each consisting of a filament and an anther, where pollen is produced (Scott *et al.*, 2004). In the most internal ring, 2 carpels are fused to form the gynoecium, the female reproductive structure of flowering plants (Irish, 2010).

Internal tissues near the margins of the fused carpels have meristematic activity and generate placenta, septum, transmitting tract, style, and stigma (Hawkins *et al.*, 2014).

External tissues generate replum, where valve, encapsulating the seeds, are fused by a specific tissue called valve margins, responsible for fruit opening and seed dispersal (Roeder *et al.*, 2006).

The mature gynoecium has at the top the stigma, required for pollen adhesion and germination; just below it, the style is found, which comprise the apical portion of the pollen-guiding cavity transmitting tract. Basal to the style, the ovary contains ovules, attached to the septum, dividing the fruit in half, by funiculi (Crawford *et al.*, 2011). Finally, the gynophore connects the gynoecium to the base of the flower (Larsson *et al.*, 2013).

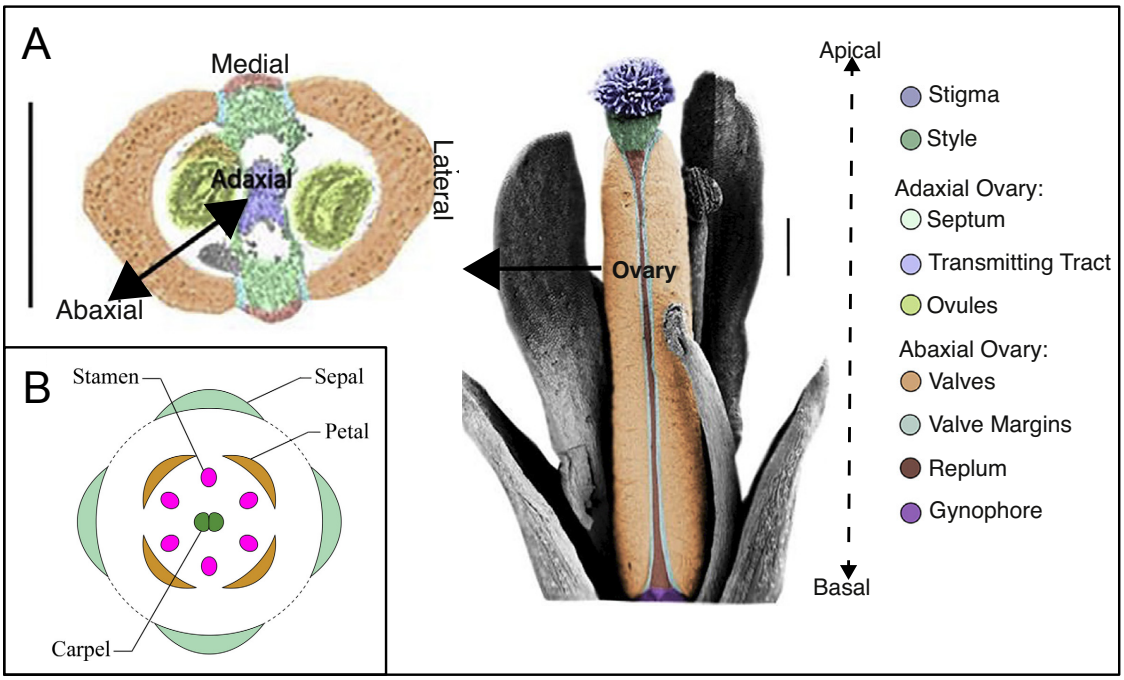

Figure 2. A) Arabidopsis gynoecium. The left panel shows a gynoecium cross-section, while the right shows a scanning electron micrograph. Both are false-colored to describe and distinguish the individual tissues (see color code on the right). Scale bars, 100 µm. Adapted from (Deb *et al.*, 2017). Under https://creativecommons.org/licenses/by/4.0/ **B) Arabidopsis floral organ arrangement**. Adapted from (Cardarelli *et al.*, 2014). Under © https://creativecommons.org/licenses/by/3.0/

2.1.2 Ovule development

The first stage of ovule development is the primordia formation: from the placenta 3 main domains grows radially: the funiculus, the chalaza, and the nucellus. The funiculus provides anchorage to placenta and allows nutrient flow to developing seeds (Khan *et al.*, 2015); the chalaza originates 2 integuments, which by anticlinal divisions enclose the female gametophyte (apart from the micropyle through which the pollen tube penetrates (Sandaklie-Nikolova *et al.*, 2007)) and differentiate into the seed coat (Enugutti *et al.*, 2012); the nucellus hosts the megaspore mother cell (which by meiosis forms the female gametophyte), and degenerates after fertilization regulating the formation of the chalazal endosperm (W. Xu *et al.*, 2016).

The second stage of ovule development is the megasporogenesis: the nucellar diploid archespore directly originates the megaspore mother cell, which undergoes meiosis; Arabidopsis megasporogenesis belongs to the monosporic type, where cell plates form with every division, generating 4 haploid mononucleate megaspores, 3 of which degenerates, leaving only the one closest to the chalaza (Yadegari *et al.*, 2004).

The last stage is the megagametogenesis: the remaining functional megaspore undergoes 3 round of mitosis, with phragmoplasts and cell plates forming only in the last round and surrounding the 8 nuclei, 4 at each pole; during this cellularization event, 2 nuclei migrate from each polar pool to the center where they will fuse. The mature female gametophyte is therefore composed of 7 cells: a binucleate central cell, 3 antipodal cells distal to the micropyle, 2 synergid cells flanking the micropyle, and one egg cell proximal to the micropyle (Yadegari *et al.*, 2004).

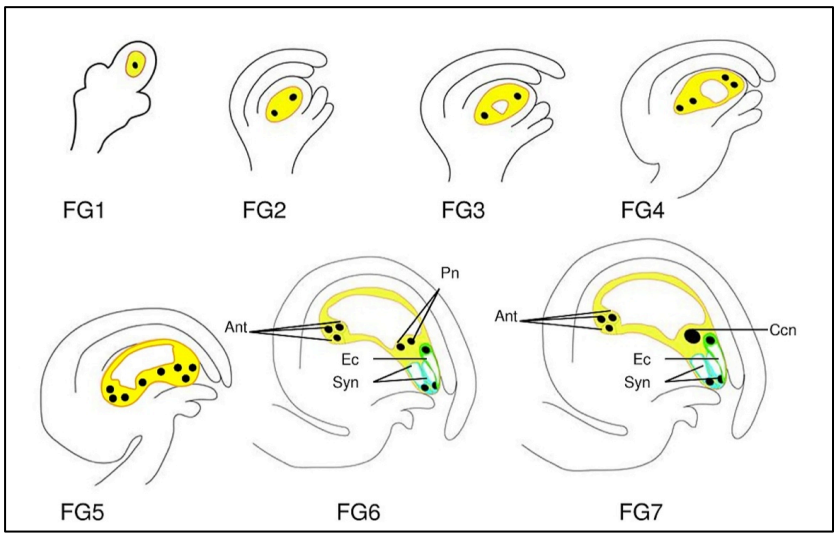

Figure 3. Schematic drawing of ovule development in Arabidopsis. Ant, antipodal; Ccn, central cell nucleus; Ec, egg cell; Pn, polar nucleus; Syn, synergid cell. Adapted from (Panoli *et al.*, 2015). Under © https://creativecommons.org/licenses/by/4.0/

2.1.3 Fertilization and embryo development

2.1.3.1 Fertilization

Adhesion of pollen grains to the stigma triggers its hydration and germination, forming a pollen tube that grows through stigma and transmitting tract, forming periodic callose plugs (Qin *et al.*, 2012), and emerges toward funiculus and micropyle (funicular guidance and micropylar guidance) (Guan *et al.*, 2014).

After entering through the micropyle, the pollen tube bursts the receptive synergid and releases the 2 sperm cells, which fuse with the egg cell and the central cell. Synergids play an important role in micropylar guidance, releasing pollen tube attractant, so the remaining synergid fuses with the fertilized central cell diluting pollen attractants and lowering the risk of politubey and therefore polyspermy (Maruyama *et al.*, 2015). The fertilized diploid egg cell develops into an embryo, while the triploid central cell originates the endosperm.

2.1.3.2 Endosperm development

Nuclear divisions without cytokinesis characterize early endosperm development, resulting in a syncytium that contains about 100 nuclei at globular embryo stage, when it begins to cellularize forming one layer (Sorensen *et al.*, 2002); endosperm cellularization starts close to the embryo and ends at the chalaza, then periclinal divisions produce more layers. Because the endosperm is consumed during embryo growth, in mature seeds only one endosperm layer remains (Brown *et al.*, 1999).

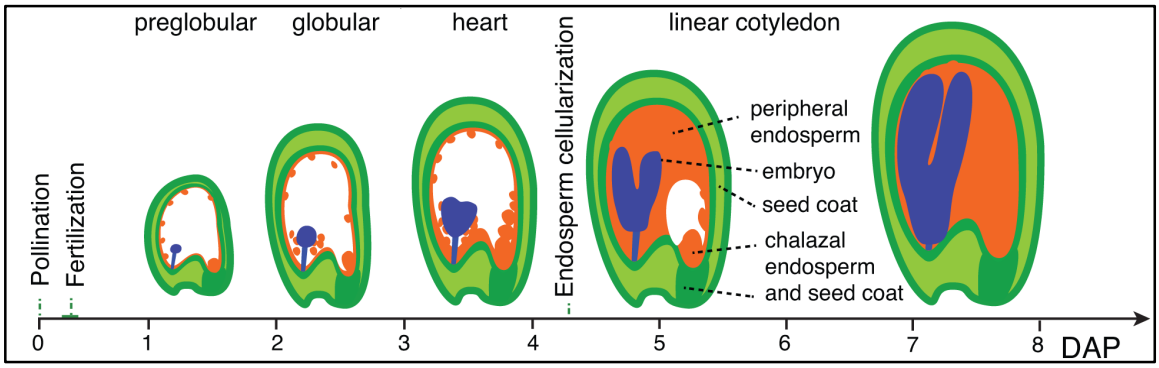

Figure 4. Arabidopsis endosperm development. Adapted from (Burkart-Waco *et al.*, 2015). Under © https://creativecommons.org/licenses/by/4.0/

2.1.3.3 Embryo development

Arabidopsis embryo develops according to a simple and predictable cell division pattern. The fertilized egg cell first elongates, creating the apical-basal axis, and then asymmetrically divides: a smaller apical cell generates most of the embryo, while the longer basal cell generates the suspensor from 7 to 9 transverse cell divisions. The uppermost cell of the suspensor will form the hypophysis, the precursor of the quiescent center (QC) and of the columella.

The apical cell first undergoes 2 orthogonal longitudinal and then one transverse divisions, reaching the octant stage. A round of periclinal cell divisions create an inner and an outer layer, precursors of ground and vascular tissues, and of the epidermis, respectively; this stage is called dermatogen. The outer layer will mostly divide anticlinally during the rest of the embryogenesis, while, already during the next early globular stage, the inner layer division pattern produces the embryo apical-basal axis. Further rounds of divisions specify basic tissue types and primordia of most major organs, already distinguishable at the early hearth stage.

In the following stages of hearth, torpedo, and bent cotyledon, the shoot apical meristem is specified, and the embryo assumes its mature form, with a tissue pattern very close to the one found in the seedling (Capron *et al.*, 2009; ten Hove *et al.*, 2015).

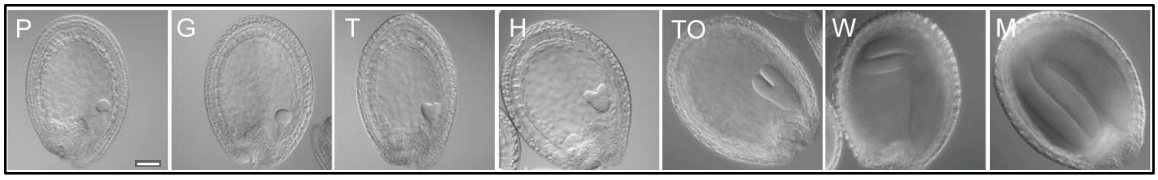

Figure 5. Embryo developmental stages in Arabidopsis. Preglobular (P), globular (G), transition (T), heart (H), torpedo (TO), walking-stick (W), and mature embryo (M). Scale bar 100 µm. Adapted from (Liu *et al.*, 2016). Under © https://creativecommons.org/licenses/by/4.0/

2.2 Post embryonic development: the Arabidopsis root system

The root system of *Arabidopsis thaliana* is essential to ensure an adequate supply of water and nutrients, to provide mechanical stability and to respond to biotic and abiotic stresses. Roots of *Arabidopsis thaliana* have both a structured tissue organization and a simple architecture. The root system of Arabidopsis consists of a primary root from which lateral roots branch.

2.2.1 Tissue organization and the root apical meristem

Tissue organization of primary and lateral roots is similar. Tissues are arranged in a concentric structure, formed, from outward to inward, by epidermis, cortex, endodermis, pericycle, and vasculature. These layers result from the activity of stem cells (or initials) at the root tip (root apical meristem): epidermal/lateral root cap initials, columella initials, ground tissue and cortex/endodermal initials, and vascular tissue/pericycle initials; radial symmetry and lack of movement means that cells originated from the same initials are disposed in vertical files (Scheres *et al.*, 2002). Along the longitudinal axis, three zones can be delineated: in the meristematic zone cells undergo several rounds of divisions, in the elongation zone they stop dividing and increase their length, and in the differentiation zone they acquire their specific characteristics (Petricka *et al.*, 2012).

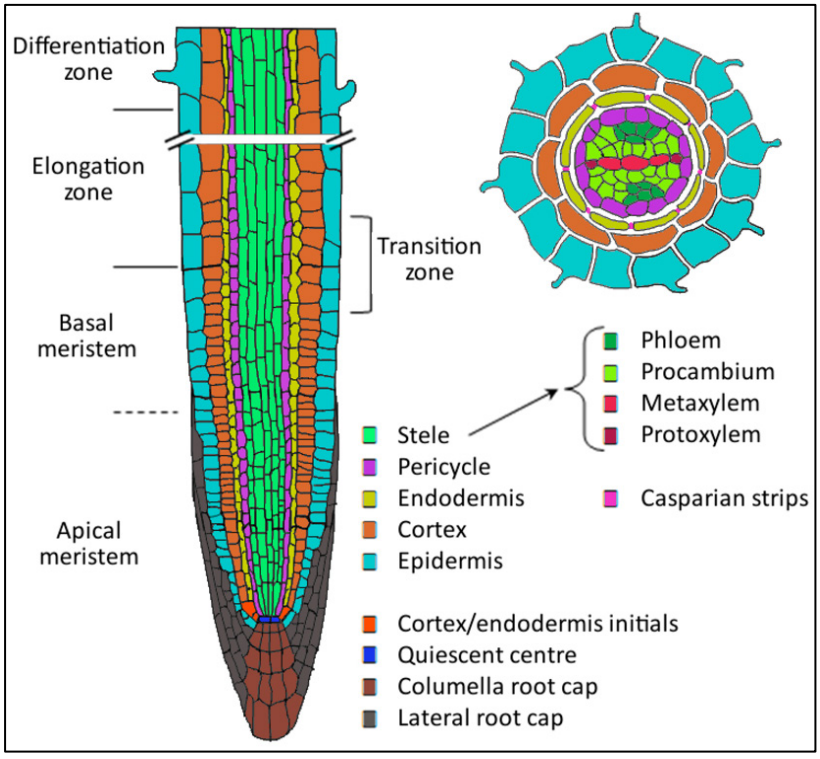

Figure 6. Organization of Arabidopsis root. Adapted from (S. De Smet *et al.*, 2015). Under © https://creativecommons.org/licenses/by/4.0/

2.2.2 Auxin control of primary root

Auxin is a key player in the organization of primary root: an auxin minimum controls the position of the transition zone, a boundary between meristematic zone and elongation zone (Verbelen *et al.*, 2006), thereby defining meristem size (Di Mambro *et al.*, 2017). On the other hand, an auxin maximum establishes the quiescent center (QC), a small group of very slow dividing cells that maintain stem cells, and creates an IAA gradient that promotes cell division at intermediate levels and differentiation at lower levels (Overvoorde *et al.*, 2010; Tian *et al.*, 2013). In auxin-dependent stem cell niche maintenance in the root apical meristem, the auxin maximum is established both by local IAA biosynthesis and polar transport (Liu *et al.*, 2017).

2.2.3 Lateral root development

2.2.3.1 Priming and specification

Lateral roots are specified in the differentiation zone from a subset of cells (founder cells) found in pericycle cells adjacent to the xylem poles (xylem pole pericycle cells). The specification of founder cells to provide the competence to form a lateral root (priming) is thought to start in the meristematic zone in concomitance with an oscillatory genes network (including auxin-induced genes), while mature founder cells display a local maximum of auxin response, defining lateral root pre-branch sites (I. De Smet, 2012; Du *et al.*, 2017). Periodic programmed cell death in the root cap has been reported to play a role in the oscillatory behavior of auxin-induced genes: root cap cells accumulate auxin through indole-3-butyric acid (IBA) conversion to IAA and AUX1 expression, and the accumulated auxin is released after their death into the oscillation zone (Moller *et al.*, 2017).

2.2.3.2 Initiation, growth, and emergence

Individual or pairs of founder divide asymmetrically and keep dividing anticlinally to form a singled-layer that can contain up to 10 cells (Stage I). In the next stage (Stage II) they divide periclinally, resulting in 2 layers. More anticlinal and periclinal divisions create a dome-shaped structure (Stages III to VII) that will emerge in stage VIII (Peret *et al.*, 2009).

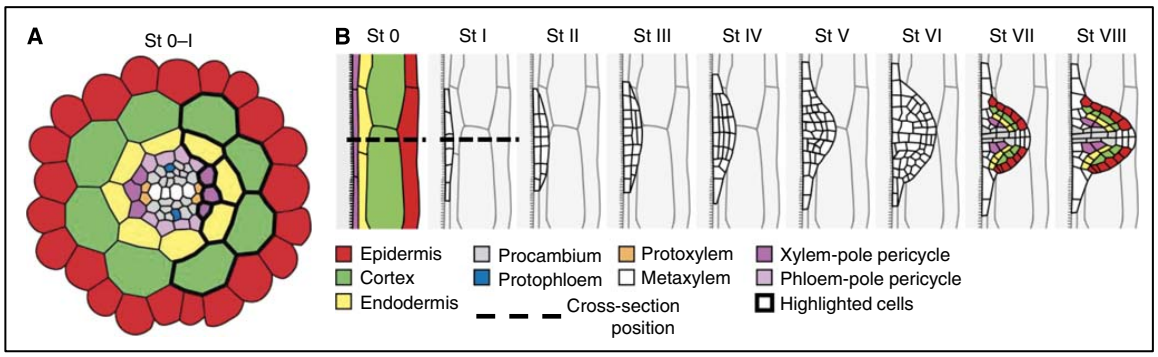

Figure 7. Lateral root formation and emergence. A, cross section. **B**, lateral section. St, stage. Adapted from (Peret *et al.*, 2013). Under © https://creativecommons.org/licenses/by/3.0/

2.2.3.3 Role of auxin signaling in lateral root development

Auxin controls through multiple auxin-signaling modules the whole development of lateral roots (Lavenus *et al.*, 2013): IAA28-ARF5, 6, 7, 8, and 19 mediate lateral root priming in the basal meristem controlling *GATA23* expression (De Rybel *et al.*, 2010); IAA14-ARF7 and ARF19 control lateral root founder cells polarization through activation of *LATERAL ORGAN BOUNDARIES-DOMAIN 16/ASYMMETRIC LEAVES2-LIKE 18* (*LBD16/ASL18*) and the other related *LBD/ASL* genes (Goh *et al.*, 2012); IAA14-ARF7 and ARF19, and IAA12-ARF5 control lateral root initiation, possibly through the control of the cell cycle (Vanneste *et al.*, 2005), and patterning, through the action of the receptor-like kinase ARABIDOPSIS CRINKLY4 (I. De Smet *et al.*, 2008); IAA14-ARF7 and ARF19 (in the cortex and in the epidermis), and IAA3-ARF7 (in the endodermis) control lateral root emergence, regulating auxin-mediated cell wall remodeling (Swarup *et al.*, 2008).

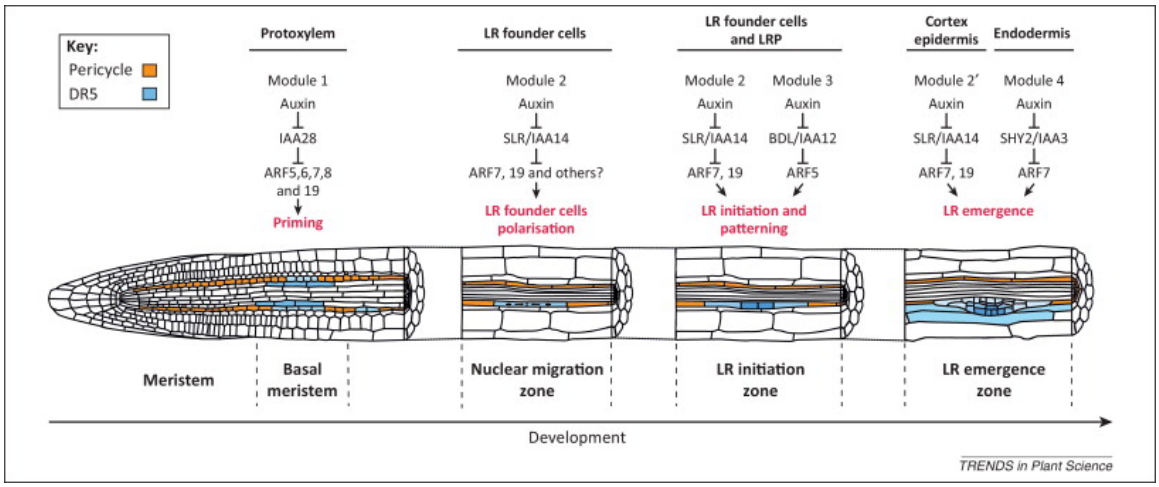

Figure 8. Auxin-signaling modules controlling LR development. Adapted from (Lavenus *et al.*, 2013), Copyright © 2013, with permission from Elsevier.

Among the ARFs playing a role in lateral root development, ARF2, ARF3, and ARF4 activity is also controlled by the TAS3-derived trans-acting small-interfering RNAs (tasiARFs)

pathway: tasiARFs inhibition of ARF2, ARF3 and ARF4 releases their repression of lateral root growth (Marin *et al.*, 2010). This part will be further developed in paragraph 3.3.2.1 below.

3 Post transcriptional gene silencing in plants

Although translation inhibition by a small molecular weight RNA was first observed in barley (Gunnery *et al.*, 1987), PTGS pioneer work has been in petunia and initially called co-suppression. It was in fact first described when, trying to increase anthocyanin production in petunia by overexpression of the limiting biosynthetic enzyme, it was observed that mRNA levels of both transgene and endogenous gene were co-suppressed (Napoli *et al.*, 1990). PTGS is mediated mainly by two classes of small RNAs: microRNAs (miRNAs) and small interfering RNAs (siRNAs). They are both DICER-LIKE ribonucleases (DCL)-mediated cleavage products of double-strand RNA (dsRNA), originated either from hairpin-forming transcripts or by RNA-DEPENDENT RNA POLYMERASEs (RDRs) with the help of SUPPRESSOR OF GENE SILENCING 3 (SGS3) RNA-binding protein. The resulting 21-24 nucleotide dsRNAs are loaded into ARGONAUTE proteins, which are part of the RNA-induced silencing complex (RISC), and only one strand (guide strand) is kept. By sequence complementary with the target mRNA, the RISC mediates target cleavage and degradation, or translational repression (Borges *et al.*, 2015; Kamthan *et al.*, 2015). miRNAs act normally in *trans*, while siRNAs, with exception of tasiRNAs, in *cis*.

3.1 MicroRNAs (miRNAs)

Plant miRNAs biogenesis can be divided in 3 main stages: pri-miRNAs, pre-miRNAs, and mature miRNAs. pri-miRNAs are transcribed by RNA POLYMERASE II from *MIR* genes, and have a 5' 7-methylguanosine cap and a 3' polyadenosine tail; thanks to complementary sequences in the primary transcript, they form a stem-loop containing the sequence of the mature miRNA. pri-miRNAs are processed mostly by DCL1, which as a molecular ruler recognizes the stem-loop structure, and, in two catalytic cycles, are converted first into pre-miRNAs and then into mature miRNAs. Mature miRNAs are also stabilized at the 3' through 2'-*O*-methylation by the HUA ENHANCER 1 (HEN1) methyltransferase (Rogers *et al.*, 2013).

3.2 Small-interfering RNAs (siRNAs)

DCL2, DCL3, and DCL4 are responsible for siRNAs biogenesis from long dsRNAs. While all three DCLs can process any long dsRNAs, they have different affinity, and are involved in different processes: DCL3 is mainly involved in transcriptional gene silencing via methylation, and DCL2 and DCL4 in PTGS, producing secondary siRNAs, such as trans-acting

siRNAs (tasiRNAs), phased siRNAs (phasiRNAs), and epigenetically activated siRNAs (easiRNAs) (Borges *et al.*, 2015).

3.2.1 Trans acting small interfering RNAs (tasiRNAs)

Trans-acting small interfering RNAs (tasiRNAs) are generated from the *TAS* gene family, comprising at least 5 gene families (*TAS1* to *4*, *TAS6*) in Arabidopsis. *TAS* genes transcripts are recognized and cleaved by specific miRNAs; the product is then processed by RNA-DEPENDENT RNA POLYMERASE6 (RDR6) and the resulting double strand is cut by DICER-LIKE4 (DCL4). The generated 21-nucleotide tasiRNAs are loaded into ARGONAUTE (AGO) family proteins and regulate their RNA targets through the RNA-induced silencing complex (RISC) (Fei *et al.*, 2013). The *TAS3* family consists of 3 loci: *TAS3a*, *TAS3b*, and *TAS3c*. The functionality of *TAS3b* and *c* remains to be determined(Howell *et al.*, 2007). *TAS3* processing is unique because the miRNA responsible for its biogenesis (miR390) specifically interacts with one AGO member, AGO7, and because it's the only well-described TAS locus in Arabidopsis with 2 miRNA recognition sites (Fei *et al.*, 2013). Only the proximal 3' site is cleaved, while a mismatch in the 5' site prevent cleavage but is nonetheless necessary for tasiARFs biogenesis (Montgomery *et al.*, 2008). Interestingly, in other plant species the 5' site can be cleaved (in *Pinus taeda* and *Physcomitrella patens*) or can behave in both ways in different *TAS3* paralogs in spruce (*Picea abies*) (de Felippes *et al.*, 2017). AGO7 specificity for miR390 has been shown to be controlled through multiple checkpoints during RISC formation: the presence in miR390 of a 5' adenosine, the 3 nucleotide central region containing a conserved G-A mismatch (conserved in monocots and eudicots) between passenger and guide strand at position 11, and the cleavage of the passenger strand, all are required to specifically assemble RISC with miR390 (Endo *et al.*, 2013). Regarding the subcellular localization for tasiARFs biogenesis, it has been proposed that based on 1) ribosomal footprinting from purified membrane-bound polysomes of *TAS3* (Hou *et al.*, 2016; Li, Le*, et al.*, 2016), and 2) AGO7, RDR6, and SGS3 subcellular localization in cytoplasm and cytoplasmic membranous siRNA bodies (Jouannet *et al.*, 2012), tasiARFs biogenesis occurs on membrane-bound polysomes, presumably at the rough endoplasmic reticulum (Axtell, 2017).

In Arabidopsis, tasiRNAs target *ARF2*, *ARF3*, and *ARF4*, which control several developmental processes. tasiRNAs-mediated downregulation of *ARF3* and *ARF4* plays a role in morphogenesis and patterning of leaves and floral organs, and in juvenile-to-adult phase transition (Fahlgren *et al.*, 2006b; Garcia *et al.*, 2006). Furthermore, as described above, the tasiARFs pathway regulates lateral root formation. Control of leaf polarity and morphogenesis through this pathway has been reported in maize (*Zea mays*) (Douglas *et al.*,

2010) and *Medicago truncatula* (Zhou *et al.*, 2013), where it affects also lateral root and nodule development (Hobecker *et al.*, 2017). The tasiARFs pathway might have a role in somatic embryo development in *Dimocarpus longan* (Lin *et al.*, 2015).

The tasiARFs pathway is highly conserved in land plants, and it is present in the oldest land plants (liverworts); interestingly, in bryophyte, tasiRNAs target also *APETALA2* (Xia *et al.*, 2017). Using the moss *Physcomitrella patens* as model for a computational approach, it has been suggested that the conservation of the tasiARFs pathway and its involvement in so many different pathways derive from the pathway's proprieties of sensitivity and robustness to noise regarding auxin response (Plavskin *et al.*, 2016).

3.3 PTGS regulation of root development

3.3.1 Primary root growth and differentiation

Several miRNAs control primary growth. Root cap formation is influenced by the miR160-ARF10/ARF16 module, while root elongation by the miR160-ARF17 module. Root cap formation and root elongation are also regulated by the miR396-GROWTH-REGULATING FACTORS (GRFs)/PLETHORA (PLT) module. SCARECROW (SCR)/SHORTROOT (SHR)-mediated miR165/miR166 gradient, highest in the endodermis and lowest in the stele, regulates PHABULOSA (PHB), determining xylem differentiation (Stauffer *et al.*, 2014); the SCR/SHR-miR165/miR166-PHB module is also implicated in root elongation and control of meristem size. Regarding xylem differentiation, miR857-LACCASE7 module has been reported to control lignin content and secondary xylem differentiation (Couzigou *et al.*, 2016). Auxin-induced inhibition of primary root growth could be mediated by the tasiARFs pathway: *MIR390* expression in the meristematic zone of primary roots, contrary to lateral roots, is repressed by the synthetic auxin 1-naphthaleneacetic acid (Yoon *et al.*, 2014).

3.3.2 Lateral root development

3.3.2.1 The tasiARFs pathway and lateral root development

In Arabidopsis there are 2 *MIR390* loci, *MIR390A* and *MIR390B*, *MIR390A* being the main locus responsible for miR390 production in roots, where its abundance is regulated by auxin (Marin *et al.*, 2010). It has been shown that miR390, tasiARFs, and ARF2 to 4 define a regulatory network controlling lateral root development. miR390 is initially expressed in the mesenchymal cells of the stele, and extends into the pericycle during the first asymmetrical division. Its expression is then restricted at the base and flanks of the developing primordium by ARF4. Because *TAS3a* and *MIR390A* are only coexpressed in the central cylinder, they probably act non-cell-autonomously. *MIR390A* expression is also

positively regulated by ARF2 and ARF3 (Marin *et al.*, 2010). miR390-tasiARFs mediated degradation of *ARFs* mRNAs releases their inhibition of lateral root growth, promoting their elongation.

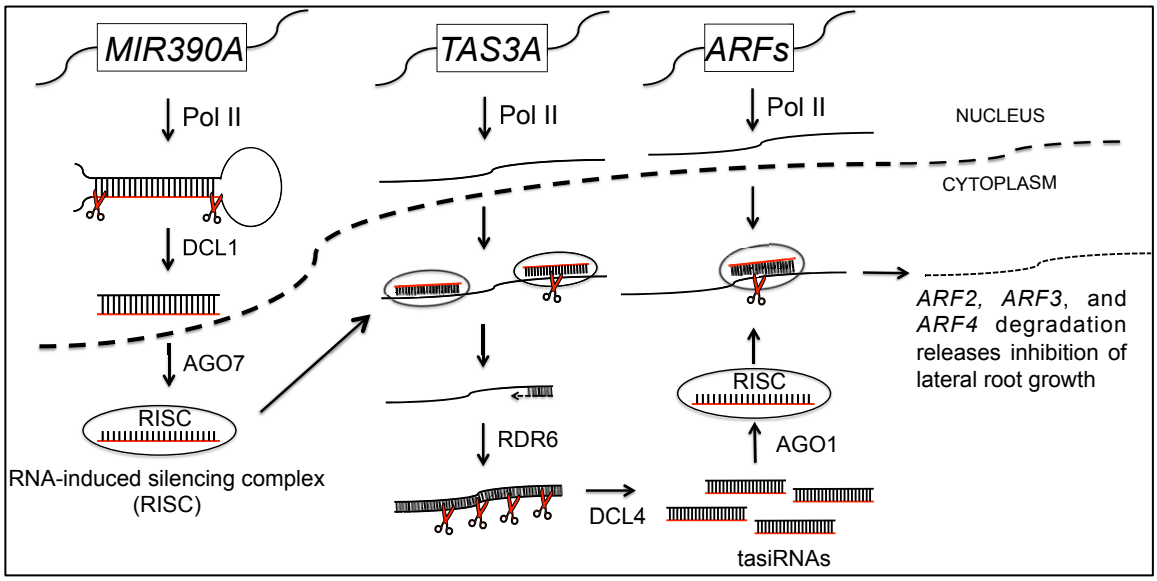

Figure 9. The tasiARFs pathway and its control of lateral root growth.

3.3.2.2 miR156/SPLs modules and lateral root development

It has been recently described that miR156/SQUAMOSA PROMOTER BINDING PROTEIN-LIKE (SPL) modules play a role in root system architecture (Yu *et al.*, 2015). miR156-mediated inhibition of *SPLs* transcription factors is involved in several developmental processes, such as juvenile-to-adult and vegetative-to-reproductive phase transitions (Shalom *et al.*, 2015). Regarding lateral root development, miR156 overexpression increases lateral root number, while overexpression of a target mimic as well as of cleavage-resistant targets reduces the number. *SPLs* and *MIR156* expressions increase after auxin treatment (Yu *et al.*, 2015).

3.3.2.3 Other miRNA pathways involved in LR development

There are several others miRNA controlling lateral root architecture: miR160 targets *ARF10*, *ARF16*, and *ARF17*, affecting root branching; miR164 targets *NAC1* transcription factor family (NAM, ATAF, CUC: NO APICAL MERISTEM, ARABIDOPSIS TRANSCRIPTION ACTIVATION FACTOR, CUP-SHAPED COTYLEDON), regulating lateral root initiation downstream of TIR1; miR393 targets *TIR1*, *AFB2*, and *AFB3*, and it modulates nitrate-induced root architecture changes; miR167 targets *IAA-Ala RESISTANT 3* (*IAR3*) to adapt root architecture to osmotic stress; miR847 targets *IAA28*, controlling lateral root

promotion. Most of these modules are affected by auxin, and are interconnected (Couzigou *et al.*, 2016).

3.4 PTGS regulation of embryo development

3.4.1 The tasiARFs pathway

The tasiARFs pathway has been implicated in the control of megaspore mother cell (MMC) numbers, restricting its formation to a single cell: tasiRNAs biogenesis is promoted by TEX1, a component of the TREX (TRanscription-EXport), to downregulate ARF3 specifically in the ovule primordia (Su *et al.*, 2017). Furthermore, miR390 has been reported by *in situ* hybridization in the filiform apparatus of the synergids in ovules, and in shoot and root apical meristems in embryos (Dastidar *et al.*, 2016).

3.4.2 Other miRNA pathways involved in embryo development

Although more than 400 miRNAs are present in embryo, only to few of them a function has been assigned: miR164 targets CUP-SHAPED COTYLEDON1 (CUC1) and CUC2 to control cotyledon separation and shoot apical meristem (SAM) formation. The SAM is also regulated by miR394 repression of LEAF CURLING RESPONSIVENESS, and by miR165/166 repression of Homeodomain-Leucine zipper III genes. The latter modules promote also vascular and adaxial fates. Finally, miR160 targets ARF10 and ARF16, controlling root cap differentiation (Seefried *et al.*, 2014).

Aims of the thesis

The tasiARFs pathway is highly conserved in higher plants and its involved in many biological processes, modulating the response of the major phytohormone auxin. However, despite its importance, many aspects of this pathway are still unknown. In this thesis we wanted to address 4 open questions:

1 Is AT1G75860, a gene of unknown function, required for *MIR390A* expression in the primary root tip?

MIR390A, the main locus responsible for miR390 production in roots, is a key component of the tasiARFs pathway, but its regulation is not yet fully understood. This first question aims to test if AT1G75860, a gene of unknown function, is required for *MIR390A* expression in the primary root tip.

2 What is the role of the tasiARFs pathway in primary root development?

miR390 is highly expressed in the primary root tip, but its function there is still unknown. This second question aims to unravel the role of the tasiARFs pathway in primary root development

3 Do the tasiARFs pathway and miR156/SPLs module interact during lateral root development?

The tasiARFs pathway controls lateral root development, but it is not the only miRNA pathway involved in this process. In this thesis, we tested if it interacts with another pathway, the miR156/SPLs, that also controls lateral root development.

4 What is the role of the tasiARFs pathway in embryo development?

miR390 expression has been reported in the embryo, but so far no function in this stage of the plant could be associated with the tasiARFs pathway. This last question addresses this gap in our knowledge and aims to uncover a possible role for this pathway in embryo development.

Results

1 Is AT1G75860, a gene of unknown function, required for *MIR390A* expression in the primary root tip?

1.1 Context of the study

To better understand how expression of *MIR390A* is controlled, an ethyl methanesulfonate (EMS) mutagenesis screening was previously performed in our lab (Dastidar, 2015). The screen relies on Col-0 plants expressing a reporter for *MIR390A* expression (*MIR390A:GUS-GFP*). This reporter consists of a 2.5Kb long fragment of the *MIR390A* promoter (AT2G38325) promoter driving the expression of two reporters, E. Coli beta-glucuronidase gene (*GUS*) and green fluorescent protein (*GFP*). This reporter line will be referred in this study as AM539. These plants present GUS staining in the primary root tip and in the lateral root primordia, consistent with the expression profile of the endogenous miR390 obtained by *in situ* hybridization (this thesis, Figure 1-13, and Dastidar, 2015). This reporter line was EMS mutagenized and the progeny was screened for alterations in the expression of the reporters. At the M3 generation 22 candidates were confirmed: 7 with no expression in the primary root tip, 8 with reduced expression, and 7 with enhanced expression. All the candidates showed smaller primary root than the parental. Further characterization of those candidates lead to select the mutant called P5-40. *In situ* hybridization and northern blot analysis showed that, in P5-40, miR390 levels in the primary root tip are significantly lower than in the parental line (Figure 1-1).

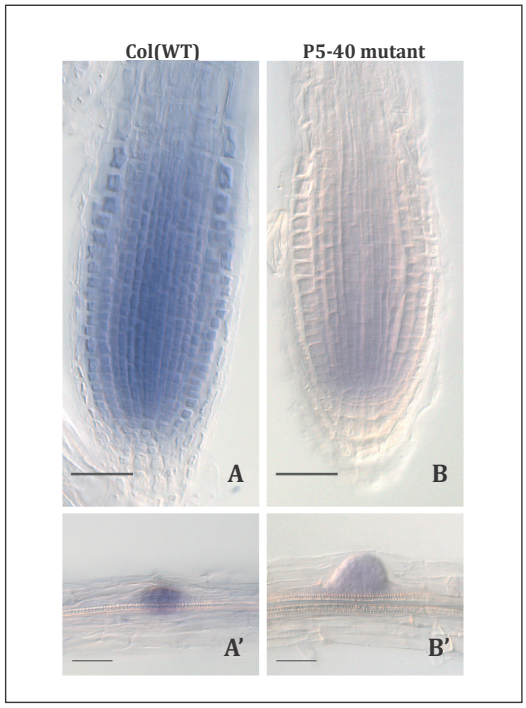

Figure 1-1. The expression pattern and abundance of endogenous miR390 was checked in P5-40 mutant and Col-0 (WT) by in-situ hybridization on whole mounts of 7 days old seedlings. (A) Strong signals for expression of miR390 at the primary root and (A') at the lateral root primordia could be detected in Col-0 (Wt) plants. (B) Very weak signals were detected both at the primary root and (B') at the lateral root primordia in P5-40 mutants. Scale bar 50μm. From (Dastidar, 2015).

The F2 population, derived from a backcross of the candidate P5-40, showed that lack of reporter expression and smaller primary root are independent traits. Next generation genome re-sequencing followed by SNP analysis of three populations (parental, backcross F2 with and without reporter expression) identified a SNP (T->C) in the coding region of AT1G75860, a gene of unknown function, causing a missense mutation (Gly/Glu) and linked with the P5-40 candidate (showing no expression of the reporter) (Dastidar, 2015). This gene (AT1G75860) of unknown function will be referred in this study as *GEORGE* (*GRG*). A *in silico* characterization of *GRG* (TAIR, PPDB, SUBA, UniProtKB) shows that this 1823 bp long gene (2 introns), expressed in most tissues and during most developmental stages, codes for a 297 amino acids (AA) protein of about 33 kDa. This predicted protein, according to automatic assertions inferred from database entries, is a DNA ligase with a 28 AA long coiled coil (positions 36 to 63), nuclearly localized. *GRG* has homologs in Arabidopsis (AT1G20100) and angiosperms.

In this section, a link between a missense mutation in *GRG* and *MIR390A* misexpression in the primary root tip is investigated.

1.2 Characterization of P5-40 and GRG

Because P5-40 is a still superficially characterized EMS mutant (Dastidar, 2015) and *GRG* has no known function, the first step has been to acquire basic information about them.

Regarding P5-40, it was investigated if its phenotype is dominant or recessive, what kind of genetic relationship it has with other yet unmapped EMS candidates and if these have also mutations in *GRG* genomic region, and if the missense mutation affects the expression of neighboring genes.

Regarding *GRG*, its subcellular localization and expression profile were explored.

1.2.1 P5-40 is a recessive mutant

P5-40 has been selected according to its phenotype and because its missense mutation was mapped in a coding sequence, but its characterization is still missing. Therefore, in order to obtain basic genetic information about its dominance and its relationship with other 3 EMS unmapped candidates (P14-6, P2-23, P5-19) that also showed no expression in the primary root tip, an allelism test was performed; GUS staining on the F1 in the primary root tip was used as readout (Figure 1-2).

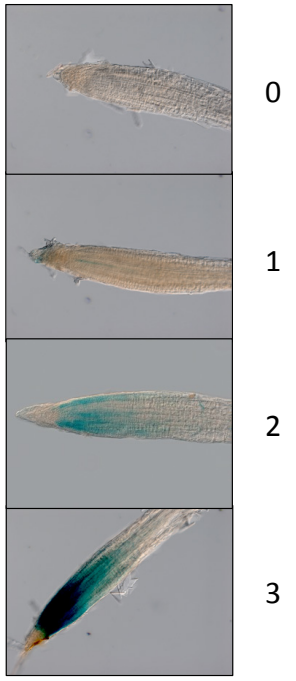

♀ \ ♂	Col-0	P5-40	P14-6	P2-23	P5-19
Col-0		3	2	1	1
P5-40	3		0	0	0
P14-6	1	0		1	n/a
P2-23	0	0	0		0
P5-19	0	0	0	0	

Figure 1-2. EMS mutants allelism test. 0, no GUS signal; 1, very faint GUS signal; 2, faint GUS signal; 3 GUS signal as in the unmutagenized reporter line *MIR390A:GUS-GFP*

By crossing each candidate with Col-0 and with all the others, in both parental directions (male/female), it was observed that P5-40 was the only recessive mutant, restoring the GUS signal in the primary root tip (as in the unmutagenized reporter line *MIR390A:GUS-GFP)* when crossed with Col-0. A genetic relationship with the other candidates could not be established, because they were all dominants.

1.2.2 Expression of GRG and flanking genes does not change in EMS mutants

GRG (AT1G75860) function is unknown, and there is no experimental data regarding the predicted protein it might code. *GRG* is flanked by 2 other genes: *VPS35B* at the 5' (AT1G75850) and AT1G75870 at the 3' (Figure 1-3), the last been also uncharacterized.

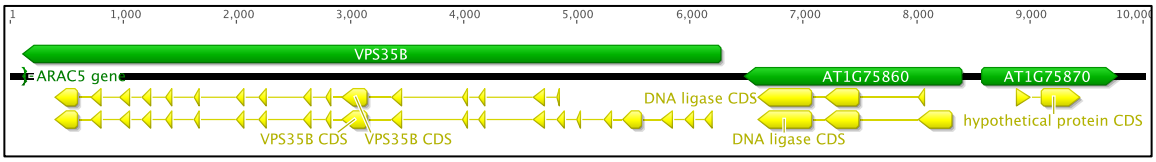

Figure 1-3. *GRG* genomic region.

Because 1) there is still uncertainty regarding *GRG* and AT1G75870 annotations, 2) *GRG* overlaps *VPS35B* promoter, and 3) only P5-40 mutation has been mapped, to check how the expression of those 3 genes is affected in P5-40 and in the other 3 EMS lines, a semi-quantitative PCR was performed (Figure 1-4).

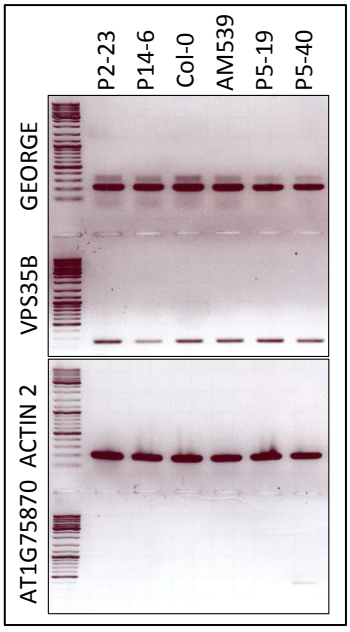

Figure 1-4. Semi-qPCR for *GRG*, *VPS35B*, and AT1G75870.
ACTIN2 was used as reference. Ladder: Thermo Scientific™ O'GeneRuler DNA Ladder Mix, Ready-to-Use 100-10,000 bp

No difference in expression levels could be observed compared to the unmutagenized reporter line AM539, furthermore, the 3 gene expression levels were consistent with the AtGenExpress expression atlas (*VPS35B* and *GRG* are expressed in roots while AT1G75870 is not). Based on these evidences, the missense mutation in P5-40 and the unmapped mutations in the other 3 EMS mutants, do not affect the expression of *GRG* and its neighboring genes.

1.2.3 VPS35B bears no mutations in EMS mutants

P5-40 miss-sense mutation was mapped by BC and NGS. To check if the mapping missed possible EMS-generated mutations in *VPS35B*, the gene was re-sequenced in AM539, P5-40 and in the other 3 EMS mutants. Because *VPS35B* is around 6 kb and the average sequencing length is around 800 bp, the gene was first PCR amplified in 3 fragments around 2 kb and then the individual fragments were sequenced (Figure 1-5).

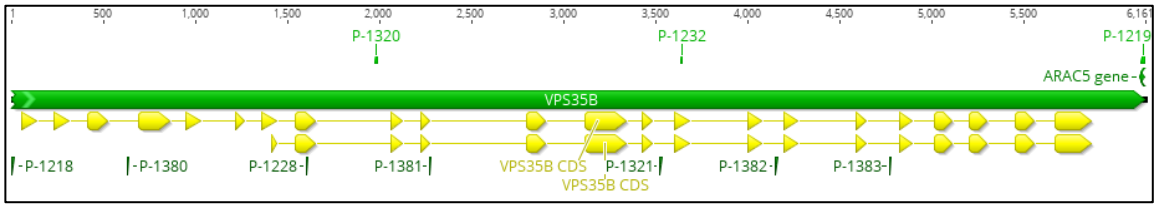

Figure 1-5. Primer setup to sequence *VPS35B*. Fragment I was amplified using P-1218 and P-1320; the following primers were used for sequencing fragment I: P-1218, P-1320, and P-1380. Fragment II was amplified using P-1228 and P-1232; the following primers were used for sequencing fragment II: P-1228, P-1381, and P-1232. Fragment III was amplified using P-1321 and P-1219; the following primers were used for sequencing fragment III: P-1321, P-1219, P-1382, and P-1383.

For every mutant and for AM539, the resulting contigs were first assembled into a consensus, and this was compared to the Araport11 Col-0 Genome Annotation (06/2016 BioProject PRJNA10719) (Figure 1-6).

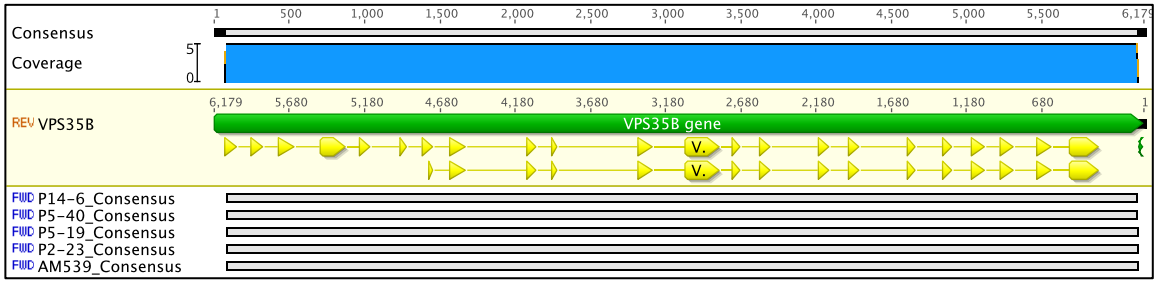

Figure 1-6. Comparison of the consensuses for AM539 and EMS mutants to the Col-0 genome annotation of *VPS35B*.

The results of the sequencing allow discarding the presence of mutations in *VPS35B* and in the other 3 EMS mutants. These evidences, together with no changes in *VPS35B* expression in the mutants (Figure 1-4), rule out this gene involvement in the lack of *MIR390A* expression in the primary root tip.

1.2.4 GRG is a nuclear protein ubiquitously expressed

To have a preliminary idea of *GRG* function, its subcellular localization and tissue expression pattern was analyzed by using fluorescent reporters. By GreenGate based cloning (Lampropoulos *et al.*, 2013), the available C-module containing *GRG* CDS plus introns (generated by Mouli G. Dastidar) was combined to obtain the final construct *UBQ10:HA-GRG-GFP. GRG* subcellular localization was tested by transient tobacco infiltration and confocal microscopy (Figure 1-7).

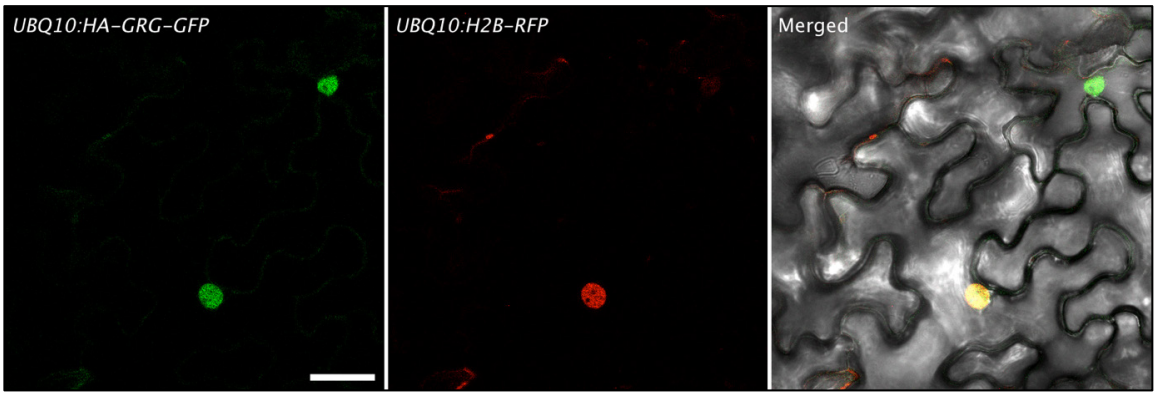

Figure 1-7. *GRG* subcellular localization by tobacco transient infiltration. In merged, GFP, RFP, and brightfield channels were merged. Scale bar: 20 µm.

GRG is nuclearly localized as it co-localizes with the co-infiltrated *UBQ10:H2B-RFP* nuclear marker.

GRG expression pattern was tested transforming a *GRG:H2B-GFP* cassette (created by GreenGate) in Col-0 and detecting the GFP fluorescence with epifluorescence and confocal microscopy. Several T1 lines were screened under stereomicroscope, and the line presenting the most common expression pattern and the highest expression was chosen for confocal microscopy (Figure 1-8,Figure 1-9).

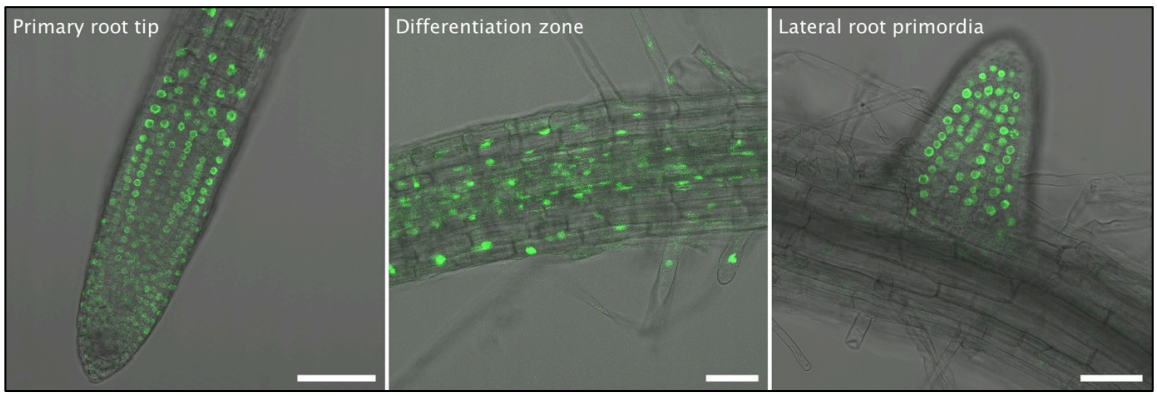

Figure 1-8. *GRG* expression pattern in roots. Merge of GFP and brightfield channels. Scale bar: 50 µm

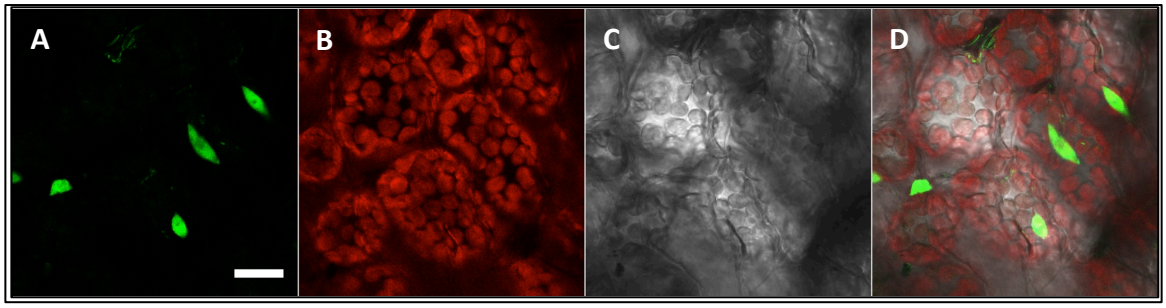

Figure 1-9. *GRG* expression pattern in palisade mesophyll cells. A: GPP channel. B: chloroplasts autofluorescence. C: bright field. D: merge of A, B, and C. Scale bar: 20 µm.

GRG is ubiquitously expressed in roots and in palisade mesophyll cells.

The experimental results agree with and confirm the bioinformatics predictions of *GRG* as a nuclear protein ubiquitously expressed.

1.3 Is P5-40 a *GRG* allele?

To test if P5-40 is a *GRG* allele, 4 main approaches were carried:

1. Allelism test between P5-40 and T-DNA insertions in *GRG*.
2. Introduction of the *MIR390A* reporter in *GRG* loss of function alleles.
3. Complementation of P5-40 molecular phenotype (loss of *MIR390A* expression in the primary root tip) by expressing *GRG* (genomic region or CDS).
4. Linkage of P5-40 phenotype to the mapped polymorphism in *GRG* (T->C) after more rounds of backcross (to clean P5-40 from other EMS-generated mutations)

1.3.1 Identification and analysis of GRG knock down alleles

1.3.1.1 Identification of T-DNA alleles for *GRG* and *BOG*

For the allelism test, 2 T-DNA insertion lines for *GRG* were identified in the stock centers: the Salk T-DNA Homozygous Line SALK_025523C and the GABI-KAT GK-839D07. Both lines carry the insertion in the first intron. Because *GRG* has a homologous gene (AT1G20100,

76% homology according to WU-BLAST 2.0), also of unknown function and called in this study *BROTHER OF GEORGE* (*BOG*), a *BOG T*-DNA insertion line was also identified (SAIL_97_B11; T-DNA inserted in the last exon).

GRG and *BOG* T-DNA lines were first genotyped to obtain homozygous lines (Figure 1-10).

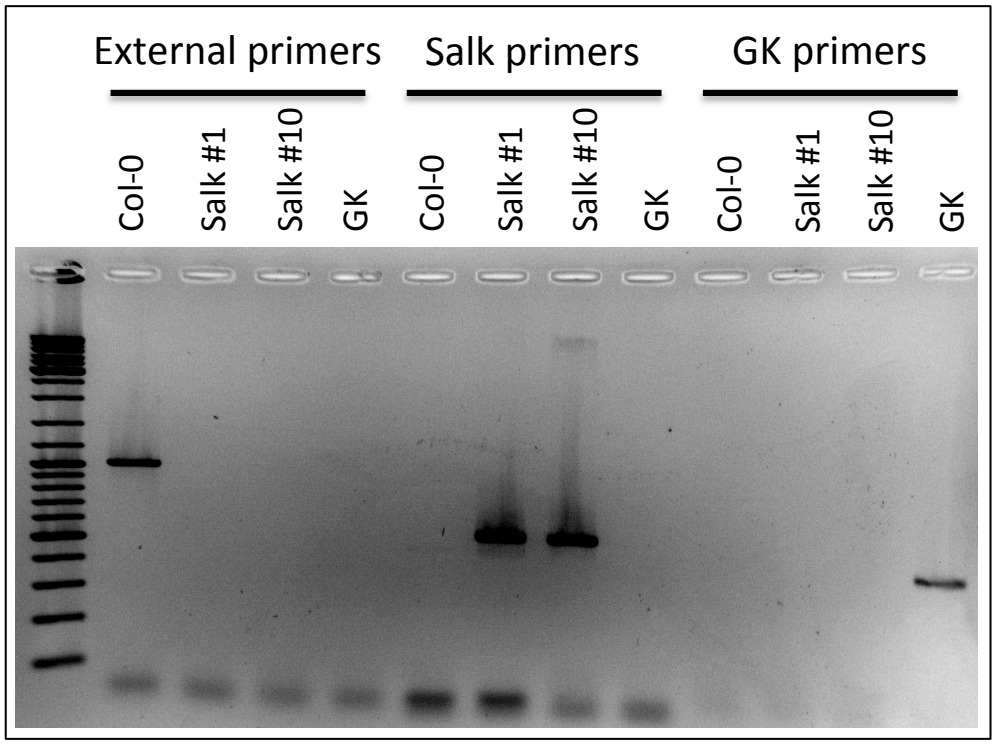

Figure 1-10. Genotyping of *GRG* T-DNA lines. External primers: LP + RP; Salk primers: LBb1 + RP; GK primers: o8409 + RP. Salk: SALK_025523C; GK: GK-839D07. Ladder: Thermo Scientific™ O'GeneRuler DNA Ladder Mix, Ready-to-Use 100-10,000 bp

1.3.1.2 In Salk and GK GRG T-DNA lines, GRG is less expressed than in Wt and it is not affected by IAA or NPA treatment.

To test if *GRG* expression is reduced in the T-DNA lines, RT-qPCR in seedling roots was performed. Because miR390 levels increase after IAA treatment (Marin *et al.*, 2010), and the scope of this section is to test if *GRG* is required for *MIR390A* expression in the primary root tip, plants were grown according to the lateral root induction system (Marin *et al.*, 2010) and also miR390 levels were tested; *mir390a-2* T-DNA line (Marin *et al.*, 2010) was included as negative control. P5-40 was also included to compare its miR390 expression profiles (Figure 1-11).

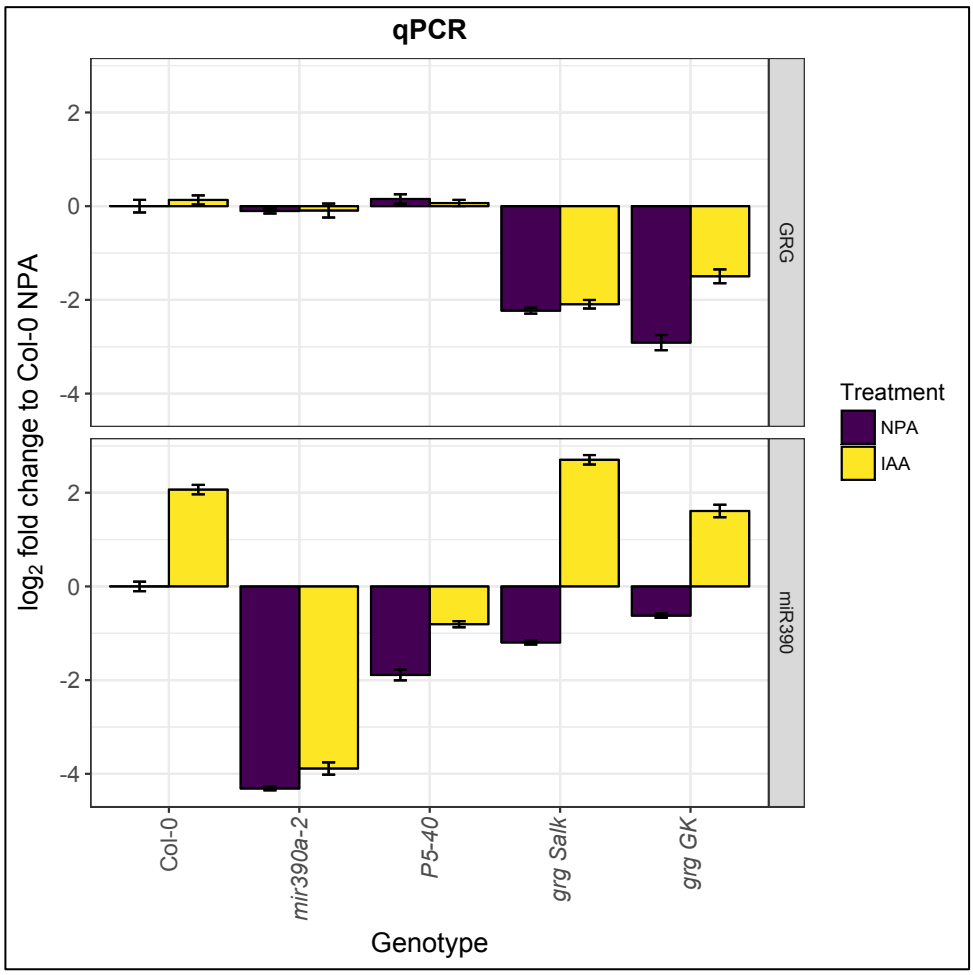

Figure 1-11. qPCR for *GRG* and miR390. Col-0 NPA is set as reference. Salk: SALK_025523C; GK: GK-839D07. NPA: 48h 10 µM NPA. IAA: 24h 10 µM NPA then 24h 10 µM IAA. *PP2AA3* (AT1G13320) was used as reference. Error bar: standard error of the mean.

GRG T-DNA lines behaves as expected: in both lines *GRG* expression was reduced regardless of treatment; compared to Wt, in the T-DNA lines and in P5-40, miR390 levels are reduced upon NPA treatment, but, while in the T-DNA lines the IAA response remains, in P5-40 the IAA-mediated induction is reduced.

The results of the qPCR show that both T-DNA lines are knockdown for *GRG* and are therefore suitable alleles; furthermore, their reduction in the untreated miR390 levels, especially in the Salk line, support a role for *GRG* in controlling *MIR390A* expression.

1.3.1.3 In BOG T-DNA line, BOG levels are the same as in Col-0

BOG levels in *BOG* T-DNA line were checked by semi-qPCR (Figure 1-12):

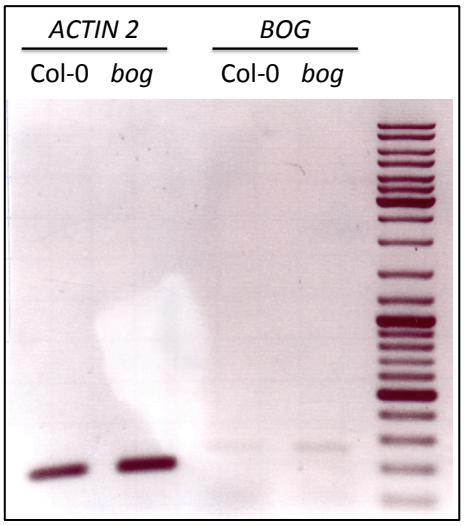

Figure 1-12. Semi-qPCR for *BOG*. *ACTIN 2* was used as reference. *bog:* SAIL_97_B11. Ladder: Thermo Scientific™ O'GeneRuler DNA Ladder Mix, Ready-to-Use 100-10,000 bp.

Because *BOG* levels in *BOG* T-DNA are the same as in Col-0, the line was not used in this study.

1.3.1.4 amiRNAs against *GRG*, *BOG*, and both gave inconsistent results

Because *BOG* T-DNA line showed no *GRG* expression difference compared to Wt, and to obtain more *GRG* knock-down alleles, artificial miRNAs against *GRG*, *BOG*, and both (3 independent miRNA for each) were cloned and tested in tobacco by transient co-infiltration with *UBQ10:GRG-GFP, UBQ10:BOG-GFP*, or both (*UBQ10:H2B-RFP* was also co-infiltrated as reference). Fluorescence was measured after protein extraction of the infiltrated disk by plate reader. No suitable amiRNA cassette was identified because the fluorescence measurements were inconsistent.

1.3.1.5 In GRG Salk T-DNA line, miR390 is not expressed in primary root tip but in GK is

To test if defects in P5-40 and in *GRG* lead to the same molecular phenotype (absence of miR390 in the primary root tip), miR390 levels were tested in *GRG* T-DNA lines by ISH (Figure 1-13).

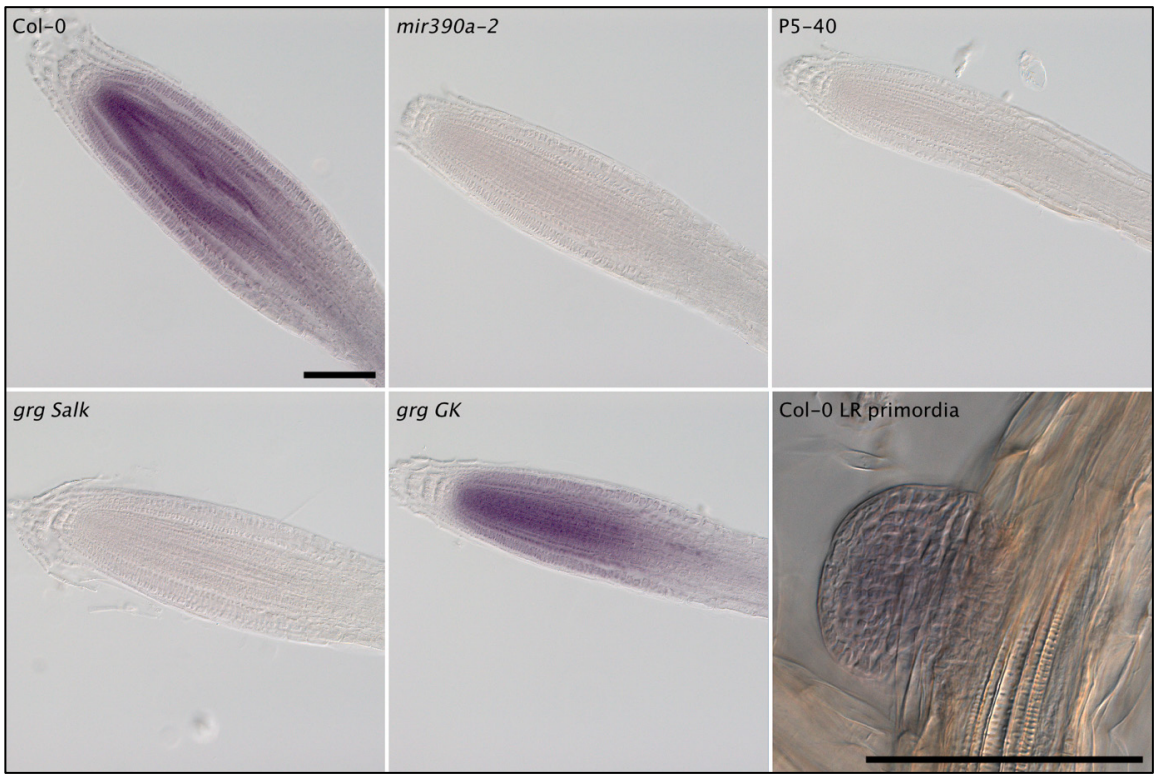

Figure 1-13. ISH at miR390. *grg* Salk: SALK_025523C; *grg* GK: GK-839D07. LR: lateral root. Scale bar: 100 µm

While negative controls (*mir390a-2* and P5-40) showed absence of signal, as well as *GRG* Salk T-DNA line, in *GRG* GK T-DNA line, miR390 was detected in the PR tip, as in the Wt positive control.

1.3.1.6 Expression of GRG flanking genes does not change in GRG Salk T-DNA and P5-40

To test if the mutation (P5-40) or the T-DNA insertion (Salk T-DNA line) in *GRG* affects the expression of its flanking genes (AT1G75870 and VPS35B), a semi-qPCR was performed (Figure 1-14).

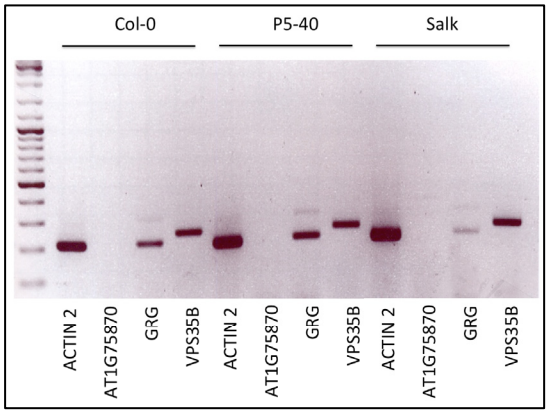

Figure 1-14. Semi-qPCR for *GRG* and flanking genes. *ACTIN 2* was used as reference. Salk: SALK_025523C. Ladder: Thermo Scientific™ O'GeneRuler DNA Ladder Mix, Ready-to-Use 100-10,000 bp.

The mutation or the T-DNA insertion in *GRG* has no effect on the expression of flanking genes. In the Salk T-DNA line, the expected reduction of *GRG* levels was observed.

1.3.2 P5-40 is a GRG allele

To check if P5-40 is *GRG* allele, P5-40 was crossed in both direction (male/female) with either Col-0 or *GRG* T-DNA lines. GUS staining on the F1 in the primary root tip was used as readout (Figure 1-15).

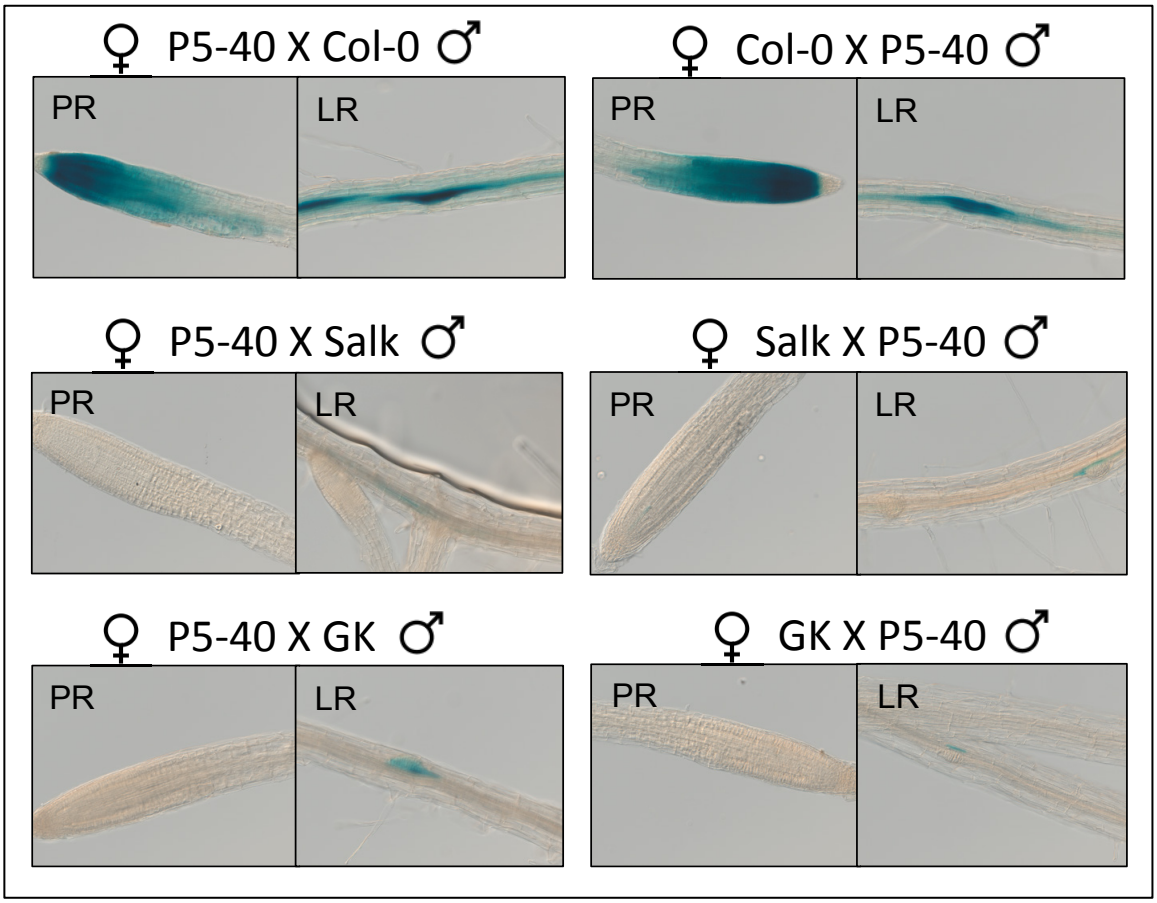

Figure 1-15. P5-40 allelism test by GUS staining in F1. PR: primary root; LR: lateral root. Salk: SALK_025523C; GK: GK-839D07.

The allelism test indicates that P5-40 is a *GRG* allele: when P5-40 was crossed with Col-0, the GUS signal in the primary root tip was restored as expected for a recessive mutant (Figure 1-2), while when crossed with T-DNA lines no GUS signal was observed. GUS expression in the lateral roots was use as control to verify that crosses and GUS reaction were successful.

1.3.3 Introduction of MIR390A (MIR390A:GUS-GFP) reporter in GRG loss of function alleles

If P5-40 is a *GRG* loss of function allele, introducing the *MIR390A* reporter (*MIR390A:GUS-GFP*) in *GRG* loss of function alleles (Salk and GK T-DNA lines) should yield the same molecular phenotype (absence of GUS signal in the primary root tip).

A new *MIR390A* reporter (*MIR390A:GFP-GUS-NLS*) was created because the original reporter used for the EMS screening (*MIR390A:GUS-GFP*) has the same resistance (kanamycin) as the Salk T-DNA line. Salk *GRG* T-DNA line was transformed with this new construct, while GK *GRG* T-DNA line and Col-0 (used as control) were transformed with the original reporter. Several T1 seedlings for every genotype were then GUS stained, and the presence and location of the GUS signal were recorded (Figure 1-16).

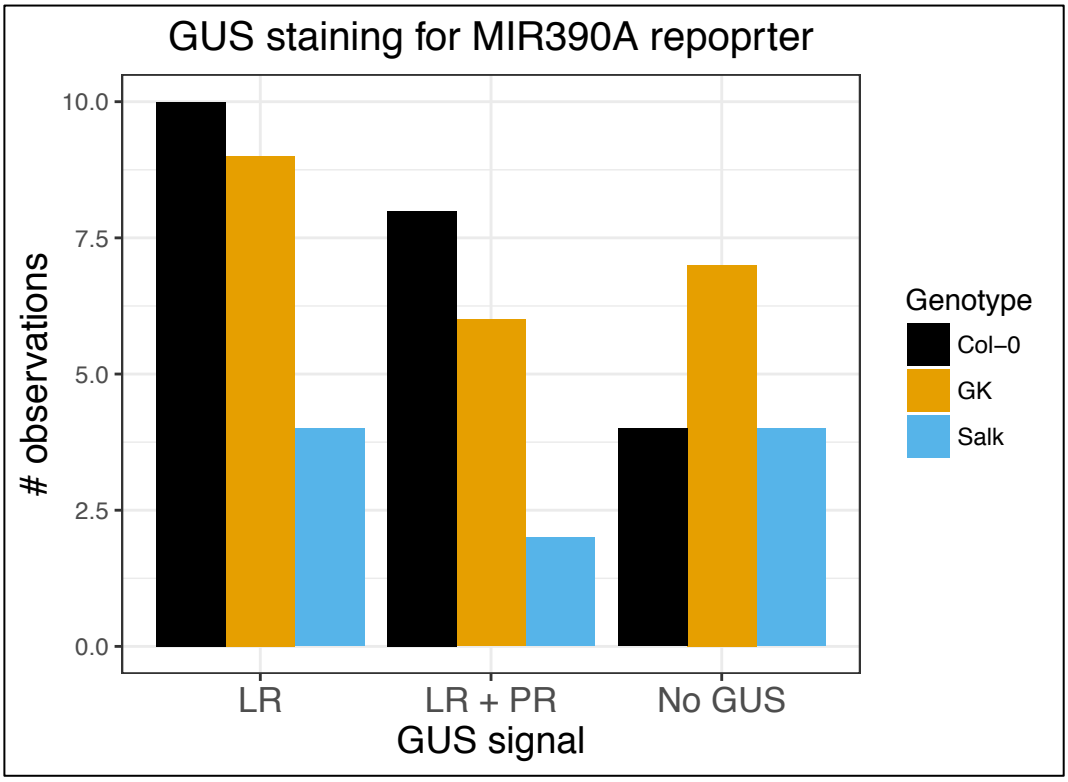

Figure 1-16. Observed GUS signal for *MI390A* reporter in T1 roots. LR: lateral root, PR: primary root, No GUS: GUS signal was absent. Col-0: *MIR390A:GUS-GFP* in Col-0 background, GK: *MIR390A:GUS-GFP* in GK-839D07 background, Salk: *MIR390A:GFP-GUS-NLS* in SALK_025523C.

The high proportion of T1 *MIR390A:GUS-GFP* in Col-0 background showing the same molecular phenotype as P5-40 (GUS signal only in lateral roots) does not allowed to draw any conclusion about the expression pattern of T1 *GRG* T-DNA lines (which anyway show no clear pattern).

1.3.4 P5-40 complementation by GRG

Another strategy to test if P5-40 is a *GRG* allele was to complement P5-40 with *GRG*. P5-40 plants were transformed either with *GRG* genomic region or with *GRG* CDS plus introns. For the genomic region, 2.1 or 4.5 kb fragments were chosen, with 146 or 554 bp terminator. In the case of constructs based on pMLBart, the empty vector was used as control. For the CDS plus intron, it was driven either by *UBQ10* promoter or by 2.1 kb *GRG* promoter. Several T1 plants for each construct were GUS stained and the presence and location of the GUS signal were recorded. A line was deemed complemented if the GUS signal in the primary root tip was restored (Table 1-1).

Table 1-1. P5-40 complementation by *GRG*. *GRG* cassette: *GRG* cassette used for P5-40 transformation. Cloning method: cloning system used to generate *GRG* cassette. Complemented: a line was deemed complemented if the GUS signal in the primary root tip was restored; in brackets, the number of complemented T1 vs. the total number is shown.

***GRG* cassette**	**Cloning system**	**Complemented T1**
2.1 kb *GRG* genomic region (146 bp terminator)	pMLBart	(0/22)
4.5 kb *GRG* genomic region (146 bp terminator)	pMLBart	(0/20)
2.1 kb *GRG* genomic region (554 bp terminator)	GreenGate	(0/6)
UBQ10:HA-GRG-GFP	GreenGate	(0/9)
GRG:GRG-GFP	GreenGate	(0/7)

Regardless of the cassette used, no complementation was observed.

1.3.5 Linkage between the P5-40 phenotype and the mutation in GRG

The last strategy was to check if the linkage between P5-40 phenotype (loss of *MIR390A* expression in the primary root tip) and *GRG* mutation (C/T) after several additional rounds of backcross (to clean P5-40 from other EMS-generated mutations) was still present

1.3.5.1 Identification of a stable line after 3 round of backcross

After 3 round of backcross with the unmutagenized reporter (AM539), choosing the absence of GUS signal in the primary root tip (P5-40 molecular phenotype) in F2 as criteria to move to the next round of backcross, a F3 line showing a homozygous P5-40 molecular phenotype was chosen (P5-40 BC3 F3) (Figure 1-17).

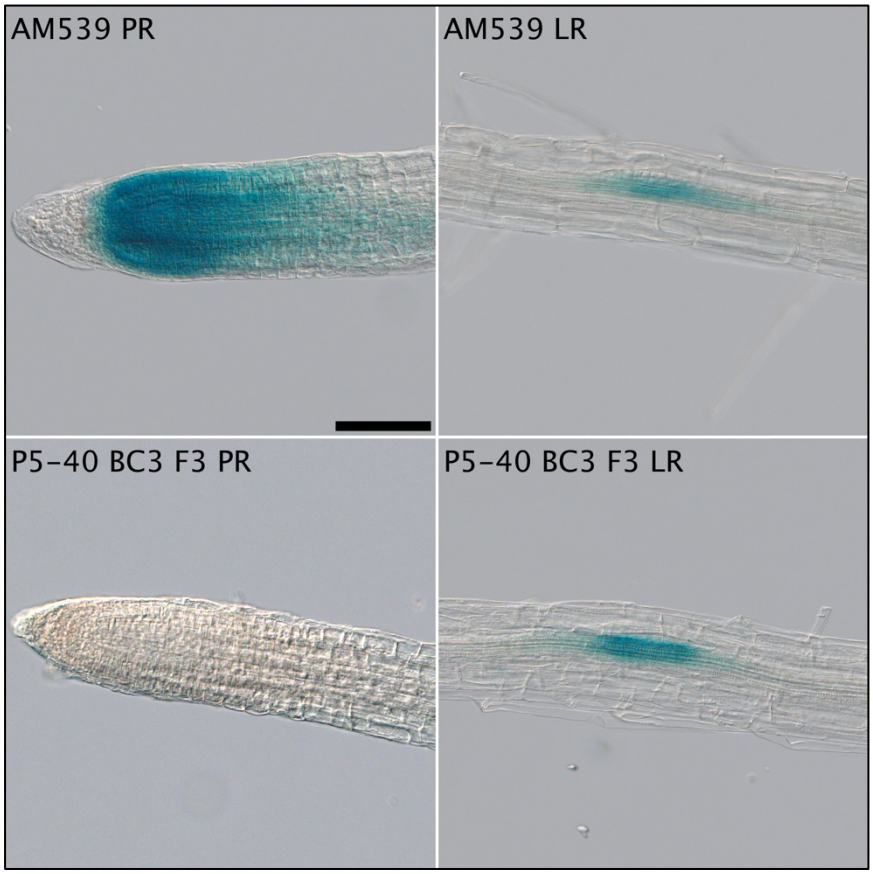

Figure 1-17. GUS staining of P5-40 BC3 F3. AM539 (*MIR390A:GUS-GFP*) was used as control. P5-40 BC3 F3 shows absence of GUS signal in the primary root in 78/78 cases. PR: primary root. LR: lateral root. Scale bar: 100 µm.

1.3.5.2 Genotyping of P5-40 BC3 F3 shows no link between *GRG* mutation and molecular phenotype

To genotype P5-40 BC3 F3, a 501 bp fragment containing P5-40 SNP (T->C) was first PCR-amplified and then digested with Eco130I (CC^WWGG), which uniquely recognizes the sequence containing P-50 SNP (**C**CAAGG in Wt and **T**CAAGG in P5-40). Therefore, in Wt, Eco310I can cut, and the 2 fragments (208 and 297 bp, respectively) can be easily separated on an agarose gel, while, in P5-40, it cannot cut. 10 seedlings of the homozygous P5-40 BC3 F3 line were genotyped using the above-described method (Figure 1-18).

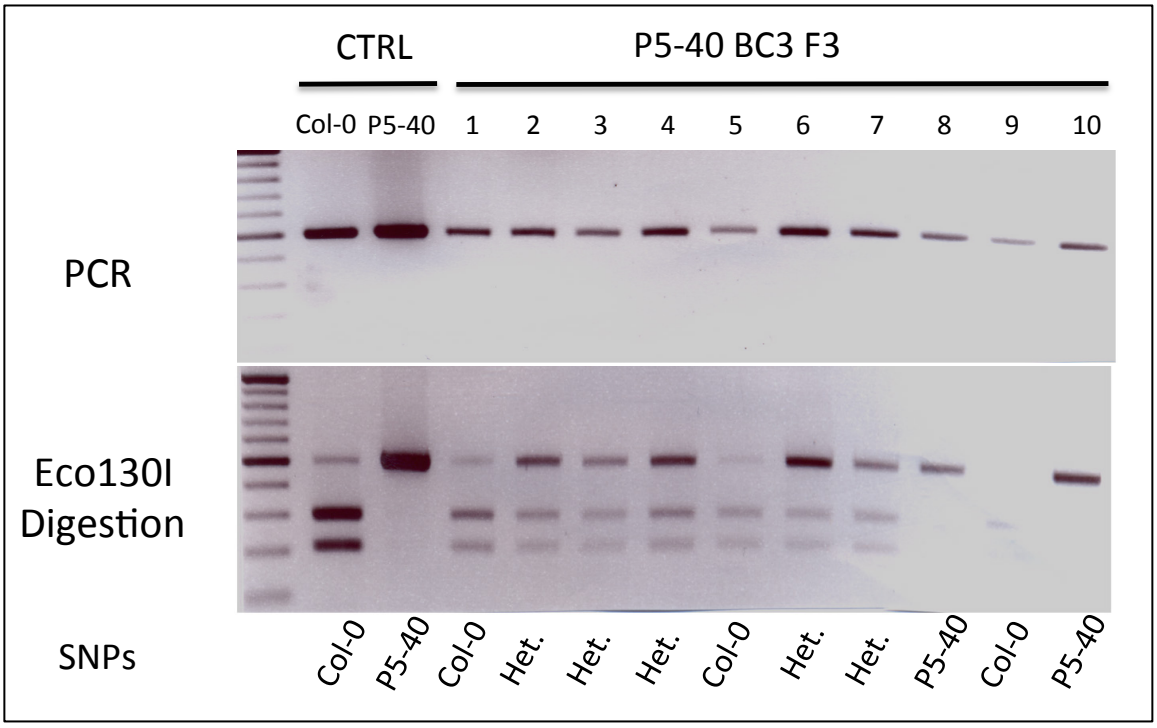

Figure 1-18. Genotyping of P5-40 BC3 F3. CTRL: controls. 1->10: individual P5-40 BC3 F3 seedlings. Het. Heterozygous. Ladder: Thermo Scientific™ O'GeneRuler DNA Ladder Mix, Ready-to-Use 100-10,000 bp.

The 10 seedlings were a mix of homozygous Wt or P5-40 SNPs, as well as heterozygous. Therefore there is no correlation between the presence of the mutation in *GRG* and the phenotype of P5-40, and the mutation in P5-40 cannot be associated with the phenotype. This result suggests that other gene(s) might be involved in the regulation of *MIR390A* expression.

1.4 Discussion

The experiments performed to link *GRG* EMS-induced missense mutation or knockdown T-DNA insertions to a lack of *MIR390A* expression (detected by GUS) or to a lack of mature miR390 presence (detected by ISH) in the primary root tip yielded contradictory results (Table 1-2).

Table 1-2. Summary of the experiments and of the respective results performed to link GRG EMS-derived miss-sense mutation or knockdown T-DNA insertions to a lack of MIR390A expression (detected by GUS) or to a lack of mature miR390 presence (detected by ISH) in the primary root tip.

Experiment	Results support the hypothesis
Allelism test between P5-40 and T-DNA insertions in GRG	YES
Introduction of the *MIR390A* reporter in *GRG* loss of function alleles	NO
Complementation of the P5-40 phenotype by expressing *GRG* (genomic region or CDS).	NO
Linkage of P5-40 phenotype to the mapped polymorphism in *GRG* (T->C) after more rounds of backcross	NO

Drawing any solid conclusion regarding the experiments performed with the non-backcrossed P5-40 EMS mutant is difficult, because of the possible presence of other EMS-generated mutations. It has been calculated that there are at least 700 mutations in each EMS-mutagenized plant (Jander *et al.*, 2003), so three to six round of backcross should be performed to reasonably "clean" the genome. This problem can be especially appreciated when, after 3 round of backcross, P5-40 still showed the molecular phenotype, but lost the original mutation in *GRG* (Figure 1-18).

A second problem arises from the *MIR390A:GUS-GFP* reporter. When the reporter was transformed in Col-0 as control in the experiment performed to introduce the reporter in *GRG* T-DNA lines, *MIR390A* expression pattern was, in the majority of T1 lines, the same as in P5-40 (Figure 1-16). Furthermore, these two problems combined when trying to complement P5-40 (Table 1-1) or in the P5-40 allelism test (Figure 1-15); and, while a lack of complementation is not particularly surprising, the allelism test results were not in agreement with the results from *GRG* T-DNA lines ISH at miR390 (Figure 1-13): in the allelism test, both *GRG* T-DNA lines (Salk and GK) seemed to be allelic to P5-40, but by ISH only the Salk line showed absence of mature miR390 in the primary root tip.

In light of these two problems, and because for the backcross only the P5-40 molecular phenotype but not the genotype (the P5-40 miss-sense mutation) was selected for, is also

not especially unexpected that P5-40, after 3 rounds of backcross, showed the molecular phenotype but not the miss-sense mutation.

Also, the presence in Arabidopsis of a *GRG* homologous, *BOG*, for which no knockout or knockdown line could be identified, complicates further the picture.

Nonetheless, despite all these negative premises, it seems reasonable to conclude that it would be worthy to further investigate *GRG* role in the control of *MIR390A* expression in the primary root tip. However, to draw more solid conclusions, finding a more reliable *MIR390A* reporter should be a priority. Another hypothesis is that the reporter itself was reliable but its expression was affected by the antibiotic selection in T1 (although prior to GUS staining seedlings were recovered few days in non-antibiotic media), a issue which would involve not only the insertion of the reporter in *GRG* T-DNA lines, but also their (and P5-40) complementation.

Also, it would be important to obtain loss-of-function lines for *BOG* to eventually create a *grg bog* double mutant. Testing artificial miRNAs lines against *GRG, BOG,* and both targets in the final organism (Arabidopsis) through stable transformation might help to obtain more loss-of-function alleles and to reduce the variability encountered in tobacco. The use of CRISPR-Cas9 targeted genome editing might also help to produce more alleles. Increasing the available number of alleles is important to get a better idea about *GRG* function, and to tackle discrepancies like the fact that miR390 is present in the primary root tip in GK T-DNA line but absent in Salk T-DNA line (Figure 1-13). Once more loss-of-function alleles are created or identified, apart from GUS staining, allelism test, and ISH, a successful complementation would definitely help to prove a role of *GRG* in controlling *MIR390A* expression. qPCRs and Northern Blots for miR390 in the root tip versus the rest of the root would strengthen the results.

Regarding P5-40, it would still be interesting to find out if there are mutation(s) (and eventually where they are located) responsible for the lack of *MIR390A* expression in the primary root tip in the backcrossed line, or if it is just an effect of the reporter. In any case, the first step should be to check by ISH the expression pattern of the mature miR390 in this line, and see if it still agrees with the expression pattern obtained by GUS staining.

A fundamental issue, which will be addressed in the next section of the results, still remains: so far there is no evidence of a primary root phenotype for *GRG* in particular and the tasiARFs pathway in general.

2 What is the role of the tasiARFs pathway in primary root development?

2.1 Context of the study

MIR390A expression by GUS staining and miR390 detection by ISH in the primary root tip point to a role of the tasiARFs pathway in primary root development. Furthermore, Yoon *et al.* (Yoon *et al.*, 2014) proposed the tasiARFs pathway as responsible for the different regulation of primary and lateral root growth by exogenously-applied auxin: high levels of auxin, in fact, promote LR growth but repress PR growth. Therefore, in this part, a primary root phenotype (root length and meristem size) under normal and abiotic stress conditions (cold, heath, pH, salt, nitrogen deficiency) in mutants for the tasiARFs pathway is sought.

2.2 Root and meristem length measures were very heterogeneous

The first step has been to check primary root length growth curve (Figure 2-1) and meristem length (Figure 2-2) in loss of function mutants and some overexpressing or gain of function alleles (*mir390a-1, mir390a-2, tas3a-1, TAS3Aox, arf2-6, ett-2, ett-3, arf3-2, mARF3-GUS, ARF3-GUS, arf4-2, arf4-7*) of the different components of the tasiARFs pathway. To make the heterogeneity in measures more evident, the different experiments (biological replicates) have not been aggregated.

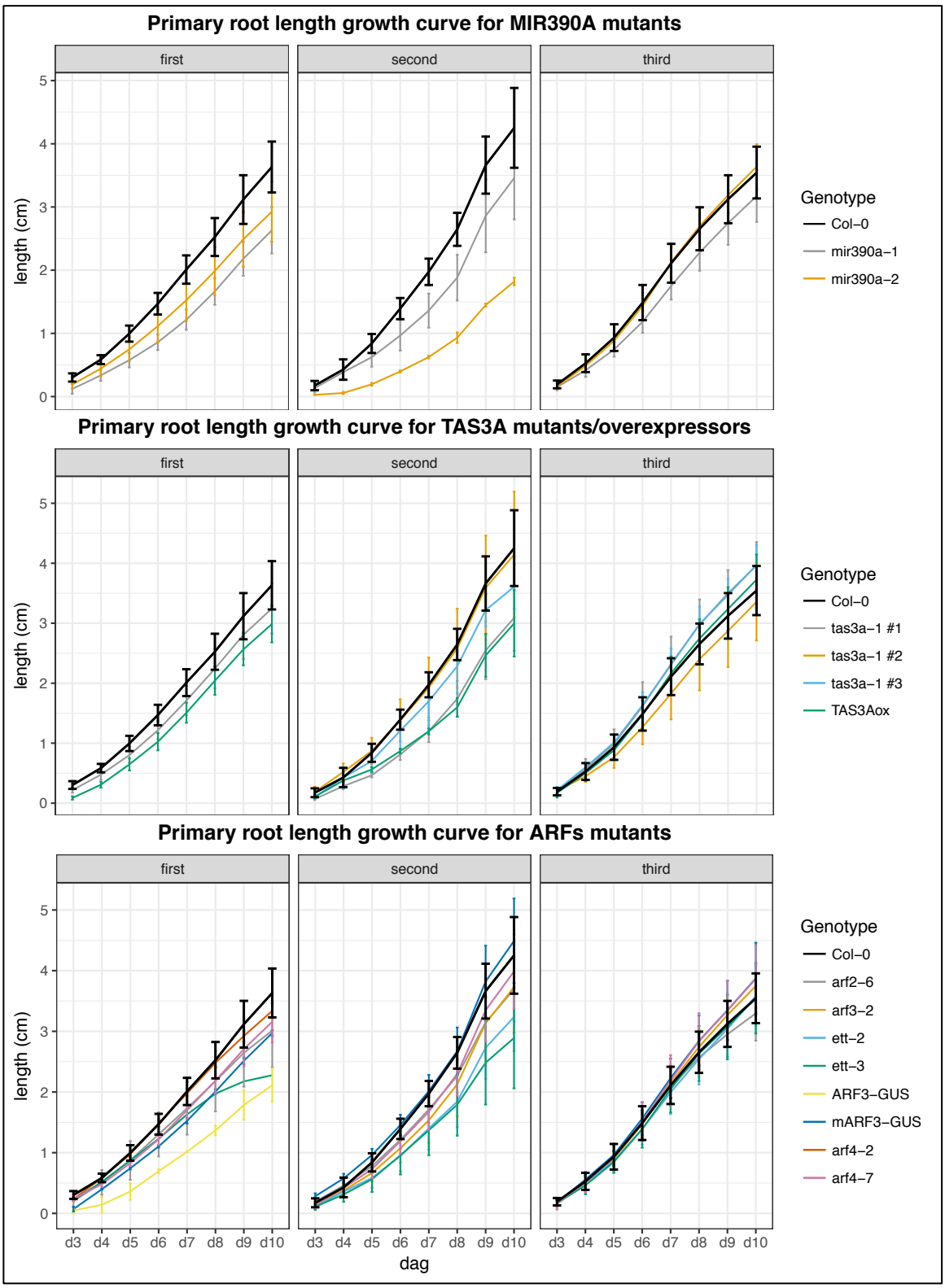

Figure 2-1. Primary root length for tasiARFs mutants. Primary root length for *MIR390A mutants, TAS3A* mutants and overexpressor, and for *ARF2, ARF3,* and *ARF4* mutants; first: first experiment; second: second experiment; third: third experiment; dag: days after germination. Error bar: standard error of the mean.

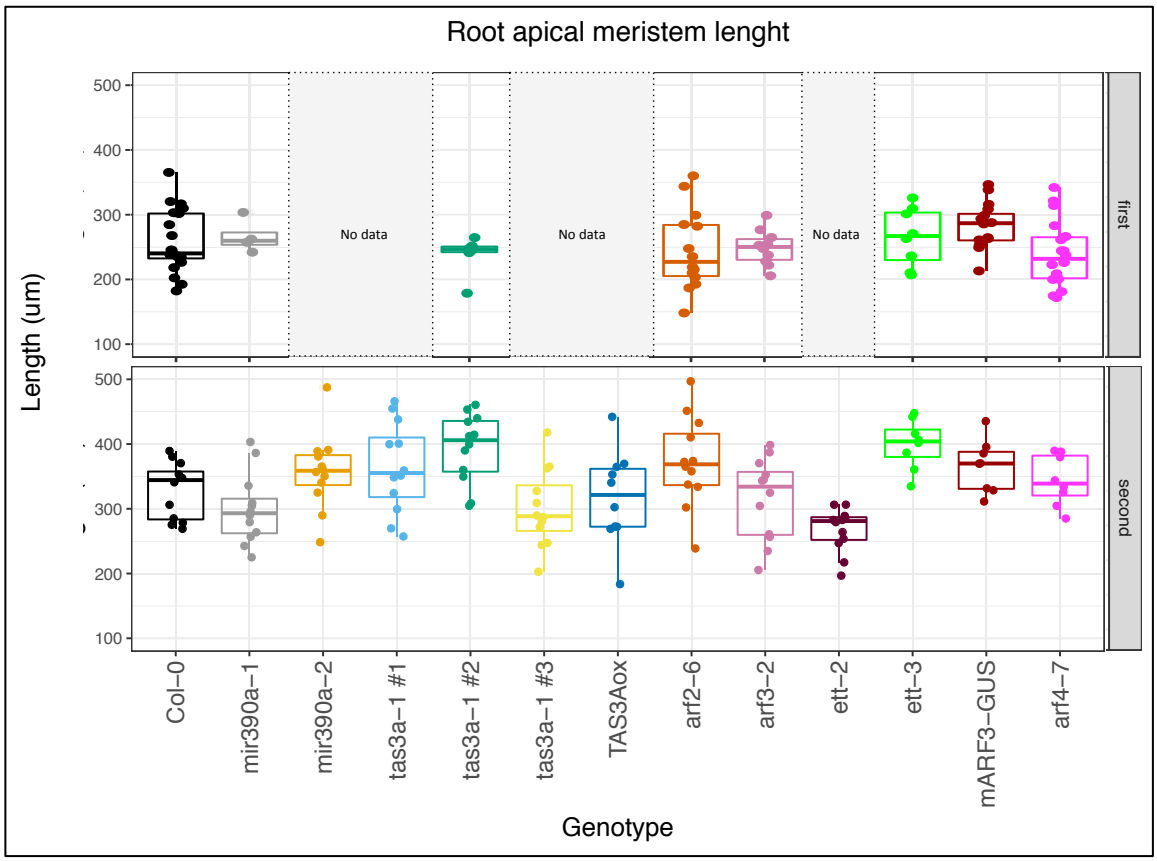

Figure 2-2. Root apical meristem length for tasiARFs mutants. Root apical meristem length for *MIR390A mutants, TAS3A* mutants and overexpressor, and for *ARF2, ARF3,* and *ARF4* mutants; first: first experiment; second: second experiment. Meristem length was measured in 7 days-old seedlings. Cell wall was stained with PI and observed under confocal microscope.

The results were very heterogeneous both among and between experiments. The heterogeneity can be easily appreciated, for example, in case of *tas3a-1* mutants, for which 3 seed batches were measured.

2.3 No difference was observed under abiotic stress (cold, heath, pH, salt, nitrogen)

Because root system architecture RSA, defined as spatial arrangement of the root and its components (Koevoets *et al.*, 2016), changes and adapts to cope with stresses (Kazan, 2013; Koevoets *et al.*, 2016), and primary root length is one of the traits determining it, root length was also checked under different abiotic stresses: cold (4°C), heath (25°C), pH (5), salt (NaCl 50 and 100mM) (Figure 2-3), and nitrogen deficiency (KNO_3 0, 0.1, 0.5, and 10 mM)

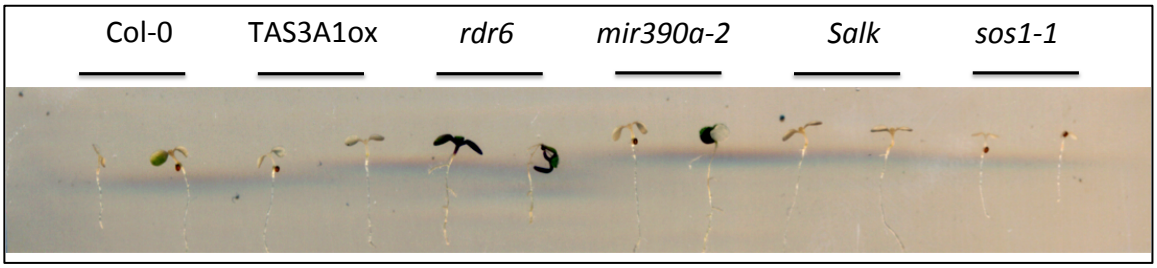

Figure 2-3. Seedlings grown at 50 mM NaCl. *sos1-1,* a salt sensitive mutant, was used as negative control. Salk: SALK_025523C.

No difference was observed, except in salt stress. At 50mM NaCl, cotyledons of all the genotypes presented various degrees of chlorosis, except for *rdr6*, in which they were still green (Figure 2-3).

2.4 No consistent root phenotype was observed in *mir390a-2*

To tackle the heterogeneity-of-measurements problem, the focus was reduced to only *mir390a-2*, using seeds derived from parents grown on the same condition and, for measuring meristem size, a modified version of the standard PI staining (mPS-PI), which yields much clearer images. Furthermore, analysis was performed in blind.

2.4.1 No PR length difference

PR length growth curve was measured for Col-0 and *mir390a-2* (Figure 2-4).

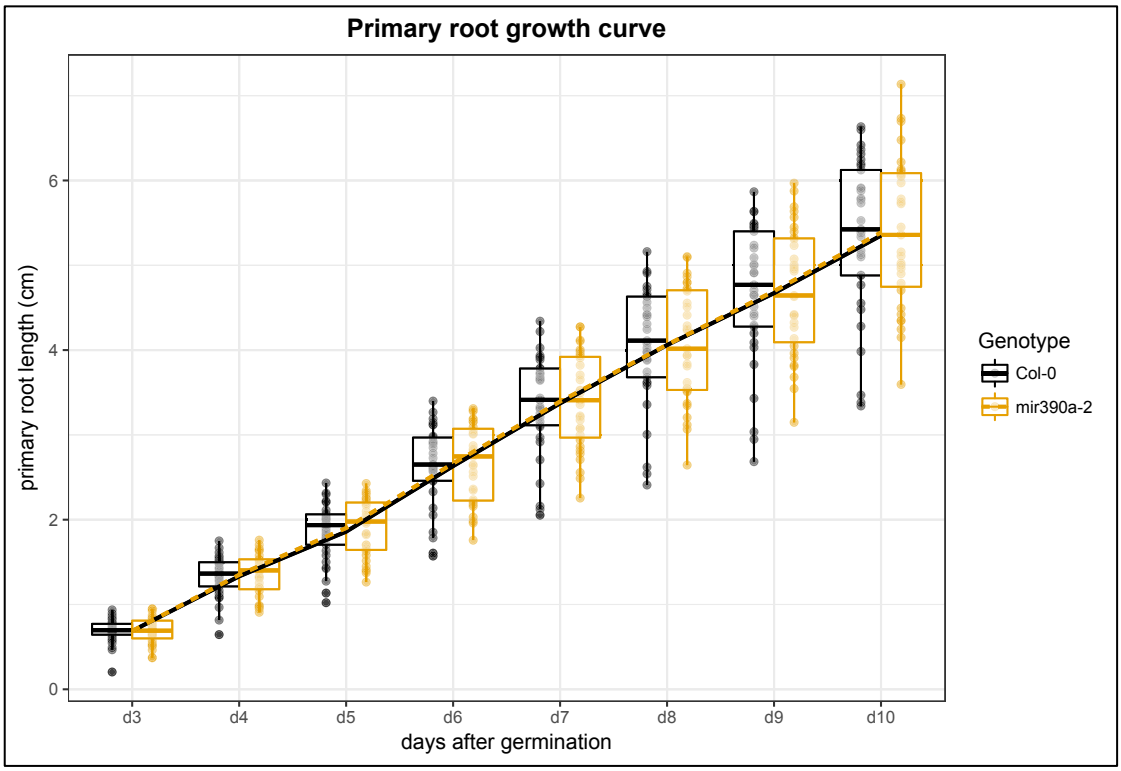

Figure 2-4. Primary root length for *mir390a-2*.

No difference was observed between *mir390a-2* and WT.

2.4.2 No meristem size difference

Meristem length and area were measured for Col-0, *mir390a-2*, and a *MIR390B* overexpressing line (MIR390Box). Cell walls in 7 days-old seedlings were stained with the modified pseudo-Schiff propidium iodide (mPS-PI) technique and imaged with confocal microscopy. Meristem length, defined as the portion of primary root axis going from the center of the quiescent center (QC) to the level of the first epidermal cell in the elongation zone, and meristem area, defined as the surface obtained by using the epidermis outer cell wall from the QC to the elongation zone as perimeter (Figure 2-5), were measured (Figure 2-6).

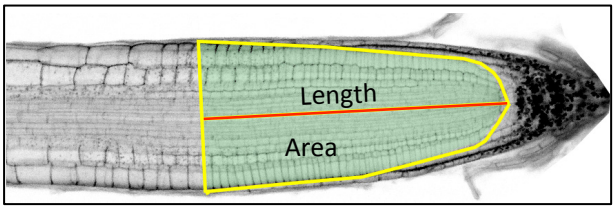

Figure 2-5. Meristem Length (red line) and Area (light green area).

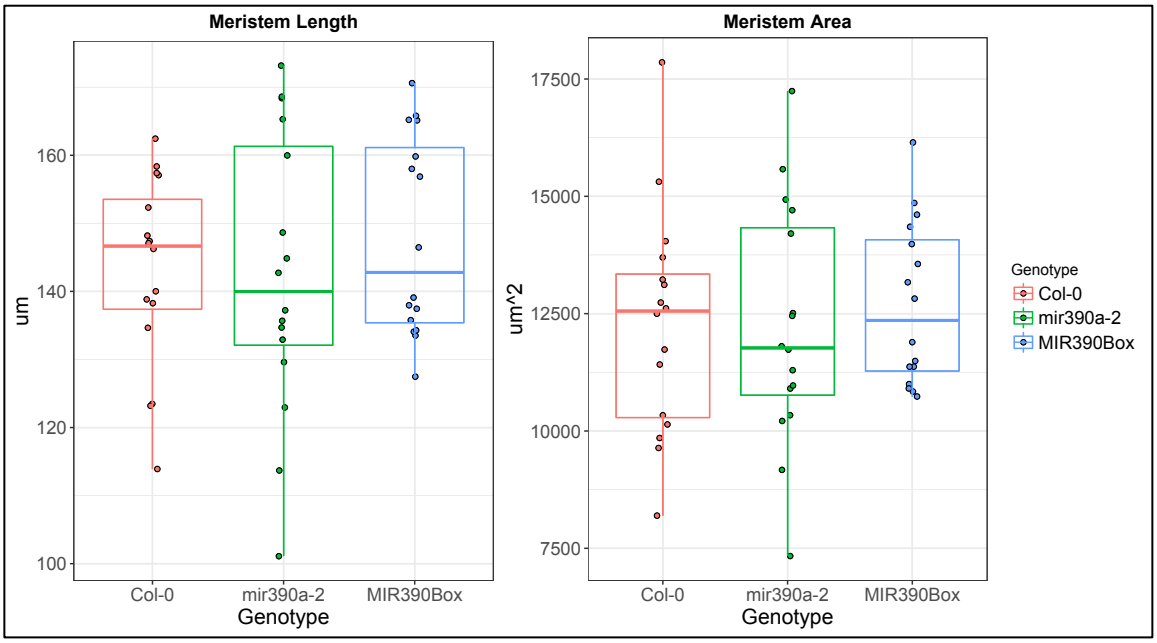

Figure 2-6. Meristem length and area by mPS-PI staining. Meristem length and area were measured in 7 days-old seedlings. Cell wall was stained with mPS-PI and observed under confocal microscope.

No difference was observed between genotypes.

Taken together, these results could not prove a role for miR390 in the control of primary root length and meristem size.

2.5 Discussion

It is puzzling that despite miR390 is highly expressed and present in the primary root tip, no primary root phenotype could be observed in *MIR390A* mutants. Only in the aerial part of *rdr6* mutants, a difference was observed, that is greener cotyledons compared to the other mutants or Col-0 (Figure 2-3). *RDR6,* though, is not specific to the tasiARFs pathway: it has been shown to be involved in the generation of 21 and 24 nucleotides natural antisense siRNAs implicated in salt tolerance (Borsani *et al.*, 2005).

However, this result should not be too surprising: in the literature (Marin *et al.*, 2010), it has already been described that plants overexpressor or mutant for *TAS3A* (the transcript target of miR390 and the direct precursor in tasiARFs biogenesis) have no difference in primary root length. It must be noticed that the growth conditions in which root length and meristem size were measured (vertical ½ MS plates in a plant growth chamber), even when abiotic stresses were applied, are very far from Arabidopsis natural environment, not only regarding the environment stability (controlled and stable temperature, relative humidity, light, and pH), but also a two dimensional root architecture with a biphasic water availability, a lack of competition for resources and an absence of pathogen or biotic stresses in general (but also of other beneficial or symbiotic microorganism associated with the rhizosphere), and a continuous exposure of roots to light. All these factors have been shown to influence root architecture (see (Morris *et al.*, 2017) for a recent review about the importance of a 3D environment and the techniques to investigate it, (W. F. Xu *et al.*, 2013) about the difference between roots grown on light versus dark, and (Philippot *et al.*, 2013) about the importance of the microbial ecology of the rhizosphere).

Given the plethora of factors contributing to the root architecture plasticity, and the fact that the tasiARFs pathway is highly conserved, it is reasonable to assume that the tasiARFs pathway might play a yet undiscovered role in the primary root. Growing plants in conditions that can cover and dissect all the above-mentioned factors could help to shed light upon this conundrum.

Because precursor and mature miR390 levels are controlled by auxin (Figure 3-1) and the tasiARFs pathway confers robustness and sensitivity onto auxin response (Plavskin *et al.*, 2016), tweaking auxin levels in *mir390a* mutants might improve the chances of revealing a phenotype. However, preliminary results (by Dr. Paola Ruiz-Duarte) on *mir390a-2* mutants grown on different auxin concentrations could not show significative differences in primary root length compared to Col-0.

On a final note, it is worth mentioning the importance of having homogenous growth conditions in the parental generation, because they will influence the following generation.

Furthermore, the effects are particular significant early in the development, affecting primary root growth and gravitropism; for root measurements, having a homogeneous seed size is also very important (Elwell *et al.*, 2011).

3 Do the tasiARFs pathway and miR156/SPLs modules interact during lateral root development?

3.1 Context of the study

The tasiARFs pathway and miR156/SPLs modules are important to control lateral root development (Marin *et al.*, 2010; Yu *et al.*, 2015). Specifically, the tasiARFs pathway is involved in the regulation of LR length, while miR156/SPLs modules play a role in determining LR density. In this section, it was tested if these two pathways interact, checking at molecular level and phenotypically what happens to one pathway when the other one is perturbed.

3.2 miR156 and miR390, mature and precursors, and their response to auxin

Mature miR156 derives from 7 loci, therefore it is important to identify which loci contribute the most to lateral root development. According to literature, *MIR156B* is the most abundant in roots, and its expression increases upon IAA treatment. In the model proposed by Yu *et al.*, in fact, auxin increases miR156 levels (Yu *et al.*, 2015). Interestingly, miR156 has been previously reported to decrease after IAA treatment (Marin *et al.*, 2010).

3.2.1 While miR390 mature and precursor increase upon IAA, miR156 mature and precursors behave less clearly

miR156 and miR390 mature and precursor levels were checked by qPCR after 0, 6, or 24h IAA treatment. 24h with or without NPA was used as pre-treatment (Figure 3-1).

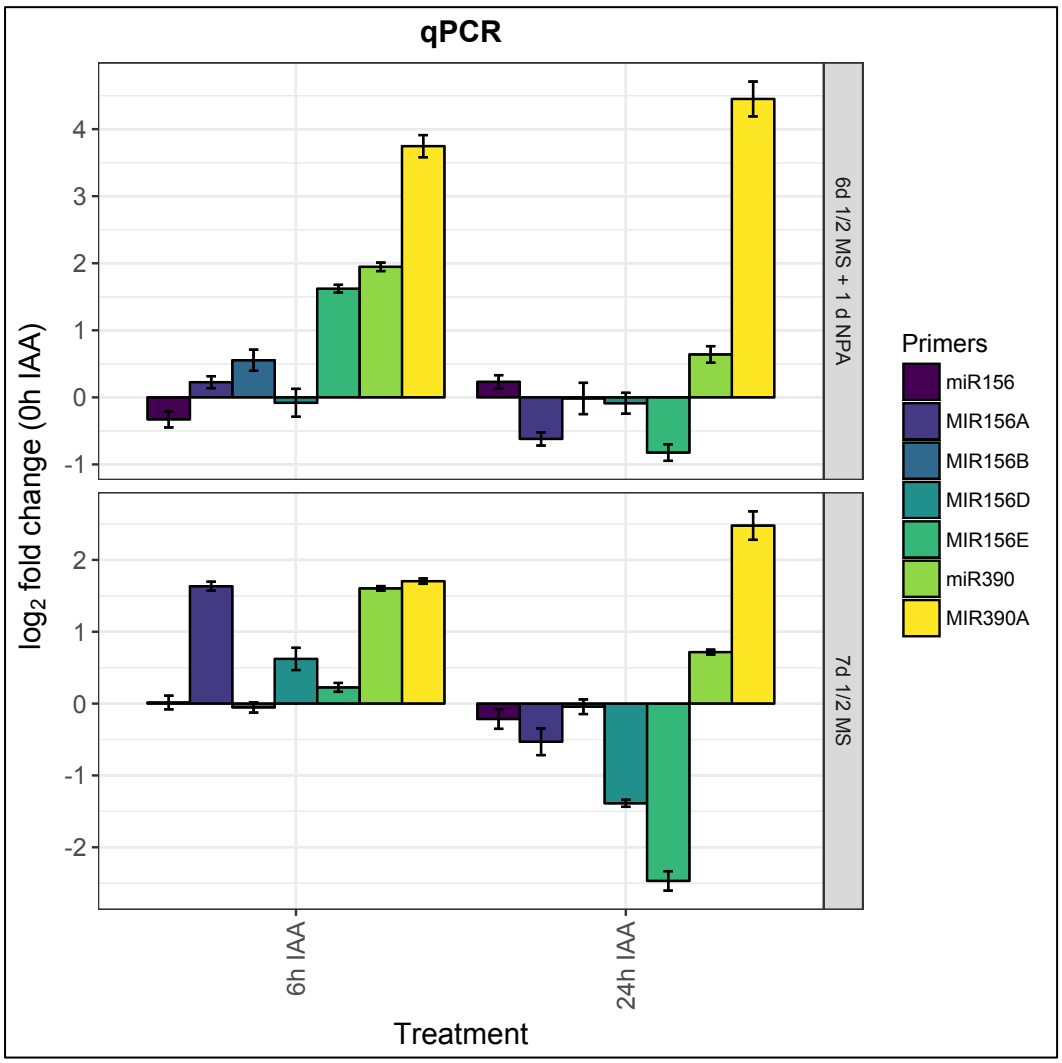

Figure 3-1. qPCR for miR156 and miR390, matures and precursors. 0 h IAA is set as reference. NPA: 10 µM, IAA: 10 µM. Facets refer to the pre-treatment conditions. *PP2AA3* (AT1G13320) was used as reference. Error bar: standard error of the mean.

While miR390 (mature and precursor) levels, regardless of pre-treatment and treatment, increase upon auxin, mir156 levels show no clear pattern. miR156 does not seem affected by pre-treatment or treatment. *MIR156A* slightly decreases after 6h IAA, and increases after 24h IAA. *MIR156B* does not seem affected by pre-treatment or treatment. *MIR156D* levels do not change if NPA-pre-treated, and, without pre-treatment, decrease after 6h and slightly increase after 24h. *MIR156E* is lower after 6h IAA, especially without pre-treatment, and is higher after 24h, especially after treatment.

To have a better understanding of miR156 behavior after IAA or NPA treatment, the following treatment were applied:

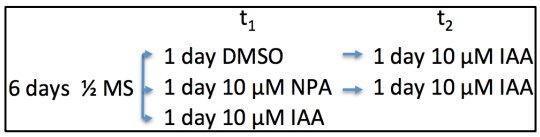

Seedlings were harvested at t_1 and t_2 and miR156 and miR390 (as control) were measured by qPCR and Northern Blot (Figure 3-2).

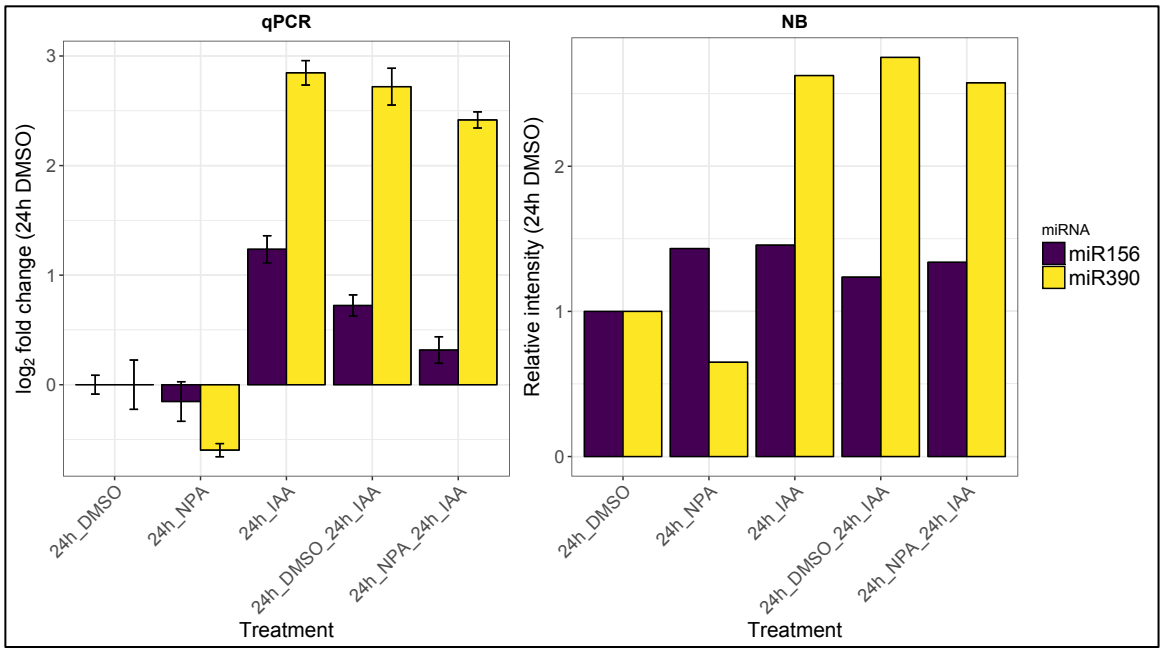

Figure 3-2. qPCR and NB for miR156 and miR390 after different treatments. 24 h DMSO is set as reference. NPA: 10 µM, IAA: 10 µM. *PP2AA3* (AT1G13320) was used as reference for qPCR. Error bar in qPCR plot: standard error of the mean.

qPCR and NB for miR390 gave the expected result: miR390 levels decrease after NPA treatment and increase after IAA treatment, regardless of pre-treatment. A similar pattern can be observed by qPCR for miR156. However, miR156 levels measured by NB did not change significantly after treatment.

Taken together, these results show that while miR390 response to different treatments is consistent with the literature and between techniques, miR156 mature and precursors levels are not, so no clear conclusion can be drawn.

3.3 The response of a pathway to perturbations in the other

To test if the two pathways interact, levels of the component of one pathway were measured in plants that were mutant, overexpressor, or gain-of-function for the other pathway.

3.3.1 By qPCR, no clear patterns were observed

miR156, miR390, and *SPL10* levels were measured by qPCR, growing seedlings according to the LRIS. Col-0, *mir390a-2*, *TAS3Aox*, *spl10,* and *spl9 spl15* were used as genotypes Figure 3-3).

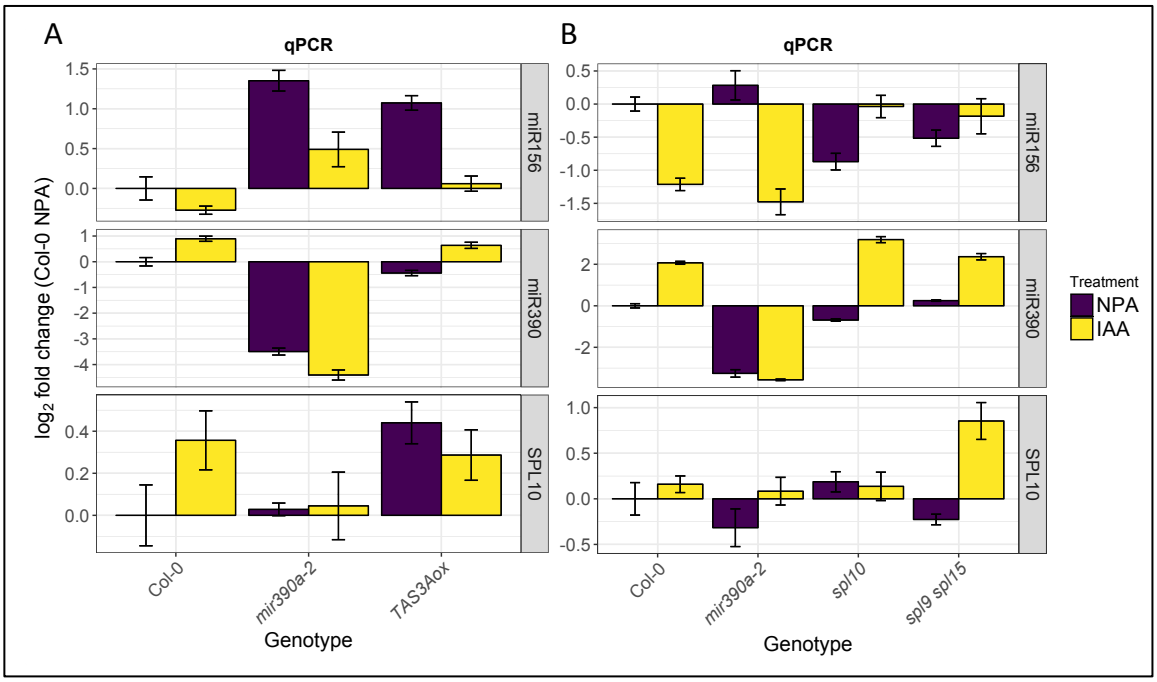

Figure 3-3. qPCR for miR156, miR390, and *SPL10*. A. Col-0, *mir390a-2*, and *TAS3Aox* were used as genotypes. **B.** Col-0, *mir390a-2*, *spl10*, and *spl9 spl15* were used as genotypes. Col-0 NPA is set as reference. NPA: 48h 10 µM NPA. IAA: 24h 10 µM NPA then 24h 10 µM IAA. *PP2AA3* (AT1G13320) was used as reference. Error bar: standard error of the mean.

In the first experiment (Figure 3-3, A), a reduction in miR390 (*mir390a-2*) increases miR156. Also, while IAA induces miR390, an opposite effect can be observed for miR156. In the second experiment (Figure 3-3, B), miR156 increase in *mir390a-2* is more modest and only NPA dependent. Interestingly, mutations in *SPLs* (*spl10* and *spl9 spl15*) reverse IAA inhibition and miR156 level is lower on NPA compared to Col-0. In these mutants, miR390 levels increase further upon IAA. Results concerning *spl10*, however, may not be valid: no decrese in *SPL10* was observed in the mutant as expected.

A third experiment was performed growing seedlings for 7 days on ½ MS and then transferred to DMSO, 10 µM NPA, or 10 µM IAA. In this experiment, miR172 instead of *SPL10* was measured. miR172 is induced by *SPL9.* Col-0, *mir390a-2, spl10, spl9 spl15,* and *MIR156A* overexpressor (*35S:5xMIR156A*) were used as genotypes (Figure 3-4).

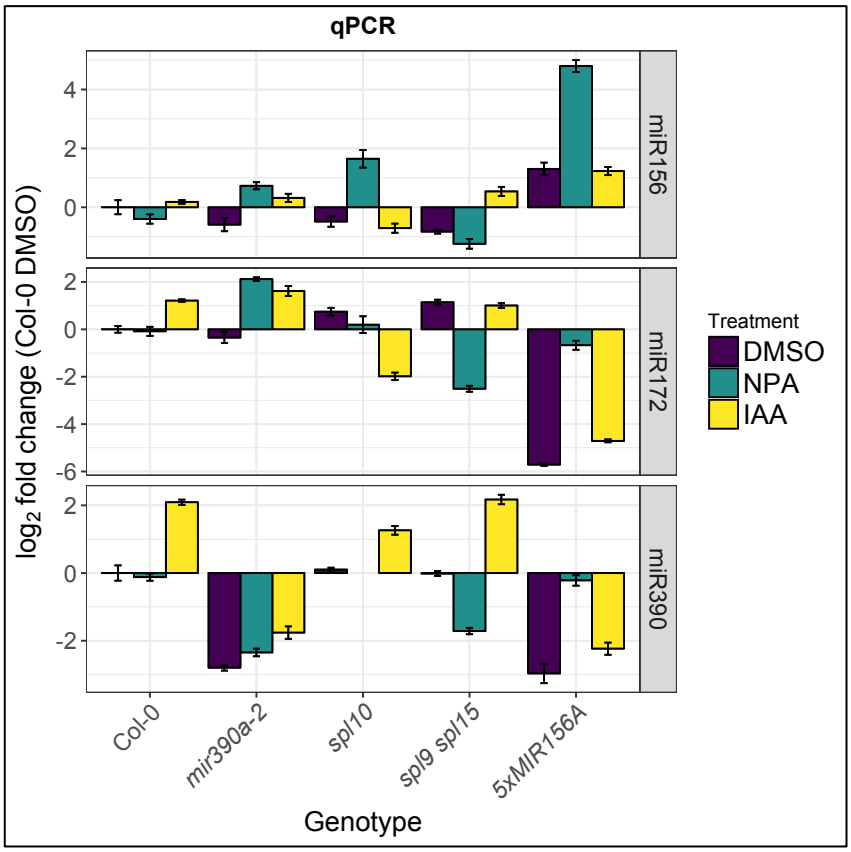

Figure 3-4. qPCR for miR156, miR172, and miR390. Col-0 DMSO is set as reference. NPA: 24h 10 µM NPA. IAA: 24h 10 µM IAA. *PP2AA3* (AT1G13320) was used as reference. Error bar: standard error of the mean.

In this experiment, mature miR156 in control conditions is, in general, less abundant than with pre-treatment, and, compare to Col-0, decreases in *mir390a-2*, *spl9 spl15*, and *spl10*. When seedling are treated with NPA or IAA, miR156 behave similarly to the LRIS: in *mir390a-2*, its level is higher than in Col-0 and decreases in IAA, while in *spl9 spl15*, and in *spl10* is lower than in Col-0 and (at least for *spl9 spl15*) increases in IAA. When *MIR156A* is overexpressed, miR156 is always more abundant than in Col-0, strongly increasing with NPA and decreasing to control levels upon IAA treatment. However, in Col-0, miR156 level is similar between treatments, slightly increasing upon IAA. Regarding mature miR390, it is interesting to notice that in *MIR156A* overexpressor there is no induction upon IAA treatment, in which case miR390 levels are even lower than in NPA. Regarding miR172, the strongest effect was observed in *MIR156A* overexpressor: miR172 levels are significantly

lower in control and IAA conditions compared to Wt. However, no clear patter regarding a possible interaction could be identified.

Finally, miR390 levels were measured by qPCR after 0h or 24h IAA treatment in Col-0 and in miR156-resistant *SPLs* (*SPLx:rSPLx-GUS, rSPLx*). The corresponding *SPLx:SPLx-GUS* (sSPLx, non resistant, sensitive) lines were used as control(M. Xu *et al.*, 2016) (Figure 3-5).

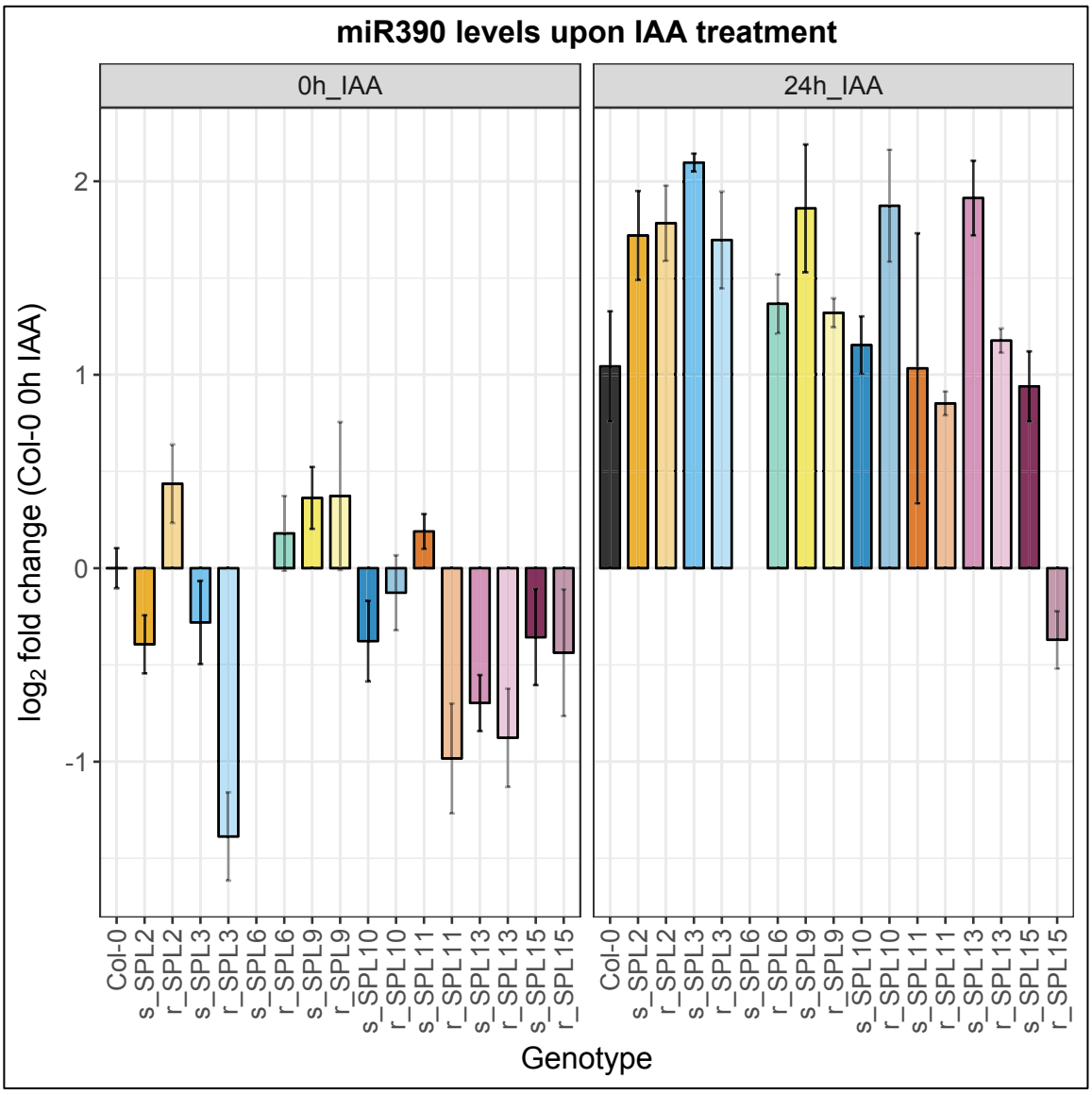

Figure 3-5. qPCR for miR390. Col-0 0h IAA is set as reference IAA: 10 µM IAA. *PP2AA3* (AT1G13320) was used as reference. Error bar: standard error of the mean. *rSPLs* have a lighter color than their corresponding sSPLs.

In this experiment sSPLs, used as control, did not behave like Col-0, so no conclusions can be drawn.

3.3.2 miR156/SPLs mutants, gain-of-functions, or overexpressors, have no impact on MIR390A expression

To check if perturbation in the miR156/SPLs pathway affect *MIR390A* expression, *MIR390A* GUS reporter (*MIR390A:GUS-GFP*), was crossed with miR156/SPLs mutants, gain-of-functions, or overexpressor.

When crossed with *spl9 spl15*, a F3 line derived from a GFP positive F2 line homozygous for the mutant was used. This line was then GUS stained and compared to the parent (*MIR390A:GUS-GFP*) (Figure 3-6).

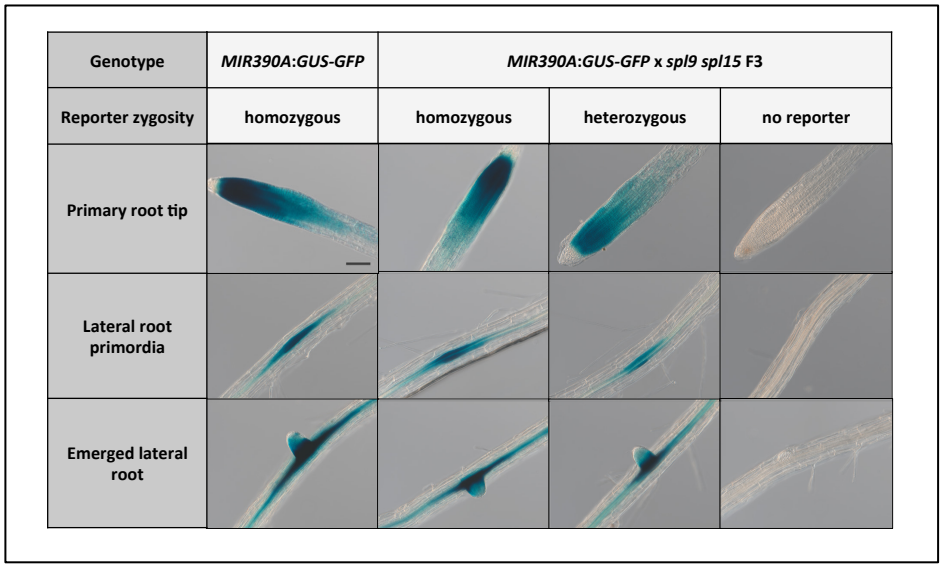

Figure 3-6. GUS staining of *MIR390A:GUS-GFP x spl9 spl15* F3. Scale bar: 100 µm.

No difference regarding the reporter expression pattern could be observed between the *spl9 spl15* F3 line and the control.

When crossed with *rSPLs*, *MIR156A* overexpressor (*35S:5xMIR156A*), or miR156 mimic overexpressor (*35S:*MIM156, miR156 target mimicry) (Franco-Zorrilla *et al.*, 2007), F1 plants were used to check the GFP reporter expression by confocal microscopy and compared to the parent (*MIR390A:GUS-GFP*) (Figure 3-7).

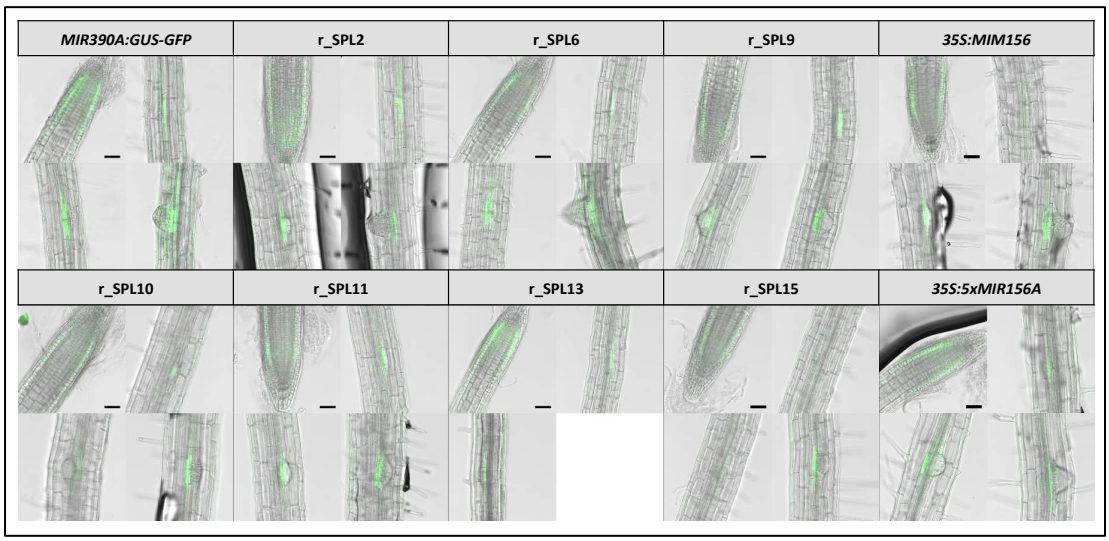

Figure 3-7. GFP signal of *MIR390A:GUS-GFP* crossed with rSPLs, *35S:5xMIR156A*, or *35S:MIM156*. Bright field and GFP channels are shown as merged. Scale bar: 100 µm.

No difference regarding the reporter expression pattern could be observed between the F1 lines and the control.

Taken together, these evidences do not support an interaction between the miR156/SPLs pathway and the tasiARFs pathway.

3.4 Phenotype of rSPLs

SPLs have been described to play a role in lateral root development; in particular, rSPL3, rSPL9, and rSPL10 show less lateral roots(Yu *et al.*, 2015). To gain a better understanding about which of them is a mayor player and how they control lateral root density, rSPLs have been phenotyped. Lateral root density and lateral root primordia morphology have been chosen as parameters for their phenotypical characterization.

3.4.1 rSPL2 and rSPL13 have less emerged lateral roots

Lateral root density was measured for every rSPL growing on the same plate Col-0, a resistant SPL and the corresponding sensitive SPL (Figure 3-8).

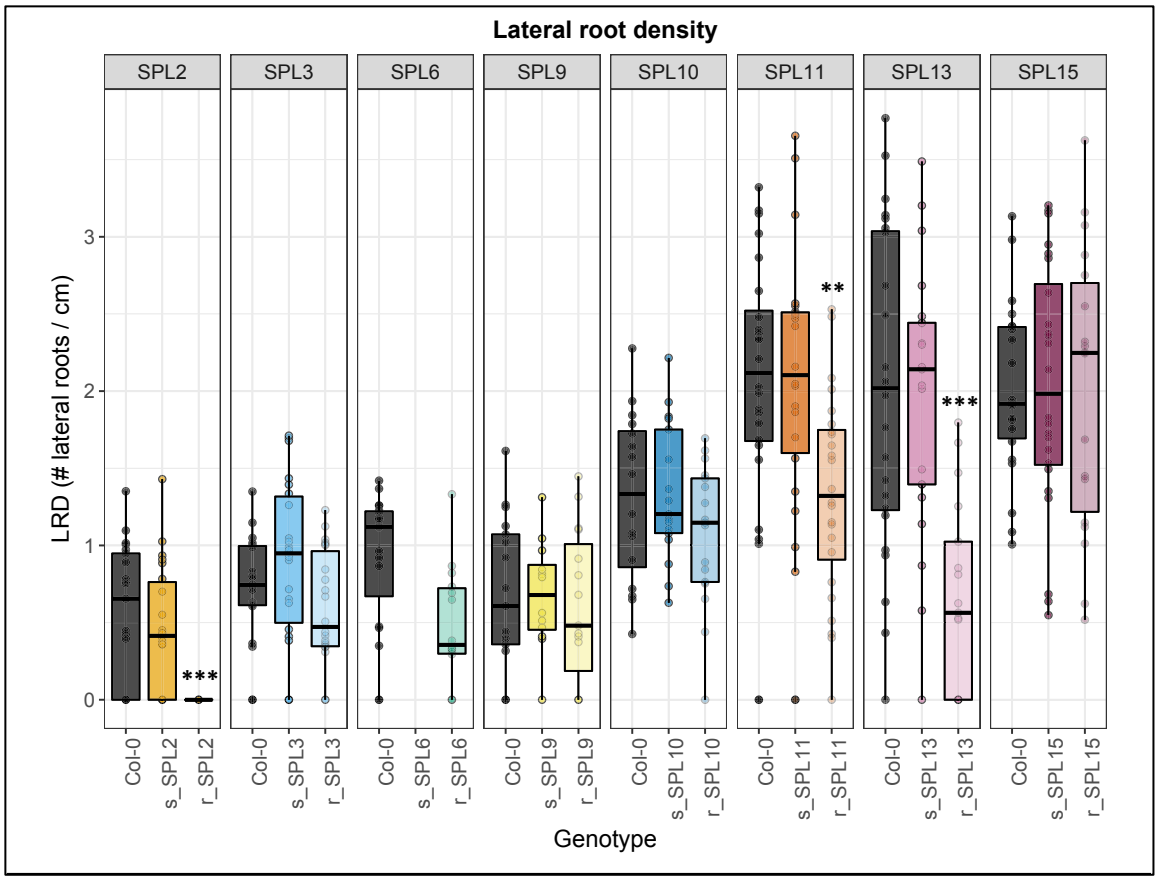

Figure 3-8. Lateral root density for r and s SPLs. For every SPL, seedlings were grown to maximize the difference, therefore SPL2 to SPL10 were grown 7d and SPL11 to SPL15 were grown 10d. *rSPLs* have a lighter color than their corresponding sSPLs. ***: p-value <0.001; **: p-value<0.01; *: p-value<0.05

sPSLs behaved Wild type-like. rSPL2 and rSPL13 showed less emerged lateral roots compared to the respective sSPLs, and were therefore chosen for further analysis. The variability in Col-0 LRD in seedlings grown during the same period (SPL2 to SPL10, and SPL11 to SPL13, respectively) suggests a plate position effect, and validates the choice to include in every plate a Col-0, and a pair of resistant and sensitive SPLs.

3.4.2 rSPL2 and rSPL13, in the bend after 48h gravistimulation, have fewer advanced stages

To check if the lower LRD found in rSPL2 and rSPL13 is due to delays in lateral root primordia development, lateral root stages in rSPL2 and rSPL13 cleared seedlings were measured in the bend created after 48h gravistimulation, which allows synchronizing lateral root initiation (Figure 3-9).

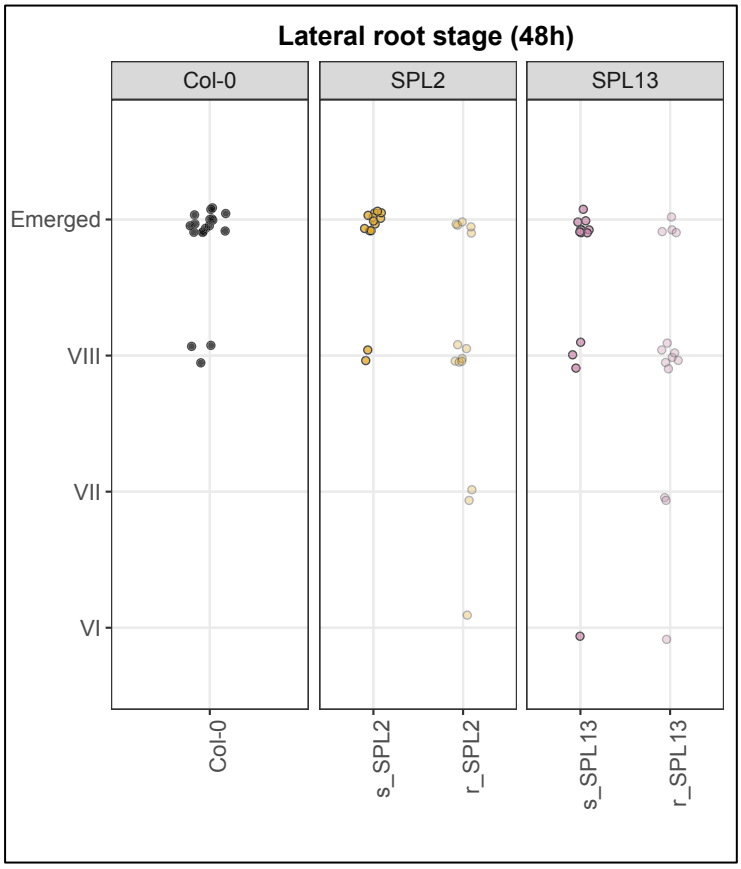

Figure 3-9. Lateral root stages in the bend after 48h gravistimulation.

rSPL2 and rSPL13 have fewer advanced stages compared to the respective sSPLs and to Col-0.

3.4.3 rSPL2 has more stage I and II and less emerged lateral roots; rSPL13 has less emerged lateral roots

To gain a more global view of LR stages in rSPL2 and rSPL13, whole-root staging was performed (Figure 3-10).

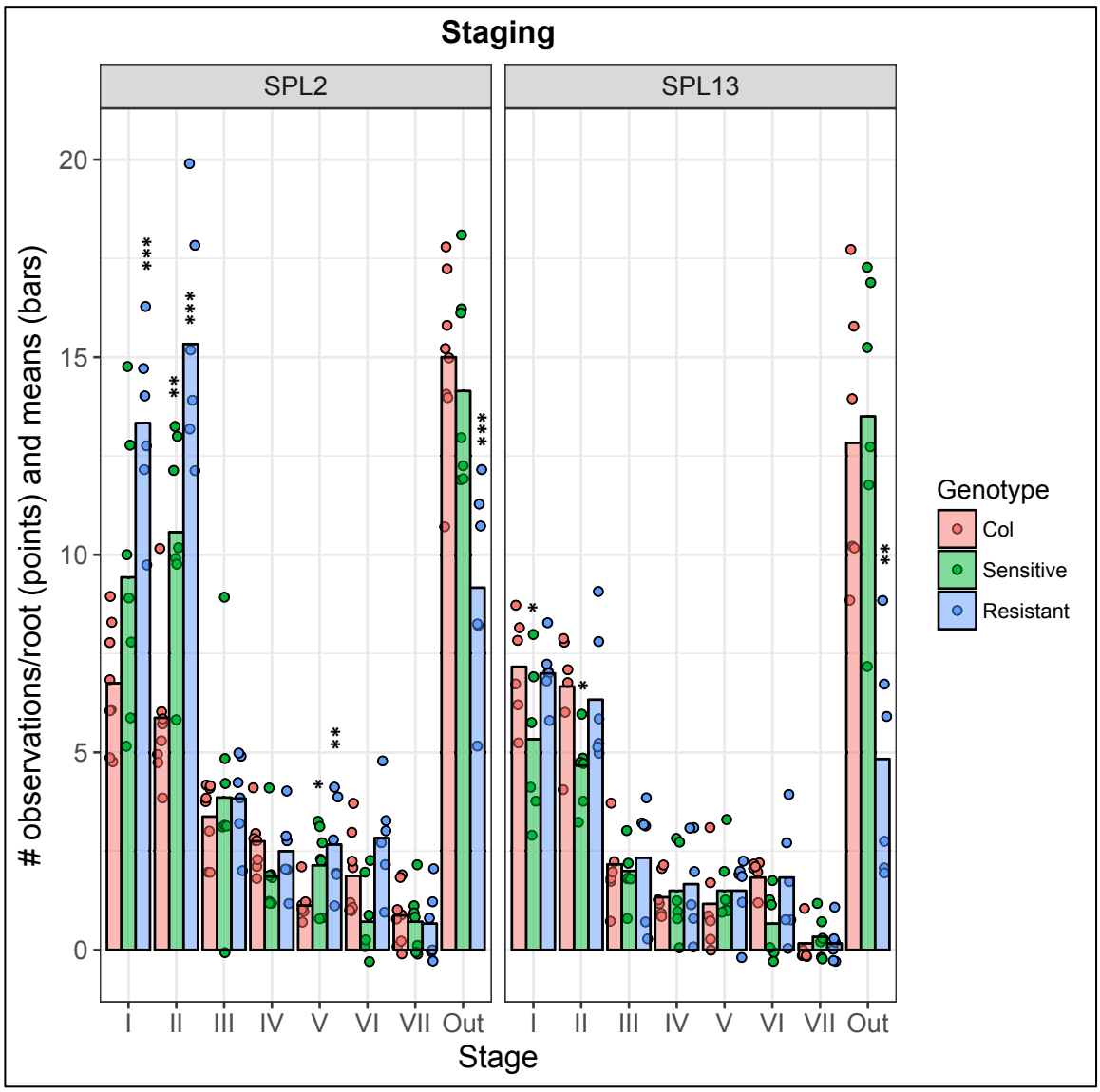

Figure 3-10. Whole-root staging. Out: emerged lateral root. ***: p-value <0.001; **: p-value<0.01; *: p-value<0.05

Regarding *SPL2*, *rSPL2* roots have a higher number of observed early stages (I and II) and a lower number of emerged lateral roots compared to Col-0, while *sSPL2* roots show an intermediate phenotype. Regarding *SPL13*, only *rSPL13* roots show a phenotype compared to Col-0 and *sSPL13*, having less emerged lateral roots.

3.4.4 Both sensitive and resistant SPL2 and SPL13 show a phenotype in the pericycle

Performing whole-root staging a continuous pericycle swelling was observed in resistant but also sensitive SPL2 and SPL13 (Figure 3-11). This is defined as a swelling of the pericycle in more and longer cells than normally associated with the first stage of lateral root primordia development. While it has already been described that up to 10 radially

enlarged pericycle cell can be observed at stage I, they are normally shorter and less numerous (Malamy *et al.*, 1997).

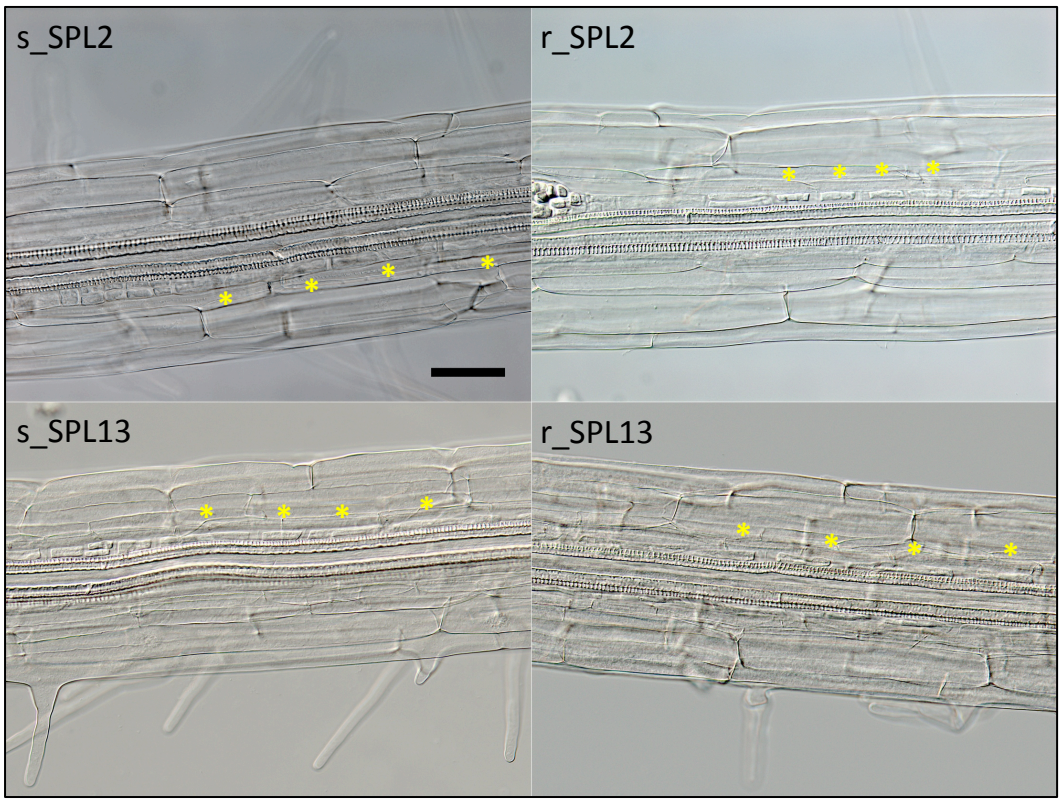

Figure 3-11. Continuous pericycle swelling in r and s SPL2 and SPL13. Asterisks are placed above swelled pericycle cells. Scale bar: 50 µm.

The difference can be easily appreciated in Figure 3-12, where a normal stage II lateral root primordium (arrow) together with the described continuous pericycle swelling (asterisks) can be observed.

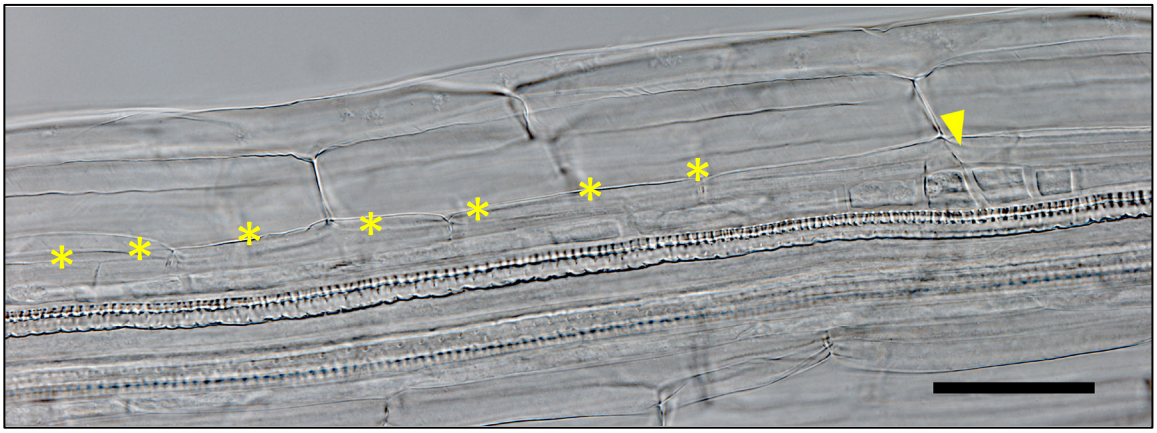

Figure 3-12. Continuous pericycle swelling in sSPL2. Asterisks are placed above swelled pericycle cells. Arrow is placed above a stage II primordium. Scale bar: 50 µm.

3.4.4.1 Pericycle swelling and SPL expression seem not to be associated

To test if SPL2 and SPL13 could directly be causing the pericycle swelling phenotype, it was examined if they are present during the first stages of lateral development. Resistant and sensitive SPL2 and SPL13 (both sensitive and resistant SPLs are fused with a GUS reporter: *SPLx:r/sSPLx-GUS)* were therefore GUS stained (Figure 3-13).

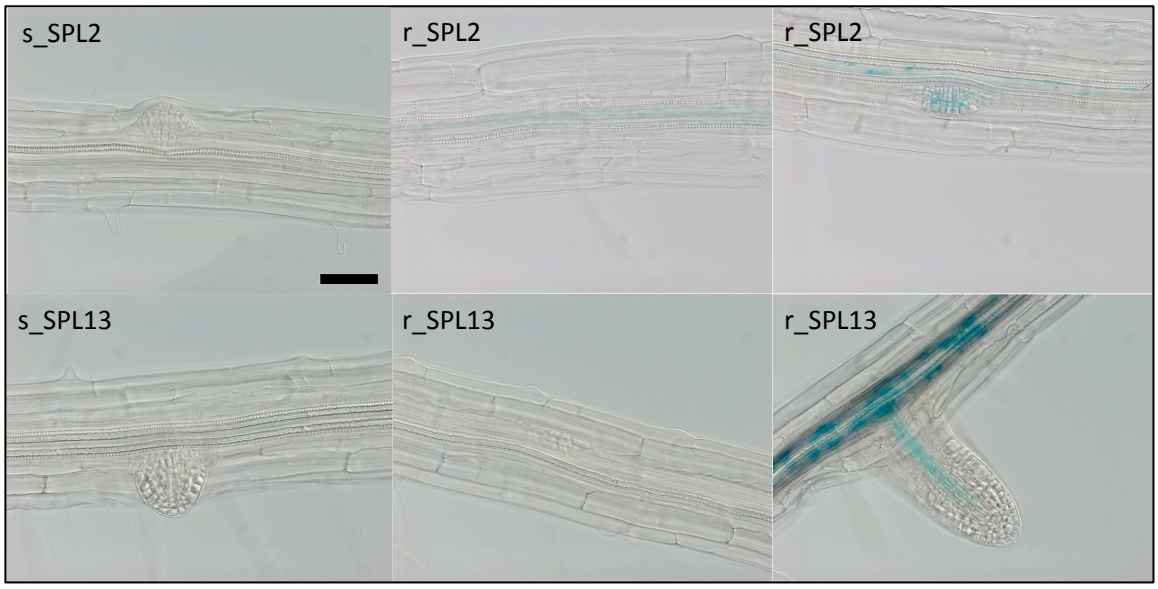

Figure 3-13. GUS staining of s and r SPL2 and SPL13. Seedlings were GUS stained and cleared. For rSPLs, pictures depict (left to right) lateral root primordia stages without staining and with the first observable GUS staining. sSPLs present no staining. Scale bar: 50 µm.

In both SPLs, GUS signal was not present during the first stages of LR development, appearing only at stage IV or V in rSPL2 and after lateral root emergency in rSPL13. sSPLs show no GUS staining. The presence of GUS signal in rSPL2 in concomitance with the absence of sSPL2 signal, suggests a miR156-mediated degradation of *SPL2* mRNA starting at stage IV or V.

These results could not provide evidences for a direct role of SPL2 and SPL13 in the early stages of lateral root development.

3.5 Discussion

The experiments performed to test a possible interaction between the tasiARFs pathway and the miR156/SPLs pathway in the control of lateral root development, and to unravel the auxin response of miR156 did not provide a clear picture.

Regarding the auxin response of miR156, as can be seen in Table 3-1, no clear pattern could be identified in the 3 different treatments (24h 10 µM NPA, 6h 10 µM IAA, 24h 10 µM IAA). Even if some variation is expected when seedlings were grown on different pre-treatments, the amount of miR156 detected on the same conditions (pre-treatment and treatment) was

not similar in different experiments and when different methods (qPCR and NB) were used. On the other hand, miR390 shows a clear pattern: it slightly decreases upon NPA and it strongly increases after auxin induction, with higher levels measured after 24h IAA compared to 6 h IAA treatment. Particularly troubling is the inconsistence between qPCR an NB. However, the use of only one biological replicate in each experiment might be the simplest explanation. Therefore, it would be important to repeat qPCR and NB with at least three biological replicates, using only simple conditions, to reach a much-needed consistency; as controls, a wider range of mutants or overexpressors for miR156 (mature and precursors) should also be introduced. Understanding the auxin response of miR156 is also very important in light of the discrepancies in the literature: according to (Marin *et al.*, 2010), miR156 decreases upon IAA treatment, while, according to (Yu *et al.*, 2015), its precursors increase. Interestingly, in (Marin *et al.*, 2010) mature miR156 levels were measured by NB, while in (Yu *et al.*, 2015) miR156 precursors were measured by qPCR. In this thesis, however, a correlation between precursors and mature miR156 levels could not be shown (Figure 3-1).

Table 3-1. miR156 and miR390 response to IAA and NPA. The results are ordered by Treatment. NB: northern blot. For qPCRs, $\log_2$ fold changes compared to Reference are shown; for NB, fold changes compared to Reference are shown. Color code: a red (low) to green (high) gradient is used.

Experiment	Method	Pre-treatment	Treatment	Reference	miR156	miR390
2 (Figure 3-2)	NB	-	24h NPA	24h DMSO	0.43	-0.35
2 (Figure 3-2)	qPCR	-		24h DMSO	-0.15	-0.60
5 (Figure 3-4)	qPCR	-		24h DMSO	-0.40	-0.12
1 (Figure 3-1)	qPCR	-	6h IAA	0h IAA	-0.22	0.72
1 (Figure 3-1)	qPCR	24h NPA		0h IAA	0.23	0.64
1 (Figure 3-1)	qPCR	-	24h IAA	0h IAA	0.02	1.60
1 (Figure 3-1)	qPCR	24h NPA		0h IAA	-0.33	1.95
2 (Figure 3-2)	NB	-		24h DMSO	0.46	1.63
2 (Figure 3-2)	qPCR	-		24h DMSO	1.24	2.85
5 (Figure 3-4)	qPCR	-		24h DMSO	0.18	2.09
6 (Figure 3-5)	qPCR	-		0h IAA	-	1.04
2 (Figure 3-2)	NB	24h DMSO		24h DMSO	0.24	1.75
2 (Figure 3-2)	qPCR	24h DMSO		24h DMSO	0.72	2.72
2 (Figure 3-2)	NB	24h NPA		24h DMSO	0.34	1.58
2 (Figure 3-2)	qPCR	24h NPA		24h DMSO	0.32	2.42
3 (Figure 3-3)	qPCR	24h NPA		48h NPA	-0.27	0.89
4 (Figure 3-3)	qPCR	24h NPA		48h NPA	-1.21	2.07

Regarding the interaction of the two pathways, for the qPCR data (Table 3-2) the discussion will focus only on what happens to miR390 when components of the miR156/SPLs pathway

are altered due to the previously discussed inconsistences in miR156 measurements. Furthermore, data obtained from *spl10* mutants will not be considered, because in those mutants *SPL10* expression levels did not differ from Col-0 (Figure 3-3). SPLs are target of miR156, so *spl9 spl15* double mutant and *MIR156A* overexpressor (*35S:5xMIR156A)* could have a similar miR390 expression profiles: this hypothesis was however not confirmed by the data.

Table 3-2. miR156 and miR390 expression by qPCR. log_2 fold change differences between mutants and Col-0 with same Pre-treatment and Treatment are shown. For the same genotype, results are order by Treatment. . Color code: a red (low) to green (high) gradient is used.

Genotype	Experiment	Pre-treatment	Treatment	miR156	miR390
mir390a-2	3 (Figure 3-4)	-	24h DMSO	-0.59	-2.80
	1 (Figure 3-3)	24h NPA	24h NPA	1.35	-3.50
	2 (Figure 3-3)			0.28	-3.26
	3 (Figure 3-4)	-		1.13	-2.23
	1 (Figure 3-3)	24h NPA	24h IAA	0.76	-5.30
	2 (Figure 3-3)			-0.26	-5.64
	3 (Figure 3-4)	-		0.14	-3.85
TAS3Aox	1 (Figure 3-3)	24h NPA	24h NPA	1.07	-0.44
			24h IAA	0.33	-0.26
spl10	3 (Figure 3-4)	-	24h DMSO	-0.49	0.10
	2 (Figure 3-3)	24h NPA	24h NPA	-0.87	-0.69
	3 (Figure 3-4)	-		2.05	-
	2 (Figure 3-3)	24h NPA	24h IAA	1.18	1.12
	3 (Figure 3-4)	-		-0.89	0.81
spl9 spl15	3 (Figure 3-4)	-	24h DMSO	-0.83	-0.02
	2 (Figure 3-3)	24h NPA	24h NPA	-0.52	0.25
	3 (Figure 3-4)	-		-0.84	-1.59
	2 (Figure 3-3)	24h NPA	24h IAA	1.03	0.30
	3 (Figure 3-4)	-		0.36	0.08
5xMIR156A	3 (Figure 3-4)	-	24h DMSO	1.30	-2.97
	3 (Figure 3-4)	-	24h NPA	5.19	-0.10
	3 (Figure 3-4)	-	24h IAA	1.05	-4.33

MIR390A expression profile in miR156/SPLs mutants, gain-of-functions, or overexpressors, measured by GUS (Figure 3-6) or GFP (Figure 3-7), was not different than in Col-0 background.

miR390 abundance in resistant or sensitive *SPLs* (*rSPLs* or *sSPLS*, Figure 3-5) was also not conclusive, because sSPLs, used as control, did not behave as the Col-0. More striking was the lateral root phenotype observed in *rSPL2* and *rSPL13* (lower lateral root density, Figure 3-8), even if a similar phenotype could not be observed in *rSPL3*, *rSPL9*, and *rSPL10* as it has been described by (Yu *et al.*, 2015). It is interesting to notice that, when lateral root

primordia stages were measured, only *rSPL2* showed more early stages and that the respective *sPLS* (*sSPL2* and *sSPL13*) displayed an intermediate phenotype (Figure 3-8). This result could be explained considering that each *sSPLs* bear an extra pair of the respective *SPLs*, becoming in theory overexpressors. This interpretation is supported by the fact that both sensitive and resistant *SPL2* and *SPL13* have a continuous pericycle swelling (Figure 3-11). However, because no GUS signal (*s*- and *r*- *SPLs* are fused to a GUS reporter) was detected during the early stages of primordia formation in those genotypes (Figure 3-13), a direct correlation between more SPL2 or SPL13 and pericycle swelling could not be drawn and such a phenotype could also be due to the effect of SPLs in the aerial part (M. Xu *et al.*, 2016). To draw more solid conclusions, a quantification of the pericycle swelling (frequency, thickness, association and distance with lateral root primordia) should be performed.

In conclusion, while an interaction between the tasiARFs and the miR156/SPLs pathway could not be proven, investigating further the role of a central pathway like the miR156/SPLs in roots would be of great interest. It would also be interesting to look at the interaction between the tasiARFs pathway and other miRNAs, beside miR156, controlling lateral root development (Couzigou *et al.*, 2016).

4 What is the role of the tasiARFs pathway in embryo development?

4.1 Context of the study

ISH(Dastidar *et al.*, 2016) and GUS staining (this study) of Arabidopsis embryos show miR390 presence and *MIR390A* expression, respectively, pointing to a possible role of the tasiARFs pathway in embryo development. Also, the tasiARFs pathway has been implicated in the control of MMC numbers(Su *et al.*, 2017): tasiARFs controls non-cell autonomously ARF3 to prevent excessive MMC formation, restricting its expression to the medio domain of ovule primordia. Furthermore, because 1) a *MIR390A* promoter deletion study (Dastidar, 2015) in the primary root found an ARF5/MONOPTEROS (MP)-specific auxin-response element required for *MIR390A* expression in PR, and 2) the MP-BODENLOS (BDL) module is critical for hypophysis specification, the tasiARFs pathway could also play a role in primary root initiation. Therefore, in this section, a role of the tasiARFs pathway in embryo development is sought.

4.2 The components of the tasiARFs pathway are expressed in embryo

To check if the tasiARFs pathway plays a role in embryo development, the first step has been to check if its components are expressed in the embryo. Embryos of plants containing GUS reporters for *MIR390A* (*MIR390A:GUS-GFP*), *TAS3A* (*TAS3A:GUS*), and *ARF3* (*ARF3:ARF3-GUS* and *ARF3:mARF3-GUS*, a tasiARFs insensitive version) were therefore GUS stained (Figure 4-1).

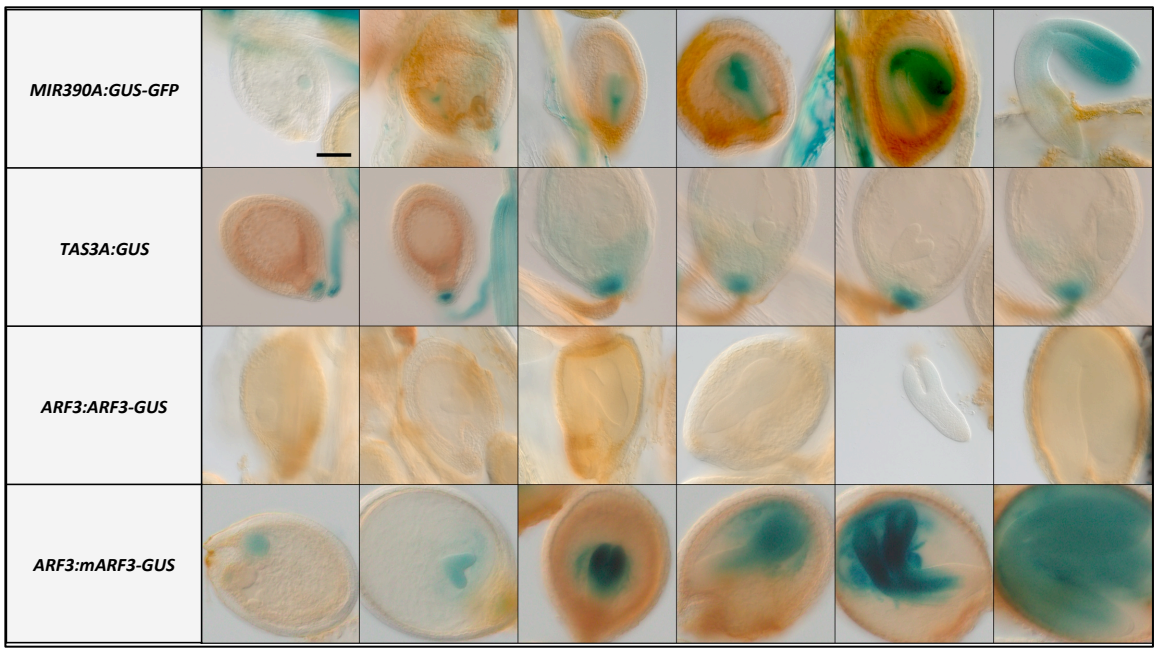

Figure 4-1. GUS staining of *MIR390A, TAS3A, ARF3,* and *mARF3* reporter. Scale bar: 100 µm.

MIR390A and *mARF3* are expressed in the embryo during all developmental stages, while *TAS3A* is expressed in the chalazal domain. No GUS staining for *ARF3* was observed. Altogether, these results suggest that elements of the tasiARFs pathway are expressed during embryo development and actively repress the expression of *ARF3*

4.3 tasiARFs mutants have less seeds per silique and more aborted seeds

The next step was to check if tasiARFs mutants have embryo development phenotypes. If that is the case, a decrease of fertility might be expected. To verify this hypothesis the number and position of normal and aborted seeds per silique were measured (Figure 4-2).

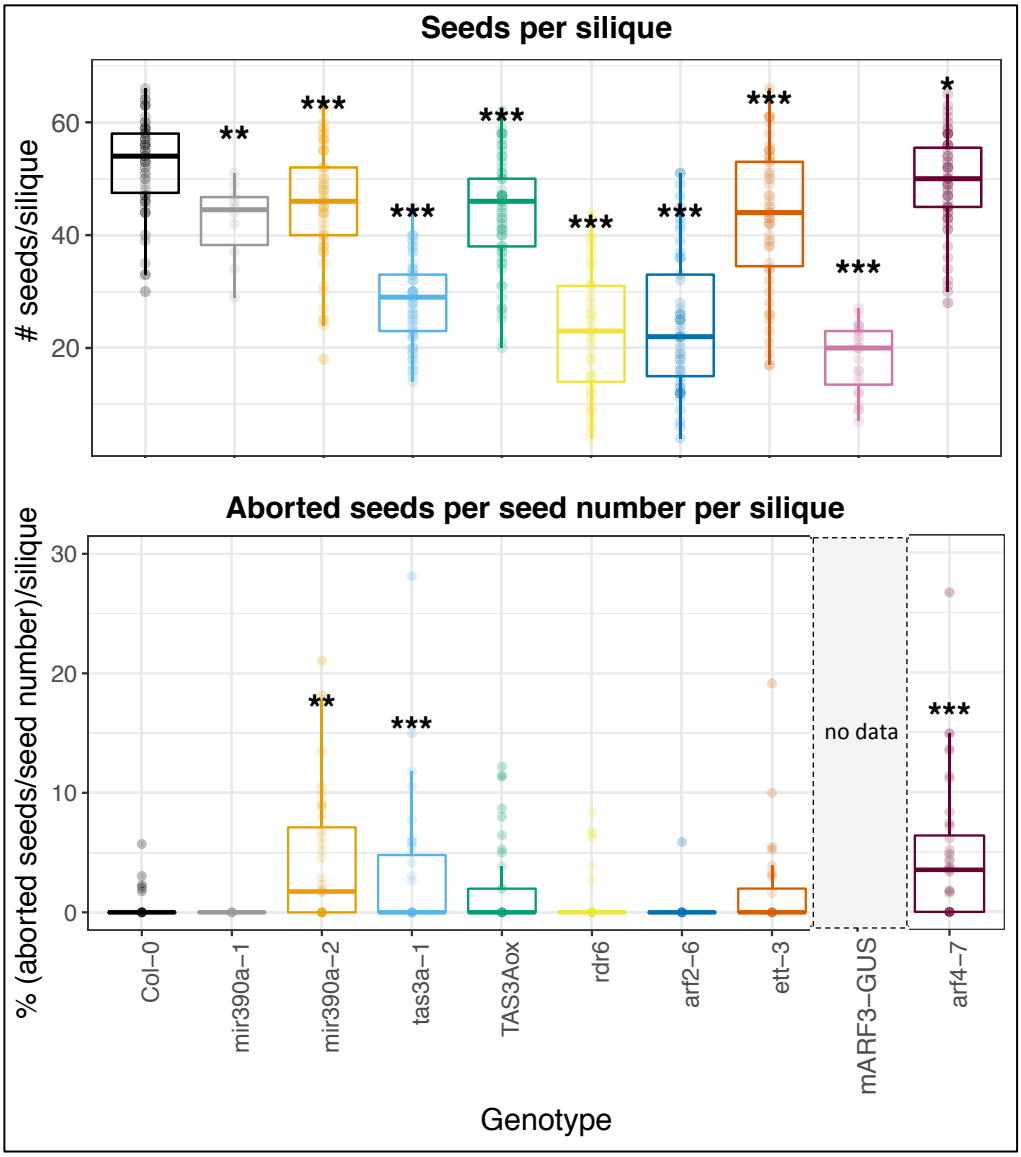

Figure 4-2. Seed number and aborted seeds per silique. ***: p-value <0.001; **: p-value<0.01; *: p-value<0.05

A strong reduction of seed number per silique was observed in *tas3a-1*, *rdr6*, and *arf2-6* mutants. *mARF3-GUS* has an already described reduced fertility phenotype, and behaved as expected (less seeds per silique)(Fahlgren *et al.*, 2006b). A higher aborted seed number was found in *mir390a-2, tas3a-1*, *TAS3A* overexpressor, *ett-3*, and *arf4*. These results strengthen the hypothesis that the tasiARFs pathway is involved in embryo development.

4.4 In *mir390a-2, tas3a-1*, and *arf4-7*, the endosperm seems undeveloped

To check if aberrant embryo division patterns were responsible for *mir390a-2, tas3a-1,* and *arf4-7* increased aborted seeds, their aborted seeds were cleared and examined for embryo defects (Figure 4-3).

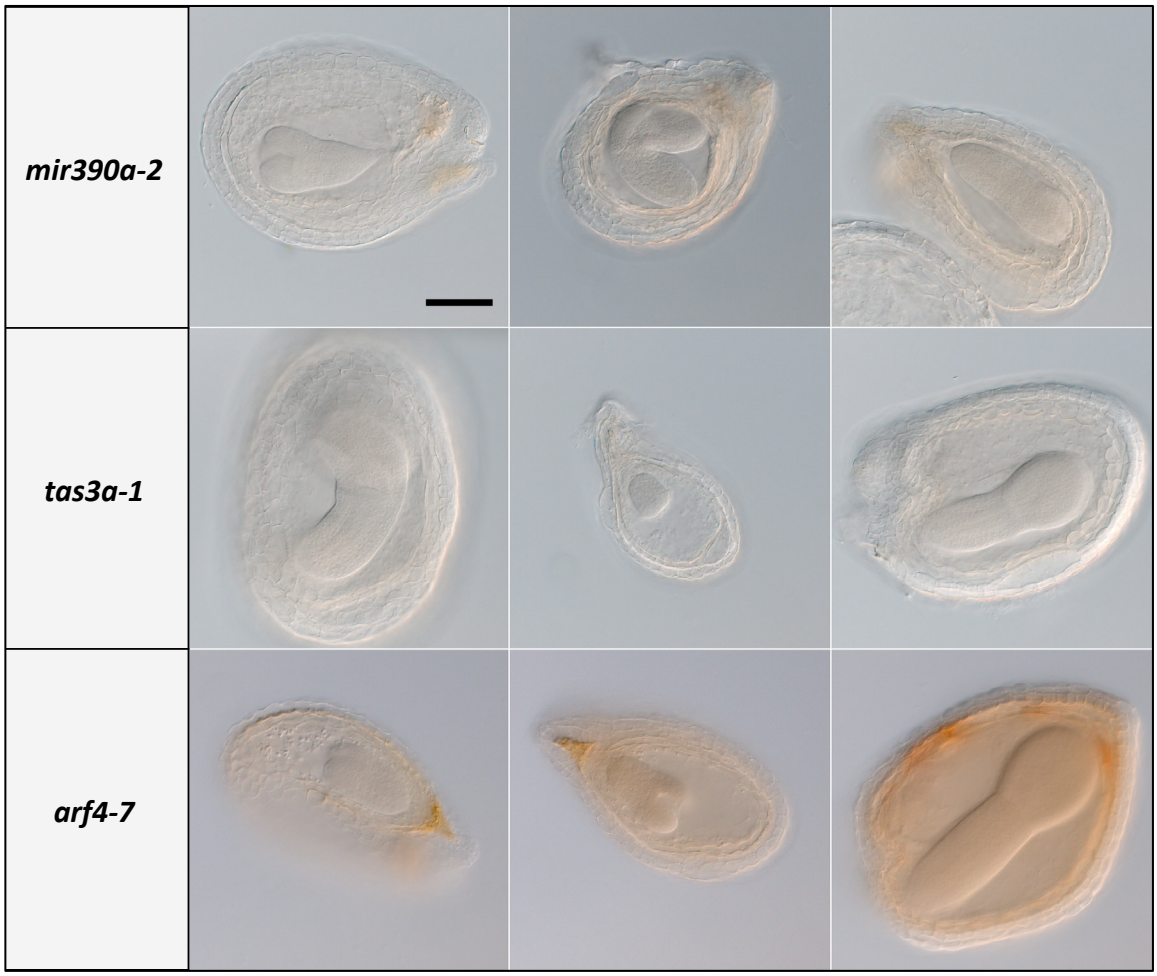

Figure 4-3. Embryo phenotype in *mir390a-2, tas3a-1,* and *arf4-7*. Scale bar: 100 µm.

When aborted seeds were cleared, no aberrant embryo division pattern could be identified, but the endosperm seemed undeveloped, smaller relative to the embryo size.

4.5 In *tas3a-1*, *rdr6*, and arf2-6, mature seeds cluster in the top part of the silique while unfertilized seed cluster in the bottom part of the silique.

In *tas3a-1*, *rdr6*, and arf2-6, an additional phenotype was observed: mature seeds cluster in the top part of the silique while unfertilized seed cluster in the bottom part of the silique (Figure 4-4).

Figure 4-4. *rdr6* opened siliques. Light green and dark green seeds mirror the different developmental stages of the siliques.

This imbalance could be due to defects in the pollen tube growth.

4.6 Mutants as female parents have less seeds and smaller silique

Expression profiles, reduced fertility, and higher abortion rate sustain the hypothesis that the tasiARFs pathway plays a role in embryo or seed development. To verify a possible involvement of the pollen tube (male contribution) in the reduced fertility of *tas3a-1*, *rdr6*, and *arf2-6*, reciprocal crosses with Col-0 were performed (Figure 4-5, Figure 4-6A); if there is a male parental effect, siliques resulting from crosses where Col-0 is use as a pollen donor should not show any imbalance in fertility or seeds distribution (Figure 4-6B).

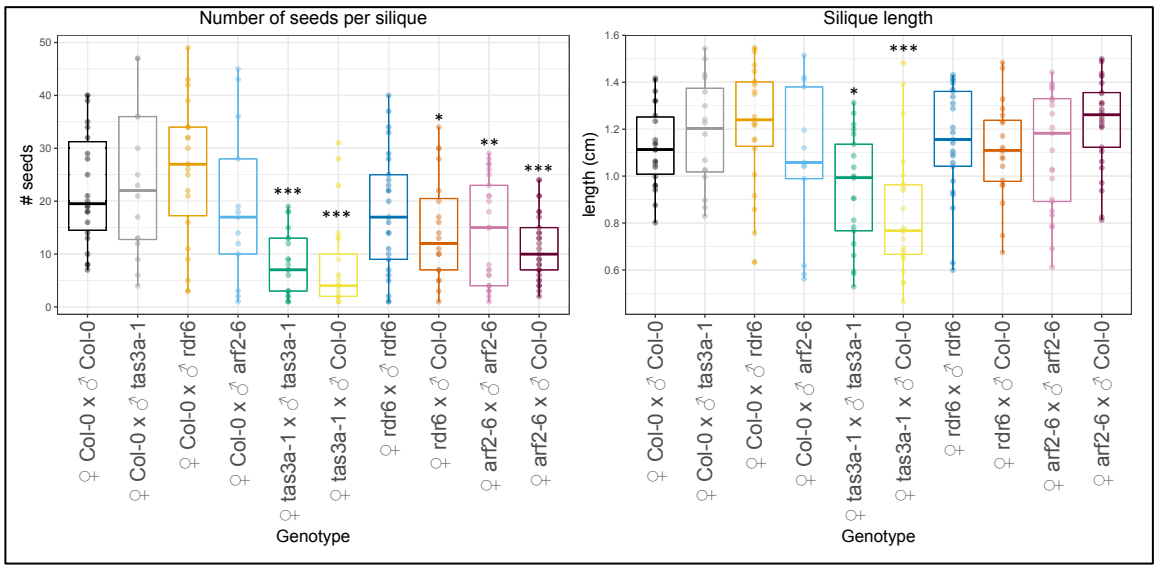

Figure 4-5. Seed number and silique length in *tas3a-1*, *rdr6*, and *arf2-6*, reciprocal crosses with Col-0. ***: p-value <0.001; **: p-value<0.01; *: p-value<0.05

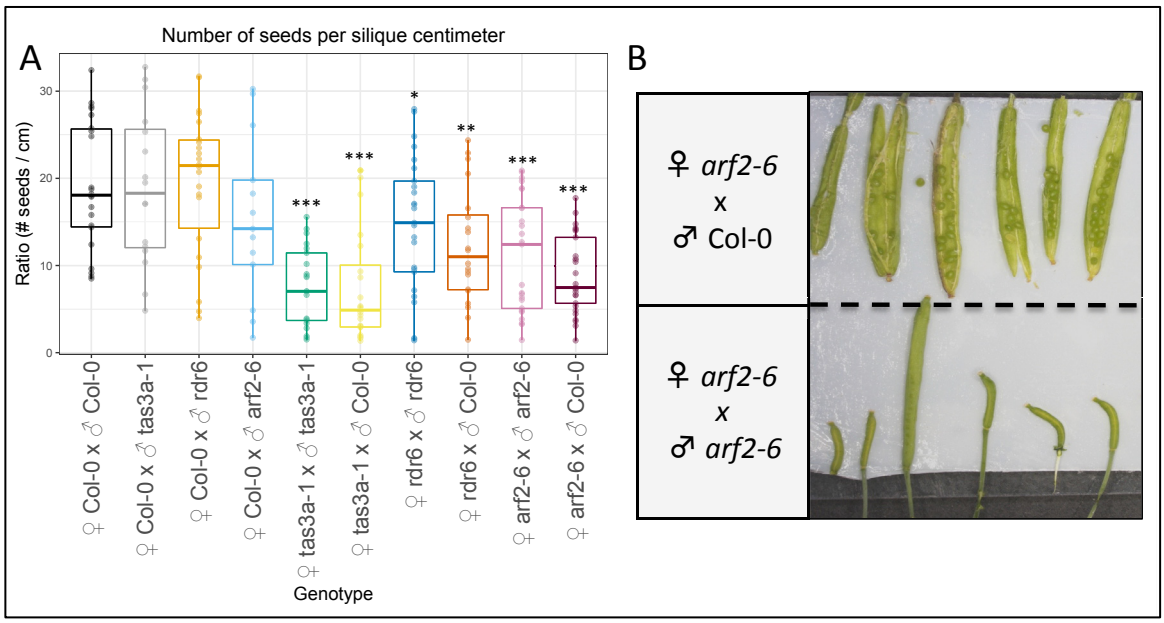

Figure 4-6. A: Number of seeds per silique cm in *tas3a-1*, *rdr6*, and *arf2-6* reciprocal crosses with Col-0. B: *arf2-6* as female parent shows the same phenotype as *arf2-6* selfed. ***: p-value <0.001; **: p-value<0.01; *: p-value<0.05

Seed number per silique, silique length, and normalized seed numbers (number of seeds per silique divided by silique length), all of them show no difference compared to Col-0 pollinated by Col-0 when using mutants as male. On the other hand, when the tasiARFs mutants were used as female, there was a reduction in fertility, especially in the case of *tas3a-1*. The imbalance in seed distribution also persists.

These results seem to exclude a male role in the fertility defects of the tasiARFs mutants.

4.7 Mutant pollen tubes can grow along the whole gynoecium

To rule out a pollen tube growth defect as cause of uneven seed distribution, aniline blue staining of pollen tube was performed (Figure 4-7).

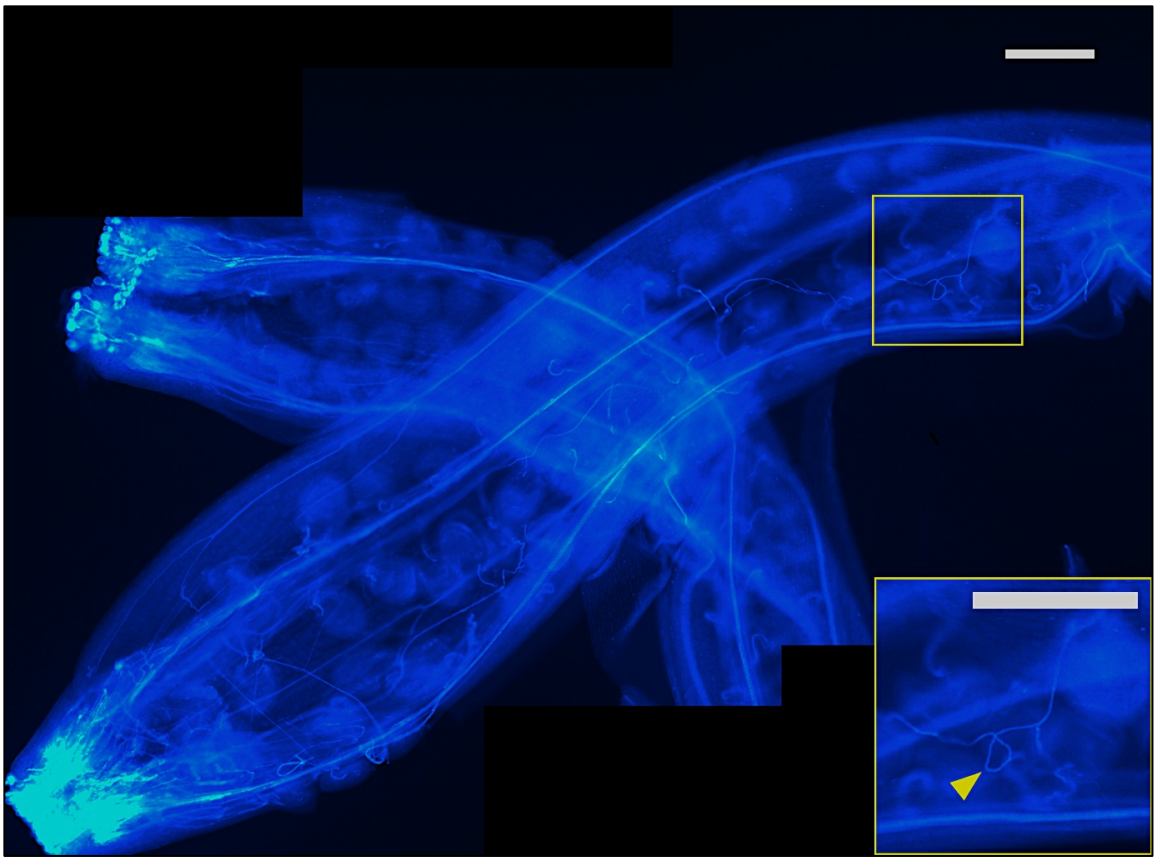

Figure 4-7. Aniline blue staining of pollen tube in *arf2-6* mutants. Yellow arrow point to the pollen tube. Scale bar: 200 µm. Images were stitched using the Pairwise Stitching function of Fiji Stitching plugin(Preibisch *et al.*, 2009).

Pollen tubes behaved normally and were able to grow along the whole gynoecium. Therefore, the hypothesis that a defect in pollen tube growth of the tasiARFs mutant might be the cause for the reduced fertility and the imbalance in seed distribution was discarded.

4.8 MIR390A promoter deletion shows no GUS in siliques or embryos

To check if the putative auxin responsive element (ARE, around 532 bp before ATG start codon) in *MIR390A* promoter, controlling *MIR390A* expression in the primary root tip, controls its expression also in the embryo, gynoecia and embryos of several *MIR390A:GUS-GFP* promoter deletion lines were GUS stained (Figure 4-8, Figure 4-9). The following deletion lines were chosen (Table 4-1):

Table 4-1. *MIR390A:GUS-GFP* promoter deletion lines.

bp before ATG start codon	ARE present	GUS signal in PR	GUS signal in LR
575	+	+	+
555	+	+	+
575	-	-	+
519	-	-	+
94	-	-	-

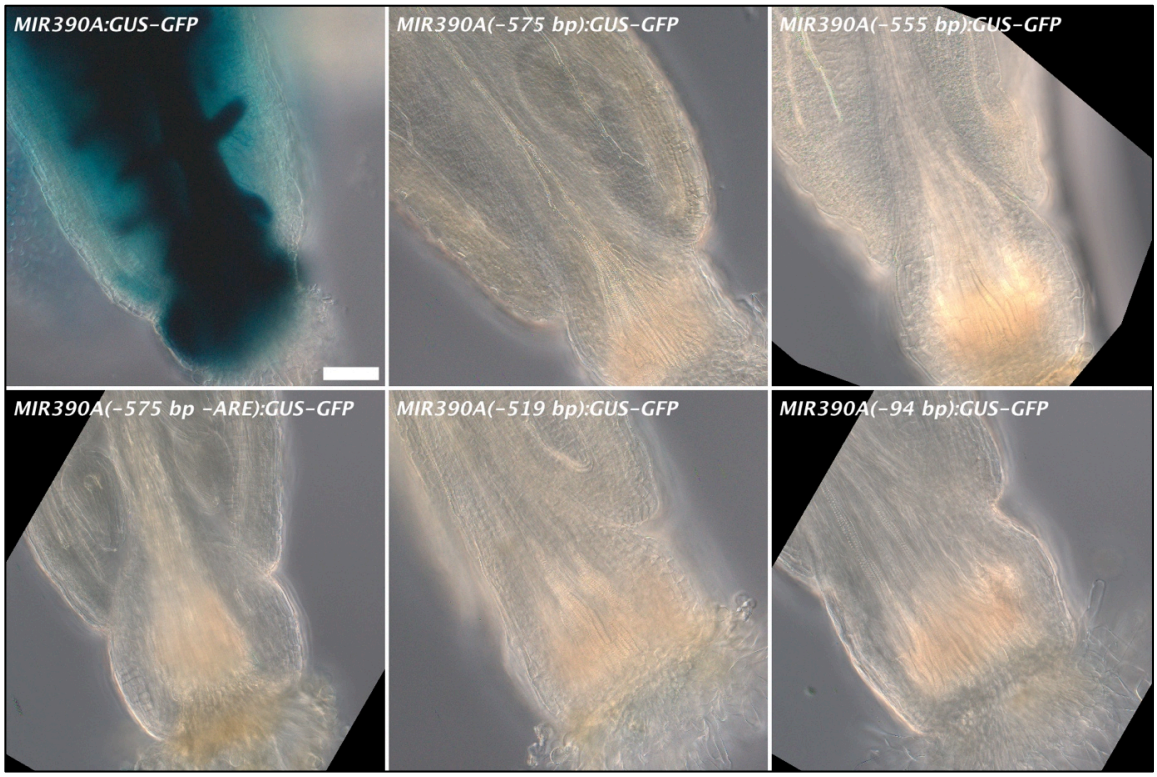

Figure 4-8. GUS staining of *MIR390A:GUS-GFP* promoter deletion line siliques. In brackets, the remaining base pare in *MIR390A* promoter counting from ATG start codon are listed. ARE: putative auxin response element, located around 532 bp before ATG start codon. Scale bar: 200 µm.

Figure 4-9. GUS staining of *MIR390A:GUS*-GFP embryos. Scale bar: 100 µm.

Only the full-length *MIR390A* promoter showed GUS staining in gynoecia and embryos. Therefore, no conclusion could be made about a possible involvement of the putative ARE in *MIR390A* expression in embryo or in the gynoecium.

4.9 Discussion

The evidences obtained from the experiments performed to test a possible role of the tasiARFs pathway in embryo development point to a novel function of this pathway.

The main elements of the tasiARFs pathway are expressed in the embryo (Figure 4-1), and, although a colocalization of the 3 components (MIR390A, *TAS3A, ARF3*) in the embryo would have been ideal, these results are still promising, especially considering that miR390 can act non-cell autonomously(Marin *et al.*, 2010) and that *ARF3* seems to be degraded (*ARF3:ARF3-GUS vs. ARF3:mARF3-GUS*).

The importance of this pathway in embryo development was confirmed by fact that tasiARFs mutants have less seeds per silique and have more aborted seeds (Figure 4-2), while the phenotype of the aborted seeds suggests defects in endosperm development (Figure 4-3). A quantification of this phenotype is however necessary to draw more solid conclusion. Reciprocal crosses between Col-0 and the tasiARFs mutants, (Figure 4-5, Figure 4-6) and aniline blue staining of their pollen tubes (Figure 4-7) do not provide evidences for a paternal role in fertility, but they further confirm a maternal role for this pathway. However, a direct link between the tasiARFs function(s) in embryo development and in the control of seed number cannot be established, because an increase in aborted seed and a decrease in seed number are two phenotypes not always present in the same genotype (Figure 4-2, confront upper and lower panel); furthermore, it has been previously shown that mutants in the tasiARFs pathway have defects in the floral organs and reduced seed number, showing a silique phenotype similar to the one shown in Figure 4-6B (Fahlgren *et al.*, 2006b).

Therefore, a more comprehensive description of the embryo (and the endosperm) development in single or multiple tasiARFs mutants or overexpressor, for example by 4D microscopy, would be necessary to pinpoint the associated developmental defects (for a review about live cell analysis of plant reproduction see (Kurihara *et al.*, 2013), and more specifically for live cell imaging of Arabidopsis early embryogenesis see (Gooh *et al.*, 2015)). Finding the auxin responsive elements (AREs) targeted by ARF2, ARF3, and ARF4 in the embryo, for example by Chip-seq, would help find the downstream genes controlled by the tasiARFs pathway. This, like MONOPTEROS (ARF5) binding to DORNROSCHEN ARE (controlling cell patterning in embryo) (Cole *et al.*, 2009) or to TARGET OF MP 5 (TMO5) and TMO7 AREs (crucial for embryonic root initiation) (Schlereth *et al.*, 2010), would

improve our understanding of auxin signaling in embryo. Furthermore, auxin has been recently showed to regulate endosperm cellularization (Figueiredo *et al.*, 2017), providing a link between the tasiARFs pathway and endosperm development.

Regarding the putative auxin responsive element controlling *MIR390A* expression in the primary root tip, a 575 bp *MIR390A* promoter is likely to short to drive the expression in the embryo (Figure 4-8), so no conclusion can be made about this ARE role in *MIR390A* expression in the embryo. A promoter deletion test with longer fragments would be necessary, and it might uncover yet unidentified AREs.

General conclusion and perspectives

The tasiARFs pathway controls several developmental processes in Arabidopsis (among which lateral root development) and other species, and is highly conserved in land plants (Xia *et al.*, 2017). miR390, the miRNA involved in the generation of the tasiARFs has been previously (Dastidar, 2015; Dastidar *et al.*, 2016), and in this thesis, shown to be present also in the primary root tip and in the embryo. The efforts to unravel how it is controlled and which function(s) it has in the primary root, as well as its role in embryo development and if it interacts with the miR156/SPLs pathway (also controlling lateral root development) were only partially successful. No primary root phenotype could be observed in *mir390a-2*, and no gene controlling its expression in the primary root tip could be clearly identified, although *GRG* is still a plausible candidate. The lack of a reliable detection of miR156 hindered the attempt to test a possible interaction of this miRNA with the tasiARFs pathway in lateral root development. However, in embryo, the expression pattern and activity of the tasiARFs components, and a phenotype in their mutants, suggest a possible role for this pathway in embryo development.

Much remains to be done: obtaining a more reliable reporter for *MIR390A* and achieving a consistency in miR156 measurements are two fundamental tools for further experiments; following in time embryo and endosperm development in tasiARFs mutants is necessary to unravel the function of the tasiARFs pathway in seed development; and testing these mutants in less artificial conditions might finally provide a role for this pathway in primary root development.

Considering the numerous biological functions associated with the tasiARFs pathway, its function as a model system to study tasiRNAs and auxin network robustness and sensitivity, its conservation and the fact that it has been coopted several times to mediate various developmental processes in plants, it is somehow surprising to find only 81 publications in PubMed containing, in the title or in the abstract, a reference to miR390. This suggests that

we are only scraping the surface of our comprehension of this pathway and there is much left worthy to be explored (and it might be not so easy to do it).

Materials and methods

1 Biological resources

1.1 Plant material and growth condition

1.1.1 Tobacco

Nicotiana benthamiana was used for all experiments. A Conviron A1000 was used for growth on soil (Einheitserde CLT SM fein). Plants were grown in long day conditions at 25 °C.

1.1.2 Arabidopsis

Arabidopsis thaliana ecotype Columbia (Col-0) was used as wild type. A Conviron A1000 was used for growth on plate. A growth chamber was used for growth on soil (Einheitserde CLT SM fein). Plants were grown in long day conditions at 22 °C.

1.1.2.1 Media for growth on plate

1.1.2.1.1 Standard

½ MS; 0.8% phyto agar; pH buffered with 0.5 g/l MES and adjusted to 5.8 with KOH.

1.1.2.1.2 Salt stress

1/10 MS; 0.8% agarose; NaCl was used for salt stress.

1.1.2.1.3 Nitrogen deficiency

MS was substituted according to (Yuan *et al.*, 2007); 0.8% phyto agar; pH buffered and adjusted to 5.8 with TRIS; KNO_3 was supplied to provide nitrogen-sufficient conditions and KCl was used to adjust K to a final concentration of 2mM.

1.1.2.1.4 Chemical stocks

MS: Duchefa Biochemie Murashige & Skoog medium and SIGMA-ALDRICH Murashige and Skoog Basal Salt Mixture, both as described by Murashige and Skoog (Murashige *et al.*, 1962).
Phyto agar: Duchefa Biochemie
Agarose: Sigma

1.1.2.2 Mutants

Table 1-1. Mutants

Gene	ATG number	Allele	Allele type	References
MIR390A	AT2G38325	*mir390a-1*	EMS mutant; G94-to-A94 foldback substitution	(Cuperus *et al.*, 2010)
MIR390A	AT2G38325	*mir390a-2*	Wisconsin DsLox T-DNA insertion (WiscDsLox440F06); 30 bp upstream of transcriptional start site	(Marin *et al.*, 2010)

TAS3A	AT3G17185	*tas3a-1*	GABI-KAT T-DNA insertion (GABI_621G08); 108 bp upstream of predicted location	(Adenot *et al.*, 2006)
RDR6	AT3G49500	*sgs2-1*	Single nucleotide substitution (G2474A) leading to a missense mutation (G825E)	(Elmayan *et al.*, 1998)
ARF2	AT5G62000	*arf2-6*	T-DNA insertion located in the 12th exon, after codon G494 (nt T2549 from ATG)	(Okushima *et al.*, 2005)
ARF3	AT2G33860	*ett-2*	T-DNA insertion located 8 bp upstream of ATG, Wassilewskija (WsO) ecotype	(R. A. Sessions *et al.*, 1995)
ARF3	AT2G33860	*arf3-2*	Salk T-DNA insertion (Salk_005658); inserted in exon 10	(Okushima *et al.*, 2005)
ARF3	AT2G33860	*ett-3*	EMS mutant; G1430-to-A1430, nonsense, Landsberg (LaO) ecotype	(R. A. Sessions, 1997)
ARF4	AT5G60450	*arf4-2*	Salk T-DNA insertion (Salk_070506); inserted in exon 10	(Pekker *et al.*, 2005)
ARF4	AT5G60450	*arf4-7*	Salk T-DNA insertion (Salk_028804C); inserted in the 5' untranslated region 376 bp upstream of ATG	(Marin *et al.*, 2010)
GRG	AT1G75860	*salk*	Salk T-DNA insertion (Salk_025523C); inserted in the first intron	(Alonso *et al.*, 2003)
GRG	AT1G75860	*gk*	GABI-KAT T-DNA insertion (GABI_839D07); inserted in the first intron	(Rosso *et al.*, 2003)
BOG	AT1G20100	*bog*	SAIL T-DNA insertion (SAIL_97_B11); inserted in the last exon	(A. Sessions *et al.*, 2002)
SPL9	AT2G42200	*spl9-4*	SAIL T-DNA insertion (SAIL_150_B05); inserted in the first intron	(Wang *et al.*, 2008)
SPL10	AT1G27370	*spl10*	Salk T-DNA insertion (Salk_055643C); inserted in the promoter	(Yu *et al.*, 2015)
SPL15	AT3G57920	*spl15-1*	Salk T-DNA insertion (Salk_074426); inserted in the first intron	(Wang *et al.*, 2008)
SOS1	AT2G01980	*sos-1-1*	EMS mutant; 14bp deletion in the 7th transmembrane domain causing a frameshift	(Shi *et al.*, 2000)

1.1.2.3 Transgenic

Table 1-2. GreenGate(Lampropoulos *et al.*, 2013) based

Name	A-module	B-module	C-module	D-module	E-module	F-module	Z-module
UBQ10:HA-GRG-GFP	$UBQ10_p$ pGGA006	Ala-3xHA	*GRG* CDS + intron	Linker-*GFP* pGGD001	$RBCS_t$ pGGE001	$BASTA^r$ pGGF001	pGGZ001
UBQ10:GRG-GFP	$UBQ10_p$ pGGA006	N-Dummy pGGB003	*GRG* CDS	Linker-*GFP* pGGD001	$UBQ10_t$ pGGE009	$Sulf^r$ pGGF012	pGGZ001
UBQ10:BOG-GFP	$UBQ10_p$ pGGA006	N-Dummy pGGB003	*BOG* CDS	Linker-*GFP* pGGD001	$UBQ10_t$ pGGE009	$Sulf^r$ pGGF012	pGGZ001
GRG:GRG-GFP	2.1 kb *GRG* promoter	N-Dummy pGGB003	*GRG* CDS + intron	Linker-*GFP* pGGD001	$UBQ10_t$ pGGE009	$Sulf^r$ pGGF012	pGGZ001
GRG:H2B-3xGFP	2.1 kb *GRG* promoter	*H2B* CDS + PGGD001 based linker	*3xGFP* pGGC025	D-Dummy pGGD002	$UBQ10_t$ pGGE009	$Sulf^r$ pGGF012	pGGZ001

MIR390A:GFP-GUS-NLS	2 kb *MIR390A* promoter	PGGC025 based *GFP*	*GUS* pGGC051	Linker-*NLS* pGGD007	*RBCSt* pGGE001	*BASTA*^{r} pGGF001	pGGZ001
4.5kb *gGRG* (554 bp terminator)	genomic region amplified with A-Z and E-F overhang primers					*BASTA*^{r} pGGF001	pGGZ001

Table 1-3. pMLBart(Gleave, 1992) based, received by M. G. Dastidar

Name
2.1 kb *gGRG* (146 bp terminator)
4.5 kb *gGRG* (146 bp terminator)

Table 1-4. Gateway (pKGWFS7)(Karimi *et al.*, 2002) based, received by M. G. Dastidar

Name	Description
AM539	*MIR390A:EGFP-GUS*
P5-40	*MIR390A:EGFP-GUS* EMS mutant
P14-6	*MIR390A:EGFP-GUS* EMS mutant
P2-23	*MIR390A:EGFP-GUS* EMS mutant
P5-19	*MIR390A:EGFP-GUS* EMS mutant

UBQ10:H2B-RFP was created by Nicolas Mattes using Gateway (pDONR221) and was available in the lab; miR156-sensitive and miR156-resistant *SPL-GUS* fusion lines ***SPLx:SPLx-GUS*** (**rSPLs** and **sSPLs**, respectively) have been received and described by Scott Poethig (M. Xu *et al.*, 2016); ***35S:MIM156*** (miR156 target mimicry) has been received from Scott Poethig and described by Franco-Zorrilla (Franco-Zorrilla *et al.*, 2007); ***35S:5xMIR156A*** has been received and described by Niu Yu (Yu *et al.*, 2015); ***TAS3A:GUS*** was created by Virginie Jouannet using pBGWFS7 and was available in the lab; ***ARF3:ARF3-GUS*** and ***ARF3:mARF3-GUS*** have been received from James C. Carrington and described by Noah Fahlgren (Fahlgren *et al.*, 2006a); ***MIR390A:GUS-GFP*** promoter deletion lines were created by Ira Mägele and described in (Dastidar, 2015).

1.2 Bacterial strains and growth condition

Lysogeny broth (Bertani, 1951, 2004) (LB) with the appropriate antibiotics was used for both liquid and solid growth media. In the latter case agarose (15g/l) was added.

1.2.1 E. coli

Invitrogen™ TOP10 based electrocompetent cells were used. Growth temperature was 37 °C.

1.2.2 Agrobacterium tumefaciens

ASE (Pruss *et al.*, 2008) electrocompetent cells where used. Growth temperature was 28 °C.

2 Methods

2.1 Recombinant DNA methods

2.1.1 GreenGate

GreenGate constructs were prepared according to (Lampropoulos *et al.*, 2013).

2.1.2 pMLBart

In the received plasmids from Mouli G. Dastidar, constructs were inserted in *Not* I site of binary vector pMLBart, a derivative of pART27 containing the *BAR* gene (Gleave, 1992).

2.1.3 amiRNAs

amiRNAs constructs were prepared according to the protocol by Rebecca Schwab, MPI for Developmental Biology, Tuebingen, 2005 (Ossowski Stephan, Fitz Joffrey, Schwab Rebecca, Riester Markus and Weigel Detlef, personal communication).
(http://wmd3.weigelworld.org/downloads/Cloning_of_artificial_microRNAs.pdf)

2.2 DNA and RNA purification

2.2.1 Agarose gel

DNA was separated by electrophoresis in 1-2% agarose gel, with ethidium bromide for detection and TAE as buffer.

2.2.2 Miniprep

QIAprep Spin Miniprep kit (Qiagen) based method was used. Columns were substituted by 1:1 isopropanol precipitation, and N3 buffer by P3 buffer.

2.2.3 gDNA extraction using Edwards buffer

gDNA extraction using Edward's buffer was performed according to (Edwards *et al.*, 1991).

2.2.4 CTAB gDNA extraction

CTAB gDNA extraction was performed following a modified version of (Healey *et al.*, 2014). DNA was precipitated by adding 1/10 volume of 3 M NA-Acetate and 2.5 volume of absolute alcohol.

2.2.5 RNA extraction kit

mRNA was extracted using and according to a GeneMATRIX Universal RNA Purification Kit (Roboklon)

2.2.6 RNA total extraction

Total RNA was extracted according to (Mallory *et al.*, 2001).

2.2.7 DNA extraction from gels

DNA was extracted from gels using and according to GeneJET Gel Extraction Kit (Thermo Scientific).

2.3 DNA and RNA amplification and quantification

2.3.1 PCR

2.3.1.1 Genotyping

For genotyping, JumpStart™ REDTaq® ReadyMix™ Reaction Mix (Sigma-Aldrich) was used according to the producer.

2.3.1.2 Cloning

For cloning, Q5® High-Fidelity DNA Polymerase (NEB) was used according to the producer.

2.3.1.3 Semi-quantitative PCR

For Semi-quantitative PCR, JumpStart™ REDTaq® ReadyMix™ Reaction Mix (Sigma-Aldrich) was used according to the producer. 1 µl cDNA was used as template.

2.3.1.4 qPCR

qPCR was performed using and according to ABsolute qPCR SYBR Green Mix (Thermo Scientific). 2 µl of 1:5 cDNA dilution were used as template. A DNA Engine Opticon 2 System (BioRad) was used for detection.

2.3.2 Diagnostic digest

Diagnostic digest was performed using and according to FastDigest Restriction Enzymes (Thermo Scientific).

2.3.3 cDNA preparation

cDNA was prepared using and according to the SuperScript™ II Reverse Transcriptase (Thermofisher) kit. 2 µg RNA were used as template. For cDNA synthesis from miRNAs, 1 µl of a 1 µM miRNA-specific stem-loop primer(Varkonyi-Gasic *et al.*, 2007) was added to the reverse transcription reaction mix.

2.3.4 Northern Blot

Northern blot was performed according to (Marin *et al.*, 2010). 5 µg RNA were separated in a denaturing 15% Acrylamide (19:1) 7M Urea gel, blotted and cross-linked with 1-Ethyl-3-[3-dimethylaminopropyl]carbodiimide hydrochloride (EDC). Probes were labeled using T4 polynucleotide kinase and ^{32}P- $^{\gamma}$ATP and RNA was hybridized overnight at 50°C. After 1day exposition, a Typhoon (GE Healthcare) bimolecular imager was used for detection and quantification.

2.3.5 NanoDrop

RNA and DNA were quantified using a NanoDrop 2000 (Thermofisher).

2.4 Transformation

2.4.1 Tobacco transient transformation and amiRNA activity

For testing amiRNAs activity in *N. benthamiana*, young leaves of 5-week old plants were infiltrated with a suspension of *A. tumefaciens* carrying the constructs of interest according to a modified version of (Batoko *et al.*, 2000). Agrobacteria were grown overnight at 28°C in LB medium plus the appropriate antibiotics. After centrifugation, the pellet was re-suspended in water to reach an OD of 0.8. A mix of equal volume of amiRNA, target-GFP, and control-RFP was infiltrated. After 3 days, transformed leaves disks were snap-frozen, grinded, and proteins were extracted adding 300 µl of extraction buffer (100 mM Tris pH 7.5, 150 mM NaCl, 0.1% Tween20, and 0.1% fresh β-mercaptoethanol). After centrifugation, the supernatant was transferred into plates and GFP and RFP were measured with a Tecan Infinite M1000 plate reader.

Table 2-1. GreenGate based plasmids for tobacco infiltration

Name	A-module	B-module	C-module	D-module	E-module	F-module	Z-module
UBQ10:GRG-GFP	$UBQ10_p$ pGGA006	N-Dummy pGGB003	GRG CDS	Linker-*GFP* pGGD001	$UBQ10_t$ pGGE009	$Sulf^r$ pGGF012	pGGZ001
UBQ10:BOG-GFP	$UBQ10_p$ pGGA006	N-Dummy pGGB003	BOG CDS	Linker-*GFP* pGGD001	$UBQ10_t$ pGGE009	$Sulf^r$ pGGF012	pGGZ001
UBQ10:amiGRG #1	$UBQ10_p$ pGGA006	-	amiRNA against *GRG* #1	-	$UBQ10_t$ pGGE009	$Sulf^r$ pGGF012	pGGZ001
UBQ10:amiGRG #2	$UBQ10_p$ pGGA006	-	amiRNA against *GRG* #2	-	$UBQ10_t$ pGGE009	$Sulf^r$ pGGF012	pGGZ001
UBQ10:amiGRG #3	$UBQ10_p$ pGGA006	-	amiRNA against *GRG* #3	-	$UBQ10_t$ pGGE009	$Sulf^r$ pGGF012	pGGZ001
UBQ10:amiBOG #1	$UBQ10_p$ pGGA006	-	amiRNA against *BOG* #1	-	$UBQ10_t$ pGGE009	$Sulf^r$ pGGF012	pGGZ001
UBQ10:amiBOG #2	$UBQ10_p$ pGGA006	-	amiRNA against *BOG* #2	-	$UBQ10_t$ pGGE009	$Sulf^r$ pGGF012	pGGZ001
UBQ10:amiBOG #3	pGGA006	-	amiRNA against *BOG* #3	-	$UBQ10_t$ pGGE009	$Sulf^r$ pGGF012	pGGZ001
UBQ10:amiGRG/BOG #1	$UBQ10_p$ pGGA006	-	amiRNA against *GRG* and *BOG* #1	-	$UBQ10_t$ pGGE009	$Sulf^r$ pGGF012	pGGZ001
UBQ10:amiGRG/BOG #2	$UBQ10_p$ pGGA006	-	amiRNA against *GRG* and *BOG* #2	-	$UBQ10_t$ pGGE009	$Sulf^r$ pGGF012	pGGZ001

UBQ10:amiGRG/BOG #3	$UBQ10_p$ pGGA006	-	amiRNA against *GRG* and *BOG* #3	-	$UBQ10_t$ pGGE009	$Sulf^r$ pGGF012	pGGZ001

2.4.2 Arabidopsis floral dip

A 3-5 ml LB pre-culture of *A. tumefaciens* carrying the constructs of interest was grown at 28° C overnight. 100 µl of pre-culture were used to inoculate 250 ml LB, and the secondary culture was grown overnight at 28°C. Cultures were pelleted and re-suspended in a solution of ½ MS, 5% sucrose, and 50 µl/l of Silwet L-77. Re-suspended pellet was used to dip the inflorescence.

2.4.3 Bacterial electroporation

Bacterial electroporation was performed using a MicroPulser™ Electroporation Apparatus (Bio-Rad) according to the producer.

2.5 Staining

2.5.1 GUS staining

GUS activity was assayed at 37°C overnight according to a modified version of (Weigel *et al.*, 2002). In this case, the initial washing with staining buffer without X-Gluc was omitted. For roots, but not for embryos, vacuum was also not applied.

2.5.2 Propidium iodide (PI) staining of roots

PI staining of roots was performed according to (Truernit & Haseloff, 2008).

2.5.3 Modified pseudo-Schiff propidium iodide (mPS-PI) staining of roots

mPS-PI staining of roots was performed according to (Truernit, Bauby, *et al.*, 2008).

2.5.4 Aniline blue staining of pollen tubes

Aniline blue staining of pollen tubes was performed according to (Mori *et al.*, 2006).

2.5.5 Root whole mount ISH to detect miR156 and miR390

Root whole mount ISH to detect miR156 and miR390 was performed according to (Dastidar *et al.*, 2016).

2.6 Clearing and fixation

2.6.1 Root clearing

Root were cleared with modified protocol from (Malamy *et al.*, 1997). Seedling were submerged in a solution of 4% HCl and 20% methanol, and incubated 15 minutes at 70°C. The solution was changed to 7% NaOH and 60% ethanol, and incubated 15 minutes at room temperature. Plants were rehydrated in 40, 20, and 10% ethanol, and 25% glycerol plus 5% ethanol 5 minutes each step, and mounted in 50% glycerol on slides.

2.6.2 Formaldehyde – acetic acid – ethanol (FAA) root fixation

Samples were submerged with FAA (50% EtOH, 10% acetic acid, 5% formaldehyde) for 30 min.

2.6.3 Embryo clearing with chloral hydrate

Clearing of embryos with chloral hydrate was performed according to the protocol written by Dr. Miguel Aguilar in Professor Robert L. Fischer laboratory at University of California, Berkley. (https://www.mcdb.ucla.edu/Research/Goldberg/HC70AL_S08/pdf/Expt8protocol.pdf)

2.7 Imaging

2.7.1 Confocal microscopy

Leica DMI8-CS with HC PL APO CS2 40x/1.30 or HC PL APO CS2 20x/0.75 objectives was used. Excitation wavelength was set at 488 nm for GFP, and 532 nm for RFP and PI. Emission was detected at 500-545 nm for GFP, and 620-670 nm for RFP and PI.

2.7.2 Epifluorescence microscopy

Zeiss Axio Imager M1 with an AxioCamHR3_552 and Plan-Apochromat 20x/0.8 M27 or EC Plan-Neofluar 40x/0.75 M27 objectives was used.

2.7.3 DIC microscopy

Zeiss Axio Imager M1 with an AxioCamHR3_552 and Plan-Apochromat 20x/0.8 M27 or EC Plan-Neofluar 40x/0.75 M27 objectives was used.

2.8 Statistical analysis

p-values were extracted from t tests running ANOVA as Linear Regression Analysis, using Col-0 as reference, with the following significance codes: ***: p-value <0.001; **: p-value<0.01; *: p-value<0.05. In case of qPCRs, no statistical analysis was performed due to the low sample number (only 1 biological replicate).

2.9 Software

R and R studio

Charts and statistical analysis were performed using R (R Core Team (2016). R: A language and environment for statistical computing. R Foundation for Statistical Computing, Vienna,Austria. URL https://www.R-project.org/) and R studio (RStudio Team (2015). RStudio: Integrated Development for R. RStudio, Inc., Boston, MA URL http://www.rstudio.com/).

Fiji

Image analysis and figure mounting were performed using Fiji (Schindelin *et al.*, 2012).

Geneious

in silico molecular biology was performed using Geneious (Kearse *et al.*, 2012).

GIMP

Jpeg2000 to TIF was performed using GIMP (URL http://gimp.org/).

HP Scan

Plates were scanned using HP Scanjet G2410 scanner and HP Scan software.

FileMaker Pro

The lab database was created and has been managed using FileMaker Pro (URL http://www.filemaker.com/).

Microsoft Office

Microsoft Office for Mac 2011(https://www.microsoft.com/) was used for text editing, spreadsheeting, and figure mounting.

EndNote

EndNote (http://endnote.com/) was used as reference manager.

Mac OSX

Mac OS X was used as operative system (https://www.apple.com/).

TAIR

For data about genetic and molecular biology of Arabidopsis, TAIR(Berardini *et al.*, 2015) was used.

miRBase

For information about miRNA, miRBase(Griffiths-Jones, 2004; Griffiths-Jones *et al.*, 2006; Griffiths-Jones *et al.*, 2008; Kozomara *et al.*, 2011, 2014) was used.

Primer-BLAST

To test primer specificity, Primer-BLAST was used.

SIGnAL

For information about T-DNA lines and primers to genotype them, SIGnAL(O'Malley *et al.*, 2015) was used.

Web MicroRNA Designer

The Web MicroRNA Designer (Ossowski Stephan, Fitz Joffrey, Schwab Rebecca, Riester Markus and Weigel Detlef, personal communication) was used to design amiRNAs

Appendix I: primers used in this thesis

Name	Sequence	Purpose
P-0015	GCACCCTGTTCTTCTTACCG	semi-qPCR for At3g18780; *ACTIN2*
P-0016	AACCCTCGTAGATTGGCACA	semi-qPCR for At3g18780; *ACTIN2*
P-0017	TAACGTGGCCAAAATGATGC	qPCR for AT1G13320; PP2A subunit PD
P-0018	GTTCTCCACAACCGCTTGGT	qPCR for AT1G13320; PP2A subunit PD
P-1372	CCCGCAATTCCTCTAGGCTT	semi-qPCR for At1G75870
P-1373	CGCAAGGTCTCTACACAAGTC	semi-qPCR for At1G75870
P-1374	ACAGATGAGCTTGAGGAACCTC	semi-qPCR for *GRG* qPCR for *GRG*
P-1375	TGGAGCAAACAACAGCCTCT	semi-qPCR for *GRG* qPCR for *GRG*
P-1376	ATGGCTAGTGCAACCAGAGG	semi-qPCR for *VPS35B*
P-1377	TCTCACCCATCAAACCACCT	semi-qPCR for *VPS35B*
P-1218	GTGCGCCCTGGAAAAAAAAAAAGA	Sequencing of *VPS35B*
P-1219	CATCTTGAGATAGATCTCTATATA	Sequencing of *VPS35B*
P-1228	TCTTTCCTGATGAGTACCATTTGC	Sequencing of *VPS35B*
P-1232	TATGTATGAGACGGGCTACTGAAT	Sequencing of *VPS35B*
P-1320	AGTGCTGATAGTGAATTCAATAGAAAA	Sequencing of *VPS35B*
P-1321	CCGTGTGGTTTGCAGTGAGAAACTCTG	Sequencing of *VPS35B*
P-1380	ACTAGAAAATGGCAATCTCCTCC	Sequencing of *VPS35B*
P-1381	GCAATTGGAAAGGTGGGTTCC	Sequencing of *VPS35B*
P-1382	GACAAGCGGTTGACTTTACGAG	Sequencing of *VPS35B*
P-1383	GGCAGAATCTGACATAGCATTCT	Sequencing of *VPS35B*
P-1363	AACAGGTCTCAACCTTTTGCGCGCTCCTTTGTTTC	Cloning of *GRG* 2.1kb promoter

P-1365	AACAGGTCTCTTGTTACCCAAGATTAGCTTCAGATTCA	Cloning of *GRG* 2.1kb promoter
P-1336	CCGAGCCAGTAGTCGTCTATG	Genotyping of *GRG* Salk (Salk_025523C) and GABI-KAT (GABI_839D07) T-DNA insertion lines
P-1337	TCCTTCTTCTCTATCCGGTGC	Genotyping of *GRG* Salk (Salk_025523C) and GABI-KAT (GABI_839D07) T-DNA insertion lines
P-0194	GCGTGGACCGCTTGCTGCAACT	Genotyping of *GRG* Salk T-DNA insertion line (Salk_025523C); Salk LBb1
P-0096	ATATTGACCATCATACTCATTGC	Genotyping of *GRG* GABI-KAT T-DNA insertion line (GABI_839D07); GK o8409
P-1420	TGATAATTTCGACGTGAAGGG	Genotyping of *BOG* SAIL T-DNA insertion (SAIL_97_B11)
P-1421	TGTTTGTTCCACTTCAGGGAC	Genotyping of *BOG* SAIL T-DNA insertion (SAIL_97_B11)
P-0120	TAGCATCTGAATTTCATAACCAATCTCGATACAC	Genotyping of *BOG* SAIL T-DNA insertion (SAIL_97_B11); Sail LB3
P-1533	CCTCAGGTTGGATATTTGTCTGA	semi-qPCR for *BOG*
P-1534	AGCCACATCATGATCACAGAT	semi-qPCR for *BOG*
P-1185	AACAGGTCTCAGGCTCAACAATGTCGCGCGTTCTCACTTGCCCAC	Cloning of *GRG* CDS + introns minus stop codon
P-1186	AACAGGTCTCTCTGAGAACGGGACAGTATAAGGTAAAGAA	Cloning of *GRG* CDS + introns minus stop codon
P-1425	AACAGGTCTCAGGCTCAACAATGTCACGATATTTCACATCCCC	Cloning of *BOG* CDS minus stop codon
P-1426	AACAGGTCTCTCTGAAAACGGGACAGTATATGGTAATGA	Cloning of *BOG* CDS minus stop codon
P-0950	AACAGGTCTCAAACACTGCAGCCCCAAACACACGC	Generating amiRNAs; oligo A
P-0951	AACAGGTCTCTGCAGCCCCATGGCGATGCC	Generating amiRNAs; oligo B
P-1428	GATGTTTATGCGATTTGTCACGCTCTCTCTTTTGTATTCC	Generating amiRNA against *GRG* #1; oligo I
P-1429	GAGCGTGACAAATCGCATAAACATCAAAGAGAATCAATGA	Generating amiRNA against *GRG* #1; oligo II
P-1430	GAGCATGACAAATCGGATAAACTTCACAGGTCGTGATATG	Generating amiRNA against *GRG* #1; oligo III
P-1431	GAAGTTTATCCGATTTGTCATGCTCTACATATATATTCCT	Generating amiRNA against *GRG* #1; oligo IV
P-1432	GATTAGTGAGTCAGACTTACCTGTCTCTCTTTTGTATTCC	Generating amiRNA against *GRG* #2; oligo I
P-1433	GACAGGTAAGTCTGACTCACTAATCAAAGAGAATCAATGA	Generating amiRNA against *GRG* #2; oligo II
P-1434	GACAAGTAAGTCTGAGTCACTATTCACAGGTCGTGATATG	Generating amiRNA against *GRG* #2; oligo III

P-1435	GAATAGTGACTCAGACTTACTTGTCTACATATATATTCCT	Generating amiRNA against *GRG* #2; oligo IV
P-1436	GATTTATGCGATTTCTCACGCGTTCTCTCTTTTGTATTCC	Generating amiRNA against *GRG* #3; oligo I
P-1437	GAACGCGTGAGAAATCGCATAAATCAAAGAGAATCAATGA	Generating amiRNA against *GRG* #3; oligo II
P-1438	GAACACGTGAGAAATGGCATAATTCACAGGTCGTGATATG	Generating amiRNA against *GRG* #3; oligo III
P-1439	GAATTATGCCATTTCTCACGTGTTCTACATATATATTCCT	Generating amiRNA against *GRG* #3; oligo IV
P-1440	GATAGTTTTGACCGTTCGCGCAGTCTCTCTTTTGTATTCC	Generating amiRNA against *BOG* #1; oligo I
P-1441	GACTGCGCGAACGGTCAAAACTATCAAAGAGAATCAATGA	Generating amiRNA against *BOG* #1; oligo II
P-1442	GACTACGCGAACGGTGAAAACTTTCACAGGTCGTGATATG	Generating amiRNA against *BOG* #1; oligo III
P-1443	GAAAGTTTTCACCGTTCGCGTAGTCTACATATATATTCCT	Generating amiRNA against *BOG* #1; oligo IV
P-1444	GATGGTAATTCGCTAGGTCGCTGTCTCTCTTTTGTATTCC	Generating amiRNA against *BOG* #2; oligo I
P-1445	GACAGCGACCTAGCGAATTACCATCAAAGAGAATCAATGA	Generating amiRNA against *BOG* #2; oligo II
P-1446	GACAACGACCTAGCGTATTACCTTCACAGGTCGTGATATG	Generating amiRNA against *BOG* #2; oligo III
P-1447	GAAGGTAATACGCTAGGTCGTTGTCTACATATATATTCCT	Generating amiRNA against *BOG* #2; oligo IV
P-1448	GATTTGGTAATTCGCTAGGTCTGTCTCTCTTTTGTATTCC	Generating amiRNA against *BOG* #3; oligo I
P-1449	GACAGACCTAGCGAATTACCAAATCAAAGAGAATCAATGA	Generating amiRNA against *BOG* #3; oligo II
P-1450	GACAAACCTAGCGAAATACCAATTCACAGGTCGTGATATG	Generating amiRNA against *BOG* #3; oligo III
P-1451	GAATTGGTATTTCGCTAGGTTTGTCTACATATATATTCCT	Generating amiRNA against *BOG* #3; oligo IV
P-1452	GACGACCAAGTTTTGACCGTCCGTCTCTCTTTTGTATTCC	Generating amiRNA against *GRG* and *BOG* #1; oligo I
P-1453	GACGGACGGTCAAAACTTGGTCGTCAAAGAGAATCAATGA	Generating amiRNA against *GRG* and *BOG* #1; oligo II
P-1454	GACGAACGGTCAAAAGTTGGTCGTCACAGGTCGTGATATG	Generating amiRNA against *GRG* and *BOG* #1; oligo III
P-1455	GACGACCAACTTTTGACCGTTCGTCTACATATATATTCCT	Generating amiRNA against *GRG* and *BOG* #1; oligo IV
P-1456	GAGTAGAGGTTTACCTGCTACAGTCTCTCTTTTGTATTCC	Generating amiRNA against *GRG* and *BOG* #2; oligo I
P-1457	GACTGTAGCAGGTAAACCTCTACTCAAAGAGAATCAATGA	Generating amiRNA against *GRG* and *BOG* #2; oligo II
P-1458	GACTATAGCAGGTAATCCTCTACTCACAGGTCGTGATATG	Generating amiRNA against *GRG* and *BOG* #2; oligo III

P-1459	GAGTAGAGGATTACCTGCTATAGTCTACATATATATTCCT	Generating amiRNA against *GRG* and *BOG* #2; oligo IV
P-1460	GATCCGTAGTGGTTTACCAGCTATCTCTCTTTTGTATTCC	Generating amiRNA against *GRG* and *BOG* #3; oligo I
P-1461	GATAGCTGGTAAACCACTACGGATCAAAGAGAATCAATGA	Generating amiRNA against *GRG* and *BOG* #3; oligo II
P-1462	GATAACTGGTAAACCTCTACGGTTCACAGGTCGTGATATG	Generating amiRNA against *GRG* and *BOG* #3; oligo III
P-1463	GAACCGTAGAGGTTTACCAGTTATCTACATATATATTCCT	Generating amiRNA against *GRG* and *BOG* #3; oligo IV
P-1518	AACAGGTCTCAACCTGTGGCCAAACTCTTGATCGT	Cloning of *MIR390A* 2kb promoter
P-1519	AACAGGTCTCTTGTTGAGGAAGAAGGAGAAGAGAAGGTGC	Cloning of *MIR390A* 2kb promoter
P-1165	ACAAAAACGTACGTACAGTGCTGCGGCCGCATTCTTAT	Cloning of 4.5 and 2.1 kb *gGRG* (146 bp terminator)
P-1166	TAAACTATGCGGCCGCATATCGGAGACTCGGACCGA	Cloning of 2.1 kb *gGRG* (146 bp terminator)
P-1167	TAAACTATGCGGCCGCCGCACTAGCAGTACGAAGGT	Cloning of 4.5 kb *gGRG* (146 bp terminator)
P-1514	AACAGGTCTCAACCTTGTCCACATGTGTTTCGCCT	Cloning of 4.5 kb *gGRG* (554 bp terminator)
P-1515	AACAGGTCTCTTAGTGGAGAGAGCTTGGAGGTTCG	Cloning of 4.5kb *gGRG* (554 bp terminator)
P-1181	AACATGATCTTCTTCTTGAATGTCT	Sequencing of *GRG* to identify P5-40 mutation
P-1092	GCGCACCGGATAGAGAAGAA	Amplification of *GRG* to identify P5-40 mutation by Eco130I digestion
P-1093	GCGACTTTGCAACTGTAGTGG	Amplification of *GRG* to identify P5-40 mutation by Eco130I digestion
P-1313	GTCGTATCCAGTGCAGGGTCCGAGGTATTCGCACTGGATACGACGTGCTC	Stem loop primer for miR156 RT
P-1317	GTCGTATCCAGTGCAGGGTCCGAGGTATTCGCACTGGATACGACGGCGCT	Stem loop primer for miR390 RT
P-1546	GTCGTATCCAGTGCAGGGTCCGAGGTATTCGCACTGGATACGACATGCAG	Stem loop primer for miR172 RT
P-1314	GCGGCGGTGACAGAAGAGAGT	Forward qPCR primer for miR156
P-1318	GAAGAGAAGCTCAGGAGGGAT	Forward qPCR primer for miR390
P-1551	GCGGGAGAATCTTGATGATG	Forward qPCR primer for miR172
P-1319	GTGCAGGGTCCGAGGT	Universal reverse qPCR primer for miRNAs
P-1697	GATCTCTGAAGTTGGACTAATT	qPCR for pri-miR156a
P-1698	AGACAGAGAAAGATTGTGTAAG	qPCR for pri-miR156a

P-1699	TCCATCTAGGTTTTTTTGAATTAGT	qPCR for pri-miR156b
P-1700	CGATCAAAGAAAGAAATGTCTAA	qPCR for pri-miR156b
P-1701	TTTAGTGTCATAACTAGATAAATATATG	qPCR for pri-miR156d
P-1702	CATAACTAGAACAATGGAATAAGG	qPCR for pri-miR156d
P-1703	GTCACATGCGTAGAGTGTGAAAGG	qPCR for pri-miR156e
P-1704	CCATGTGTGCTCACTCTCTTCTGT	qPCR for pri-miR156e
P-1309	TAGAGAAGAATCTGTAAAGCTCAGGA	qPCR for pri-miR390a
P-1310	AGAAGAGCCAATGAAACTCAGG	qPCR for pri-miR390a
P-1554	GTTCTCAGCAGGGAAATCCAACA	qPCR for *SPL10*
P-1555	CGGTGGTTCGGCCACGGGAGTGT	qPCR for *SPL10*

References

Adenot, X., Elmayan, T., Lauressergues, D., Boutet, S., Bouche, N., Gasciolli, V., & Vaucheret, H. (2006). DRB4-dependent TAS3 trans-acting siRNAs control leaf morphology through AGO7. *Current Biology, 16*(9), 927-932. doi:10.1016/j.cub.2006.03.035

Alonso, J. M., Stepanova, A. N., Leisse, T. J., Kim, C. J., Chen, H. M., Shinn, P., . . . Ecker, J. R. (2003). Genome-wide Insertional mutagenesis of Arabidopsis thaliana. *Science, 301*(5633), 653-657. doi:DOI 10.1126/science.1086391

Axtell, M. J. (2017). Lost in translation? microRNAs at the rough ER. *Trends in Plant Science, 22*(4), 273-274. doi:10.1016/j.tplants.2017.03.002

Band, L. R., Wells, D. M., Fozard, J. A., Ghetiu, T., French, A. P., Pound, M. P., . . . Bennett, M. J. (2014). Systems Analysis of Auxin Transport in the Arabidopsis Root Apex. *Plant Cell, 26*(3), 862-875. doi:10.1105/tpc.113.119495

Batoko, H., Zheng, H. Q., Hawes, C., & Moore, I. (2000). A Rab1 GTPase is required for transport between the endoplasmic reticulum and Golgi apparatus and for normal Golgi movement in plants. *Plant Cell, 12*(11), 2201-2217. doi:DOI 10.1105/tpc.12.11.2201

Berardini, T. Z., Reiser, L., Li, D. H., Mezheritsky, Y., Muller, R., Strait, E., & Huala, E. (2015). The arabidopsis information resource: Making and mining the "gold standard" annotated reference plant genome. *Genesis, 53*(8), 474-485. doi:10.1002/dvg.22877

Bertani, G. (1951). Studies on Lysogenesis .1. The Mode of Phage Liberation by Lysogenic Escherichia-Coli. *Journal of Bacteriology, 62*(3), 293-300.

Bertani, G. (2004). Lysogeny at mid-twentieth century: P1, P2, and other experimental, systems. *Journal of Bacteriology, 186*(3), 595-600. doi:10.1128/Jb.186.3.595-600.2004

Boer, D. R., Freire-Rios, A., van den Berg, W. A., Saaki, T., Manfield, I. W., Kepinski, S., . . . Coll, M. (2014). Structural basis for DNA binding specificity by the auxin-dependent ARF transcription factors. *Cell, 156*(3), 577-589. doi:10.1016/j.cell.2013.12.027

Borges, F., & Martienssen, R. A. (2015). The expanding world of small RNAs in plants. *Nat Rev Mol Cell Biol, 16*(12), 727-741. doi:10.1038/nrm4085

Borsani, O., Zhu, J., Verslues, P. E., Sunkar, R., & Zhu, J. K. (2005). Endogenous siRNAs derived from a pair of natural cis-antisense transcripts regulate salt tolerance in Arabidopsis. *Cell, 123*(7), 1279-1291. doi:10.1016/j.cell.2005.11.035

Brown, R. C., Lemmon, B. E., Nguyen, H., & Olsen, O. A. (1999). Development of endosperm in Arabidopsis thaliana. *Sexual Plant Reproduction, 12*(1), 32-42. doi:DOI 10.1007/s004970050169

Burkart-Waco, D., Ngo, K., Lieberman, M., & Comai, L. (2015). Perturbation of parentally biased gene expression during interspecific hybridization. *Plos One, 10*(2), e0117293. doi:10.1371/journal.pone.0117293

Capron, A., Chatfield, S., Provart, N., & Berleth, T. (2009). Embryogenesis: pattern formation from a single cell. *Arabidopsis Book, 7*, e0126. doi:10.1199/tab.0126

Cardarelli, M., & Cecchetti, V. (2014). Auxin polar transport in stamen formation and development: how many actors? *Front Plant Sci, 5*. doi:ARTN 333
10.3389/fpls.2014.00333

Cole, M., Chandler, J., Weijers, D., Jacobs, B., Comelli, P., & Werr, W. (2009). DORNROSCHEN is a direct target of the auxin response factor MONOPTEROS in the Arabidopsis embryo. *Development, 136*(10), 1643-1651. doi:10.1242/dev.032177

Couzigou, J. M., & Combier, J. P. (2016). Plant microRNAs: key regulators of root architecture and biotic interactions. *New Phytologist, 212*(1), 22-35. doi:10.1111/nph.14058

Crawford, B. C., & Yanofsky, M. F. (2011). HALF FILLED promotes reproductive tract development and fertilization efficiency in Arabidopsis thaliana. *Development, 138*(14), 2999-3009. doi:10.1242/dev.067793

Cuperus, J. T., Montgomery, T. A., Fahlgren, N., Burke, R. T., Townsend, T., Sullivan, C. M., & Carrington, J. C. (2010). Identification of MIR390a precursor processing-defective mutants in Arabidopsis by direct genome sequencing. *Proc Natl Acad Sci U S A, 107*(1), 466-471. doi:10.1073/pnas.0913203107

da Costa, C. T., de Almeida, M. R., Ruedell, C. M., Schwambach, J., Maraschin, F. S., & Fett-Neto, A. G. (2013). When stress and development go hand in hand: main hormonal controls of adventitious rooting in cuttings. *Front Plant Sci, 4*. doi:ARTN 133
10.3389/fpls.2013.00133

Dastidar, M. G. (2015). Identification and characterization of MIR390 regulators in *Arabidopsis thaliana* root development. *Dissertation submitted to the Combined Faculties for the Natural Sciences and for Mathematics of the Ruperto-Carola University of Heidelberg, Germany*.

Dastidar, M. G., Mosiolek, M., Bleckmann, A., Dresselhaus, T., Nodine, M. D., & Maizel, A. (2016). Sensitive whole mount in situ localization of small RNAs in plants. *Plant J, 88*(4), 694-702. doi:10.1111/tpj.13270

de Felippes, F. F., Marchais, A., Sarazin, A., Oberlin, S., & Voinnet, O. (2017). A single miR390 targeting event is sufficient for triggering TAS3-tasiRNA biogenesis in Arabidopsis. *Nucleic Acids Res, 45*(9), 5539-5554. doi:10.1093/nar/gkx119

De Rybel, B., Vassileva, V., Parizot, B., Demeulenaere, M., Grunewald, W., Audenaert, D., . . . Beeckman, T. (2010). A novel aux/IAA28 signaling cascade activates GATA23-dependent specification of lateral root founder cell identity. *Curr Biol, 20*(19), 1697-1706. doi:10.1016/j.cub.2010.09.007

De Smet, I. (2012). Lateral root initiation: one step at a time. *New Phytologist, 193*(4), 867-873. doi:Doi 10.1111/J.1469-8137.2011.03996.X

De Smet, I., Vassileva, V., De Rybel, B., Levesque, M. P., Grunewald, W., Van Damme, D., . . . Beeckman, T. (2008). Receptor-like kinase ACR4 restricts formative cell divisions in the Arabidopsis root. *Science, 322*(5901), 594-597. doi:10.1126/science.1160158

De Smet, S., Cuypers, A., Vangronsveld, J., & Remans, T. (2015). Gene Networks Involved in Hormonal Control of Root Development in Arabidopsis thaliana: A Framework for Studying Its Disturbance by Metal Stress. *Int J Mol Sci, 16*(8), 19195-19224. doi:10.3390/ijms160819195

Deb, J., Bland, H. M., & Ostergaard, L. (2017). Developmental cartography: coordination via hormonal and genetic interactions during gynoecium formation. *Curr Opin Plant Biol, 41*, 54-60. doi:10.1016/j.pbi.2017.09.004

Di Mambro, R., De Ruvo, M., Pacifici, E., Salvi, E., Sozzani, R., Benfey, P. N., . . . Sabatini, S. (2017). Auxin minimum triggers the developmental switch from cell division to cell differentiation in the Arabidopsis root. *Proc Natl Acad Sci U S A, 114*(36), E7641-E7649. doi:10.1073/pnas.1705833114

Dinesh, D. C., Villalobos, L. I., & Abel, S. (2015). Structural Biology of Nuclear Auxin Action. *Trends in Plant Science*. doi:10.1016/j.tplants.2015.10.019

Douglas, R. N., Wiley, D., Sarkar, A., Springer, N., Timmermans, M. C. P., & Scanlon, M. J. (2010). ragged seedling2 Encodes an ARGONAUTE7-Like Protein Required for Mediolateral Expansion, but Not Dorsiventrality, of Maize Leaves. *Plant Cell, 22*(5), 1441-1451. doi:10.1105/tpc.109.071613

Du, Y., & Scheres, B. (2017). Lateral root formation and the multiple roles of auxin. *Journal of Experimental Botany*. doi:10.1093/jxb/erx223

Edwards, K., Johnstone, C., & Thompson, C. (1991). A Simple and Rapid Method for the Preparation of Plant Genomic DNA for Pcr Analysis. *Nucleic Acids Res, 19*(6), 1349-1349. doi:DOI 10.1093/nar/19.6.1349

Elmayan, T., Balzergue, S., Beon, F., Bourdon, V., Daubremet, J., Guenet, Y., . . . Vaucheret, H. (1998). Arabidopsis mutants impaired in cosuppression. *Plant Cell, 10*(10), 1747-1757.

Elwell, A. L., Gronwall, D. S., Miller, N. D., Spalding, E. P., & Brooks, T. L. D. (2011). Separating parental environment from seed size effects on next generation growth and development in Arabidopsis. *Plant Cell and Environment, 34*(2), 291-301. doi:10.1111/j.1365-3040.2010.02243.x

Endo, Y., Iwakawa, H. O., & Tomari, Y. (2013). Arabidopsis ARGONAUTE7 selects miR390 through multiple checkpoints during RISC assembly. *EMBO Rep, 14*(7), 652-658. doi:10.1038/embor.2013.73

Enugutti, B., Kirchhelle, C., Oelschner, M., Torres Ruiz, R. A., Schliebner, I., Leister, D., & Schneitz, K. (2012). Regulation of planar growth by the Arabidopsis AGC protein kinase UNICORN. *Proc Natl Acad Sci U S A, 109*(37), 15060-15065. doi:10.1073/pnas.1205089109

Fahlgren, N., Montgomery, T. A., Howell, M. D., Allen, E., Dvorak, S. K., Alexander, A. L., & Carrington, J. C. (2006a). Regulation of AUXIN RESPONSE FACTOR3 by TAS3 ta-siRNA affects developmental timing and patterning in Arabidopsis. *Current Biology, 16*(9), 939-944. doi:10.1016/j.cub.2006.03.065

Fahlgren, N., Montgomery, T. A., Howell, M. D., Allen, E., Dvorak, S. K., Alexander, A. L., & Carrington, J. C. (2006b). Regulation of AUXIN RESPONSE FACTOR3 by TAS3 ta-siRNA affects developmental timing and patterning in Arabidopsis. *Curr Biol, 16*(9), 939-944. doi:10.1016/j.cub.2006.03.065

Fei, Q., Xia, R., & Meyers, B. C. (2013). Phased, secondary, small interfering RNAs in posttranscriptional regulatory networks. *Plant Cell, 25*(7), 2400-2415. doi:10.1105/tpc.113.114652

Figueiredo, D. D., Batista, R. A., & Kohler, C. (2017). Auxin regulates endosperm cellularization in Arabidopsis. *bioRxiv*. doi:10.1101/239301

Franco-Zorrilla, J. M., Valli, A., Todesco, M., Mateos, I., Puga, M. I., Rubio-Somoza, I., . . . Paz-Ares, J. (2007). Target mimicry provides a new mechanism for regulation of microRNA activity. *Nature Genetics, 39*(8), 1033-1037. doi:10.1038/ng2079

Gao, Y. B., Zhang, Y., Zhang, D., Dai, X. H., Estelle, M., & Zhao, Y. D. (2015). Auxin binding protein 1 (ABP1) is not required for either auxin signaling or Arabidopsis development. *Proc Natl Acad Sci U S A, 112*(7), 2275-2280. doi:10.1073/pnas.1500365112

Garcia, D., Collier, S. A., Byrne, M. E., & Martienssen, R. A. (2006). Specification of leaf polarity in Arabidopsis via the trans-acting siRNA pathway. *Curr Biol, 16*(9), 933-938. doi:10.1016/j.cub.2006.03.064

Gleave, A. P. (1992). A Versatile Binary Vector System with a T-DNA Organizational-Structure Conducive to Efficient Integration of Cloned DNA into the Plant Genome. *Plant Molecular Biology, 20*(6), 1203-1207. doi:Doi 10.1007/Bf00028910

Goh, T., Joi, S., Mimura, T., & Fukaki, H. (2012). The establishment of asymmetry in Arabidopsis lateral root founder cells is regulated by LBD16/ASL18 and related LBD/ASL proteins. *Development, 139*(5), 883-893. doi:10.1242/dev.071928

Gooh, K., Ueda, M., Aruga, K., Park, J., Arata, H., Higashiyama, T., & Kurihara, D. (2015). Live-Cell Imaging and Optical Manipulation of Arabidopsis Early Embryogenesis. *Developmental Cell, 34*(2), 242-251. doi:10.1016/j.devcel.2015.06.008

Griffiths-Jones, S. (2004). The microRNA Registry. *Nucleic Acids Res, 32*, D109-D111. doi:10.1093/nar/gkh023

Griffiths-Jones, S., Grocock, R. J., van Dongen, S., Bateman, A., & Enright, A. J. (2006). miRBase: microRNA sequences, targets and gene nomenclature. *Nucleic Acids Res, 34*, D140-D144. doi:10.1093/nar/gkj112

Griffiths-Jones, S., Saini, H. K., van Dongen, S., & Enright, A. J. (2008). miRBase: tools for microRNA genomics. *Nucleic Acids Res, 36*, D154-D158. doi:10.1093/nar/gkm952

Guan, Y. F., Lu, J. P., Xu, J., McClure, B., & Zhang, S. Q. (2014). Two Mitogen-Activated Protein Kinases, MPK3 and MPK6, Are Required for Funicular Guidance of Pollen Tubes in Arabidopsis. *Plant Physiol, 165*(2), 528-533. doi:10.1104/pp.113.231274

Gunnery, S., & Datta, A. (1987). An Inhibitor Rna of Translation from Barley Embryo. *Biochemical and Biophysical Research Communications, 142*(2), 383-388. doi:Doi 10.1016/0006-291x(87)90285-3

Hawkins, C., & Liu, Z. (2014). A model for an early role of auxin in Arabidopsis gynoecium morphogenesis. *Front Plant Sci, 5*, 327. doi:10.3389/fpls.2014.00327

Healey, A., Furtado, A., Cooper, T., & Henry, R. J. (2014). Protocol: a simple method for extracting next-generation sequencing quality genomic DNA from recalcitrant plant species. *Plant Methods, 10*. doi:Artn 21

10.1186/1746-4811-10-21

Hobecker, K. V., Reynoso, M. A., Bustos-Sanmamed, P., Wen, J., Mysore, K. S., Crespi, M., . . . Zanetti, M. E. (2017). The MicroRNA390/TAS3 Pathway Mediates Symbiotic Nodulation and Lateral Root Growth. *Plant Physiol, 174*(4), 2469-2486. doi:10.1104/pp.17.00464

Hou, C. Y., Lee, W. C., Chou, H. C., Chen, A. P., Chou, S. J., & Chen, H. M. (2016). Global Analysis of Truncated RNA Ends Reveals New Insights into Ribosome Stalling in Plants. *Plant Cell, 28*(10), 2398-2416. doi:10.1105/tpc.16.00295

Howell, M. D., Fahlgren, N., Chapman, E. J., Cumbie, J. S., Sullivan, C. M., Givan, S. A., . . . Carrington, J. C. (2007). Genome-wide analysis of the RNA-DEPENDENT RNA POLYMERASE6/DICER-LIKE4 pathway in Arabidopsis reveals dependency on miRNA- and tasiRNA-directed targeting. *Plant Cell, 19*(3), 926-942. doi:10.1105/tpc.107.050062

Irish, V. F. (2010). The flowering of Arabidopsis flower development. *Plant J, 61*(6), 1014-1028. doi:10.1111/j.1365-313X.2009.04065.x

Jander, G., Baerson, S. R., Hudak, J. A., Gonzalez, K. A., Gruys, K. J., & Last, R. L. (2003). Ethylmethanesulfonate saturation mutagenesis in Arabidopsis to determine frequency of herbicide resistance. *Plant Physiol, 131*(1), 139-146. doi:10.1104/pp.102.010397

Jouannet, V., Moreno, A. B., Elmayan, T., Vaucheret, H., Crespi, M. D., & Maizel, A. (2012). Cytoplasmic Arabidopsis AGO7 accumulates in membrane-associated siRNA bodies and is required for ta-siRNA biogenesis. *Embo Journal, 31*(7), 1704-1713. doi:Doi 10.1038/Emboj.2012.20

Kamthan, A., Chaudhuri, A., Kamthan, M., & Datta, A. (2015). Small RNAs in plants: recent development and application for crop improvement. *Front Plant Sci, 6*. doi:UNSP 208
10.3389/fpls.2015.00208

Karimi, M., Inze, D., & Depicker, A. (2002). GATEWAY((TM)) vectors for Agrobacterium-mediated plant transformation. *Trends in Plant Science, 7*(5), 193-195. doi:Pii S1360-1385(02)02251-3
Doi 10.1016/S1360-1385(02)02251-3

Kazan, K. (2013). Auxin and the integration of environmental signals into plant root development. *Annals of Botany, 112*(9), 1655-1665. doi:10.1093/aob/mct229

Kearse, M., Moir, R., Wilson, A., Stones-Havas, S., Cheung, M., Sturrock, S., . . . Drummond, A. (2012). Geneious Basic: An integrated and extendable desktop software platform for the organization and analysis of sequence data. *Bioinformatics, 28*(12), 1647-1649. doi:10.1093/bioinformatics/bts199

Khan, D., Millar, J. L., Girard, I. J., Chan, A., Kirkbride, R. C., Pelletier, J. M., . . . Belmonte, M. F. (2015). Transcriptome atlas of the Arabidopsis funiculus--a study of maternal seed subregions. *Plant J, 82*(1), 41-53. doi:10.1111/tpj.12790

Koevoets, I. T., Venema, J. H., Elzenga, J. T. M., & Testerink, C. (2016). Roots Withstanding their Environment: Exploiting Root System Architecture Responses to Abiotic Stress to Improve Crop Tolerance. *Front Plant Sci, 7*. doi:ARTN 1335
10.3389/fpls.2016.01335

Kozomara, A., & Griffiths-Jones, S. (2011). miRBase: integrating microRNA annotation and deep-sequencing data. *Nucleic Acids Res, 39*, D152-D157. doi:10.1093/nar/gkq1027

Kozomara, A., & Griffiths-Jones, S. (2014). miRBase: annotating high confidence microRNAs using deep sequencing data. *Nucleic Acids Res, 42*(D1), D68-D73. doi:10.1093/nar/gkt1181

Kurihara, D., Hamamura, Y., & Higashiyama, T. (2013). Live-cell analysis of plant reproduction: Live-cell imaging, optical manipulation, and advanced microscopy technologies. *Development Growth & Differentiation, 55*(4), 462-473. doi:10.1111/dgd.12040

Lampropoulos, A., Sutikovic, Z., Wenzl, C., Maegele, I., Lohmann, J. U., & Forner, J. (2013). GreenGate - A Novel, Versatile, and Efficient Cloning System for Plant Transgenesis. *Plos One, 8*(12). doi:ARTN e83043
DOI 10.1371/journal.pone.0083043

Larsson, E., Franks, R. G., & Sundberg, E. (2013). Auxin and the Arabidopsis thaliana gynoecium. *Journal of Experimental Botany, 64*(9), 2619-2627. doi:10.1093/jxb/ert099

Lavenus, J., Goh, T., Roberts, I., Guyomarc'h, S., Lucas, M., De Smet, I., . . . Laplaze, L. (2013). Lateral root development in Arabidopsis: fifty shades of auxin. *Trends in Plant Science, 18*(8), 455-463. doi:Doi 10.1016/J.Tplants.2013.04.006

Li, S. B., Le, B., Ma, X., Li, S. F., You, C. J., Yu, Y., . . . Chen, X. M. (2016). Biogenesis of phased siRNAs on membrane-bound polysomes in Arabidopsis. *Elife, 5*. doi:ARTN e22750
10.7554/eLife.22750

Li, S. B., Xie, Z. Z., Hu, C. G., & Zhang, J. Z. (2016). A Review of Auxin Response Factors (ARFs) in Plants. *Front Plant Sci, 7*, 47. doi:10.3389/fpls.2016.00047

Lin, Y. L., Lin, L. X., Lai, R. L., Liu, W. H., Chen, Y. K., Zhang, Z. H., . . . Lai, Z. X. (2015). MicroRNA390-Directed TAS3 Cleavage Leads to the Production of tasiRNA-ARF3/4 During Somatic Embryogenesis in Dimocarpus longan Lour. *Front Plant Sci, 6*. doi:ARTN 119
10.3389/fpls.2075.07719

Liu, Y., Li, S., Chen, Y., Kimberlin, A. N., Cahoon, E. B., & Yu, B. (2016). snRNA 3' End Processing by a CPSF73-Containing Complex Essential for Development in Arabidopsis. *PLoS Biol, 14*(10), e1002571. doi:10.1371/journal.pbio.1002571

Liu, Y., Xu, M., Liang, N., Zheng, Y., Yu, Q., & Wu, S. (2017). Symplastic communication spatially directs local auxin biosynthesis to maintain root stem cell niche in Arabidopsis. *Proc Natl Acad Sci U S A, 114*(15), 4005-4010. doi:10.1073/pnas.1616387114

Malamy, J. E., & Benfey, P. N. (1997). Organization and cell differentiation in lateral roots of Arabidopsis thaliana. *Development, 124*(1), 33-44.

Mallory, A. C., Ely, L., Smith, T. H., Marathe, R., Anandalakshmi, R., Fagard, M., . . . Vance, V. B. (2001). HC-Pro suppression of transgene silencing eliminates the small RNAs but not transgene methylation or the mobile signal. *Plant Cell, 13*(3), 571-583. doi:DOI 10.1105/tpc.13.3.571

Marin, E., Jouannet, V., Herz, A., Lokerse, A. S., Weijers, D., Vaucheret, H., . . . Maizel, A. (2010). miR390, Arabidopsis TAS3 tasiRNAs, and their AUXIN RESPONSE FACTOR targets define an autoregulatory network quantitatively regulating lateral root growth. *Plant Cell, 22*(4), 1104-1117. doi:10.1105/tpc.109.072553

Maruyama, D., Volz, R., Takeuchi, H., Mori, T., Igawa, T., Kurihara, D., . . . Higashiyama, T. (2015). Rapid Elimination of the Persistent Synergid through a Cell Fusion Mechanism. *Cell, 161*(4), 907-918. doi:10.1016/j.cell.2015.03.018

Mironova, V. V., Omelyanchuk, N. A., Wiebe, D. S., & Levitsky, V. G. (2014). Computational analysis of auxin responsive elements in the Arabidopsis thaliana L. genome. *Bmc Genomics, 15*. doi:Artn S4
10.1186/1471-2164-15-S12-S4

Moller, B. K., Xuan, W., & Beeckman, T. (2017). Dynamic control of lateral root positioning. *Curr Opin Plant Biol, 35*, 1-7. doi:10.1016/j.pbi.2016.09.001

Montgomery, T. A., Howell, M. D., Cuperus, J. T., Li, D., Hansen, J. E., Alexander, A. L., . . . Carrington, J. C. (2008). Specificity of ARGONAUTE7-miR390 interaction and dual functionality in TAS3 trans-acting siRNA formation. *Cell, 133*(1), 128-141. doi:10.1016/j.cell.2008.02.033

Mori, T., Kuroiwa, H., Higashiyama, T., & Kuroiwa, T. (2006). GENERATIVE CELL SPECIFIC 1 is essential for angiosperm fertilization. *Nat Cell Biol, 8*(1), 64-71. doi:10.1038/ncb1345

Morris, E. C., Griffiths, M., Golebiowska, A., Mairhofer, S., Burr-Hersey, J., Goh, T., . . . Bennett, M. J. (2017). Shaping 3D Root System Architecture. *Current Biology, 27*(17), R919-R930. doi:10.1016/j.cub.2017.06.043

Murashige, T., & Skoog, F. (1962). A Revised Medium for Rapid Growth and Bio Assays with Tobacco Tissue Cultures. *Physiologia Plantarum, 15*(3), 473-497. doi:DOI 10.1111/j.1399-3054.1962.tb08052.x

Napoli, C., Lemieux, C., & Jorgensen, R. (1990). Introduction of a Chimeric Chalcone Synthase Gene into Petunia Results in Reversible Co-Suppression of Homologous Genes in Trans. *Plant Cell, 2*(4), 279-289. doi:DOI 10.1105/tpc.2.4.279

O'Malley, R. C., Barragan, C. C., & Ecker, J. R. (2015). A User's Guide to the Arabidopsis T-DNA Insertional Mutant Collections. *Methods in molecular biology (Clifton, N.J.), 1284*, 323-342. doi:10.1007/978-1-4939-2444-8_16

Okushima, Y., Mitina, I., Quach, H. L., & Theologis, A. (2005). AUXIN RESPONSE FACTOR 2 (ARF2): a pleiotropic developmental regulator. *Plant Journal, 43*(1), 29-46. doi:10.1111/j.1365-313X.2005.02426.x

Overvoorde, P., Fukaki, H., & Beeckman, T. (2010). Auxin control of root development. *Cold Spring Harb Perspect Biol, 2*(6), a001537. doi:10.1101/cshperspect.a001537

Panoli, A., Martin, M. V., Alandete-Saez, M., Simon, M., Neff, C., Swarup, R., . . . Sundaresan, V. (2015). Auxin Import and Local Auxin Biosynthesis Are Required for Mitotic Divisions, Cell Expansion and Cell Specification during Female Gametophyte Development in Arabidopsis thaliana. *Plos One, 10*(5), e0126164. doi:10.1371/journal.pone.0126164

Pekker, I., Alvarez, J. P., & Eshed, Y. (2005). Auxin response factors mediate Arabidopsis organ asymmetry via modulation of KANADI activity. *Plant Cell, 17*(11), 2899-2910. doi:10.1105/tpc.105.034876

Peret, B., De Rybel, B., Casimiro, I., Benkova, E., Swarup, R., Laplaze, L., . . . Bennett, M. J. (2009). Arabidopsis lateral root development: an emerging story. *Trends in Plant Science, 14*(7), 399-408. doi:Doi 10.1016/J.Tplants.2009.05.002

Peret, B., Middleton, A. M., French, A. P., Larrieu, A., Bishopp, A., Njo, M., . . . Bennett, M. J. (2013). Sequential induction of auxin efflux and influx carriers regulates lateral root emergence. *Molecular Systems Biology, 9*. doi:ARTN 699
10.1038/msb.2013.43

Petricka, J. J., Winter, C. M., & Benfey, P. N. (2012). Control of Arabidopsis root development. *Annual Review of Plant Biology, Vol 63, 63*, 563-590. doi:10.1146/annurev-arplant-042811-105501

Philippot, L., Raaijmakers, J. M., Lemanceau, P., & van der Putten, W. H. (2013). Going back to the roots: the microbial ecology of the rhizosphere. *Nature Reviews Microbiology, 11*(11), 789-799. doi:10.1038/nrmicro3109

Plavskin, Y., Nagashima, A., Perroud, P. F., Hasebe, M., Quatrano, R. S., Atwal, G. S., & Timmermans, M. C. P. (2016). Ancient trans-Acting siRNAs Confer Robustness and Sensitivity onto the Auxin Response. *Developmental Cell, 36*(3), 276-289. doi:10.1016/j.devcel.2016.01.010

Preibisch, S., Saalfeld, S., & Tomancak, P. (2009). Globally optimal stitching of tiled 3D microscopic image acquisitions. *Bioinformatics, 25*(11), 1463-1465. doi:10.1093/bioinformatics/btp184

Pruss, G. J., Nester, E. W., & Vance, V. (2008). Infiltration with Agrobacterium tumefaciens Induces Host Defense and Development-Dependent Responses in the Infiltrated Zone. *Molecular Plant-Microbe Interactions, 21*(12), 1528-1538. doi:10.1094/Mpmi-21-12-1528

Qin, P., Ting, D., Shieh, A., & McCormick, S. (2012). Callose plug deposition patterns vary in pollen tubes of Arabidopsis thaliana ecotypes and tomato species. *BMC Plant Biol, 12*, 178. doi:10.1186/1471-2229-12-178

Roeder, A. H., & Yanofsky, M. F. (2006). Fruit development in Arabidopsis. *Arabidopsis Book, 4*, e0075. doi:10.1199/tab.0075

Rogers, K., & Chen, X. (2013). Biogenesis, turnover, and mode of action of plant microRNAs. *Plant Cell, 25*(7), 2383-2399. doi:10.1105/tpc.113.113159

Rosso, M. G., Li, Y., Strizhov, N., Reiss, B., Dekker, K., & Weisshaar, B. (2003). An Arabidopsis thaliana T-DNA mutagenized population (GABI-Kat) for flanking sequence tag-based reverse genetics. *Plant Molecular Biology, 53*(1), 247-259. doi:DOI 10.1023/B:PLAN.0000009297.37235.4a

Salehin, M., Bagchi, R., & Estelle, M. (2015). SCFTIR1/AFB-Based Auxin Perception: Mechanism and Role in Plant Growth and Development. *Plant Cell, 27*(1), 9-19. doi:10.1105/tpc.114.133744

Sandaklie-Nikolova, L., Palanivelu, R., King, E. J., Copenhaver, G. P., & Drews, G. N. (2007). Synergid cell death in Arabidopsis is triggered following direct interaction with the pollen tube(1[W][OA]). *Plant Physiol, 144*(4), 1753-1762. doi:DOI 10.1104/pp.107.098236

Scheres, B., Benfey, P., & Dolan, L. (2002). Root Development. *The Arabidopsis Book*, e0101. doi:10.1199/tab.0101

Schindelin, J., Arganda-Carreras, I., Frise, E., Kaynig, V., Longair, M., Pietzsch, T., . . . Cardona, A. (2012). Fiji: an open-source platform for biological-image analysis. *Nature Methods, 9*(7), 676-682. doi:10.1038/Nmeth.2019

Schlereth, A., Moller, B., Liu, W. L., Kientz, M., Flipse, J., Rademacher, E. H., . . . Weijers, D. (2010). MONOPTEROS controls embryonic root initiation by regulating a mobile transcription factor. *Nature, 464*(7290), 913-U128. doi:10.1038/nature08836

Scott, R. J., Spielman, M., & Dickinson, H. G. (2004). Stamen structure and function. *Plant Cell, 16 Suppl*, S46-60. doi:10.1105/tpc.017012

Seefried, W. F., Willmann, M. R., Clausen, R. L., & Jenik, P. D. (2014). Global Regulation of Embryonic Patterning in Arabidopsis by MicroRNAs. *Plant Physiol, 165*(2), 670-687. doi:10.1104/pp.114.240846

Sessions, A., Burke, E., Presting, G., Aux, G., McElver, J., Patton, D., . . . Goff, S. A. (2002). A high-throughput Arabidopsis reverse genetics system. *Plant Cell, 14*(12), 2985-2994. doi:10.1105/tpc.004630

Sessions, R. A. (1997). Arabidopsis (Brassicaceae) flower development and gynoecium patterning in wild type and Ettin mutants. *American Journal of Botany, 84*(9), 1179-1191. doi:Doi 10.2307/2446041

Sessions, R. A., & Zambryski, P. C. (1995). Arabidopsis Gynoecium Structure in the Wild-Type and in Effin Mutants. *Development, 121*(5), 1519-1532.

Shalom, L., Shlizerman, L., Zur, N., Doron-Faigenboim, A., Blumwald, E., & Sadka, A. (2015). Molecular characterization of SQUAMOSA PROMOTER BINDING PROTEIN-LIKE (SPL) gene family from Citrus and the effect of fruit load on their expression. *Front Plant Sci, 6*, 389. doi:10.3389/fpls.2015.00389

Shi, H. Z., Ishitani, M., Kim, C. S., & Zhu, J. K. (2000). The Arabidopsis thaliana salt tolerance gene SOS1 encodes a putative Na+/H+ antiporter. *Proc Natl Acad Sci U S A, 97*(12), 6896-6901. doi:DOI 10.1073/pnas.120170197

Sorensen, M. B., Mayer, U., Lukowitz, W., Robert, H., Chambrier, P., Jurgens, G., . . . Berger, F. (2002). Cellularisation in the endosperm of Arabidopsis thaliana is coupled to mitosis and shares multiple components with cytokinesis. *Development, 129*(24), 5567-5576. doi:10.1242/dev.00152

Stauffer, E., & Maizel, A. (2014). Post-transcriptional regulation in root development. *Wiley Interdisciplinary Reviews-Rna, 5*(5), 679-696. doi:10.1002/wrna.1239

Su, Z. X., Zhao, L. H., Zhao, Y. Y., Li, S. F., Won, S., Cai, H. Y., . . . Chen, X. M. (2017). The THO Complex Non-Cell-Autonomously Represses Female Germline Specification through the TAS3-ARF3 Module. *Current Biology, 27*(11), 1597-+. doi:10.1016/j.cub.2017.05.021

Swarup, K., Benkova, E., Swarup, R., Casimiro, I., Peret, B., Yang, Y., . . . Bennett, M. J. (2008). The auxin influx carrier LAX3 promotes lateral root emergence. *Nat Cell Biol, 10*(8), 946-954. doi:10.1038/ncb1754

ten Hove, C. A., Lu, K. J., & Weijers, D. (2015). Building a plant: cell fate specification in the early Arabidopsis embryo. *Development, 142*(3), 420-430. doi:10.1242/dev.111500

Tian, H., Niu, T., Yu, Q., Quan, T., & Ding, Z. (2013). Auxin gradient is crucial for the maintenance of root distal stem cell identity in Arabidopsis. *Plant Signal Behav, 8*(12), e26429. doi:10.4161/psb.26429

Truernit, E., Bauby, H., Dubreucq, B., Grandjean, O., Runions, J., Barthelemy, J., & Palauqui, J. C. (2008). High-resolution whole-mount imaging of three-dimensional tissue organization and gene expression enables the study of Phloem development and structure in Arabidopsis. *Plant Cell, 20*(6), 1494-1503. doi:10.1105/tpc.107.056069

Truernit, E., & Haseloff, J. (2008). A simple way to identify non-viable cells within living plant tissue using confocal microscopy. *Plant Methods, 4*. doi:Artn 15

10.1186/1746-4811-4-15

Vanneste, S., De Rybel, B., Beemster, G. T. S., Ljung, K., De Smet, I., Van Isterdael, G., . . . Beeckman, T. (2005). Cell cycle progression in the pericycle is not sufficient for SOLITARY ROOT/IAA14-mediated lateral root initiation in Arabidopsis thaliana. *Plant Cell, 17*(11), 3035-3050. doi:10.1105/tpc.105.035493

Varkonyi-Gasic, E., Wu, R., Wood, M., Walton, E. F., & Hellens, R. P. (2007). Protocol: a highly sensitive RT-PCR method for detection and quantification of microRNAs. *Plant Methods, 3*, 12. doi:10.1186/1746-4811-3-12

Verbelen, J. P., De Cnodder, T., Le, J., Vissenberg, K., & Baluska, F. (2006). The Root Apex of Arabidopsis thaliana Consists of Four Distinct Zones of Growth Activities: Meristematic Zone, Transition Zone, Fast Elongation Zone and Growth Terminating Zone. *Plant Signal Behav, 1*(6), 296-304.

Wang, J. W., Schwab, R., Czech, B., Mica, E., & Weigel, D. (2008). Dual effects of miR156-targeted SPL genes and CYP78A5/KLUH on plastochron length and organ size in Arabidopsis thaliana. *Plant Cell, 20*(5), 1231-1243. doi:10.1105/tpc.108.058180

Weigel, D., & Glazebrook, J. (2002). *Arabidopsis: A Laboratory Manual*: Cold Spring Harbor Laboratory Press.

Xia, R., Xu, J., & Meyers, B. C. (2017). The Emergence, Evolution, and Diversification of the miR390-TAS3-ARF Pathway in Land Plants. *Plant Cell, 29*(6), 1232-1247. doi:10.1105/tpc.17.00185

Xu, M., Hu, T., Zhao, J., Park, M. Y., Earley, K. W., Wu, G., . . . Poethig, R. S. (2016). Developmental Functions of miR156-Regulated SQUAMOSA PROMOTER BINDING PROTEIN-LIKE (SPL) Genes in Arabidopsis thaliana. *PLoS Genet, 12*(8), e1006263. doi:10.1371/journal.pgen.1006263

Xu, T. D., Dai, N., Chen, J. S., Nagawa, S., Cao, M., Li, H. J., . . . Yang, Z. B. (2014). Cell Surface ABP1-TMK Auxin-Sensing Complex Activates ROP GTPase Signaling. *Science, 343*(6174), 1025-1028. doi:10.1126/science.1245125

Xu, W., Fiume, E., Coen, O., Pechoux, C., Lepiniec, L., & Magnani, E. (2016). Endosperm and Nucellus Develop Antagonistically in Arabidopsis Seeds. *Plant Cell, 28*(6), 1343-1360. doi:10.1105/tpc.16.00041

Xu, W. F., Ding, G. C., Yokawa, K., Baluska, F., Li, Q. F., Liu, Y. G., . . . Zhang, J. H. (2013). An improved agar-plate method for studying root growth and response of Arabidopsis thaliana. *Scientific Reports, 3*. doi:ARTN 1273

10.1038/srep01273

Yadegari, R., & Drews, G. N. (2004). Female gametophyte development. *Plant Cell, 16*, S133-S141. doi:10.1105/tpc.018192

Yoon, E., Kim, J.-W., Yang, J., Kim, S.-H., Lim, J., & Lee, W. (2014). A Molecular framework for the differential responses of primary and lateral roots to auxin in Arabidopsis thaliana. *Journal of Plant Biology, 57*(5), 274-281. doi:10.1007/s12374-013-0239-7

Yu, N., Niu, Q. W., Ng, K. H., & Chua, N. H. (2015). The role of miR156/SPLs modules in Arabidopsis lateral root development. *Plant J, 83*(4), 673-685. doi:10.1111/tpj.12919

Yuan, L. X., Loque, D., Kojima, S., Rauch, S., Ishiyama, K., Inoue, E., . . . von Wiren, N. (2007). The organization of high-affinity ammonium uptake in Arabidopsis roots depends on the spatial

arrangement and biochemical properties of AMT1-type transporters. *Plant Cell, 19*(8), 2636-2652. doi:10.1105/tpc.107.052134

Zhou, C. N., Han, L., Fu, C. X., Wen, J. Q., Cheng, X. F., Nakashima, J., . . . Wang, Z. Y. (2013). The Trans-Acting Short Interfering RNA3 Pathway and NO APICAL MERISTEM Antagonistically Regulate Leaf Margin Development and Lateral Organ Separation, as Revealed by Analysis of an argonaute7/lobed leaflet1 Mutant in Medicago truncatula. *Plant Cell, 25*(12), 4845-4862. doi:10.1105/tpc.113.117788

Acknowledgments

George Orwell suggested in “Politics and the English Language” 6 elementary rules to clear and concise writing (I hope you will be curious and google it!). While in this thesis I violated all of them, I will try to remedy in this more personal part. I want to thank Alexis for supervising me almost 4 years, always in a straight and honest way. I want to thank Karin, Sebastian, and Sascha for our constructive TAC meetings. I want to thank all my **friends** at COS for all the fun. And of course I want to thank Zaida for everything.